REP

AD-A270 084

Form Approved
OMB No 0704-0188

1. AGENCY USE ONLY (Leave blank)	2. REPORT DATE	3. REPORT TYPE AND DATES COVERED
	93 Aug	Final 89 Jun 01 - 92 Sep 30

(2)

4. TITLE AND SUBTITLE

Photodissociation Studies of Polyatomic Free Radicals

5. FUNDING NUMBERS

~~F49620-89-C-0070~~

2303/ES

61102F

6. AUTHOR(S)

Brad R. Weiner

7. PERFORMING ORGANIZATION NAME(S) AND ADDRESS(ES)

University of Puerto Rico
Department of Chemistry
Box 23346 UPR Station
Rio Piedras, PR 00931

8. PERFORMING ORGANIZATION REPORT NUMBER

AFOSR-TR- 93 0703

9. SPONSORING/MONITORING AGENCY NAME(S) AND ADDRESS(ES)

AFOSR
Building 410
Bolling AFB, DC 20332-6448

NC

10. SPONSORING/MONITORING AGENCY REPORT NUMBER

F49620-89-C-0070

11. SUPPLEMENTARY NOTES

12a. DISTRIBUTION/AVAILABILITY STATEMENT

Approved for public release
Distribution is unlimited

N CODE

13. ABSTRACT *(Maximum 200 words)*

An experimental program in gas phase polyatomic photochemistry and photophysics has been extablished in the Department of Chemistry at the University of Puerto Rico. Real time dynamics of sulfur monoxide photoelimination reactions have been studied by laser induced fluorescence spectroscopy of the nascent SO fragment on the $B^3\Sigma^- - X^3\Sigma^-$ transition in the region of 237-295 nm. The group of molecules under investigation are Sulfur dioxide (SO_2), dimethyl sulfoxide ($(CH_3)_2SO$), and the thionyl halides (SOX_2; where X=F,Cl or Br). In all of these experiments, the parent molecule is irradiated with an excimer laser (either 193 or 248 nm) and the energy disposal into the nascent SO photofragment is determined, and used as a mechanistic probe. The experiments indicate that the several of these parent molecules undergo three body dissociations. A second set of experiments measures kinetic decay constants of the C_2H_3O, both in the ground state and in the excited state. The temperature (295-374K) and pressure (2.5-100 torr) dependences for the rate constant of the $C_2H_3O + NO_2$ reaction have been measured by laser flash photolysis/laser induced fluorescence kinetic spectroscopy. The temperature dependent reaction for the decay of C_2H_3O in the presence of NO_2 is characterized over the measured region by the rate expression, $k_{II} = (1.48 \pm 0.70) \times 10^{-11} \exp(80.7 \pm 23.4K/T) cm^3 molecule^{-1} s^{-1}$. Fluorescence decay rates were determined in the presence to ten collision partners: He, Ar, N_2, O_2, CO, H_2, HCl, CO_2, C_2H_4, and $CH_3OCH=CH_2$. The measured electronic quenching cross-sections vary from 0.01 - 66.5 Å^2. A vibrational level dependence was found for the radiative lifetimes. Finally, a general procedure to evaluate the rotational state population distributions of the nascent photofragments from the photodissociation of polyatomic molecules has been implemented with the use of a kinematic distribution function. The calculated rotational state population distributions are compared with the most recent experimental data on OH and SH photofragments to obtain the information on the kinematic aspects of the photodissociating H_2O and H_2S molecules.

14. SUBJECT TERMS	15. NUMBER OF PAGES
Photodissociation Dynamics	17 + Appendices
	16. PRICE CODE

17. SECURITY CLASSIFICATION OF REPORT	18. SECURITY CLASSIFICATION OF THIS PAGE	19. SECURITY CLASSIFICATION OF ABSTRACT	20. LIMITATION OF ABSTRACT
Unclassified	Unclassified	Unclassified	

AIR FORCE OFFICE OF SCIENTIFIC RESEARCH

FINAL REPORT

for

Contract Number F49620-89-C-0070

PHOTODISSOCIATION STUDIES OF POLYATOMIC FREE RADICALS

Principal Investigator: Brad R. Weiner

Department of Chemistry
University of Puerto Rico
Río Piedras, PR 00931

November 30, 1992

ABSTRACT

An experimental program in gas phase polyatomic photochemistry and photophysics has been extablished in the Department of Chemistry at the University of Puerto Rico. Real time dynamics of sulfur monoxide photoelimination reactions have been studied by laser induced fluorescence spectroscopy of the nascent SO fragment on the $B^3\Sigma^- - X^3\Sigma^-$ transition in the region of 237-295 nm. The group of molecules currently under investigation are Sulfur dioxide $\{SO_2\}$, dimethyl sulfoxide $\{(CH_3)_2SO\}$, and the thionyl halides $\{SOX_2$; where X=F,Cl or Br$\}$. In all of these experiments, the parent molecule is irradiated with an excimer laser (either 193 or 248 nm) and the energy disposal into the nascent SO photofragment is determined, and used as a mechanistic probe. The experiments indicate that the several of these parent molecules undergo three body dissociations. A second set of experiments measures kinetic decay constants of the C_2H_3O, both in the ground state and in the excited state. The temperature (295-374K) and pressure (2.5-100 torr) dependences for the rate constant of the $C_2H_3O + NO_2$ reaction have been measured by laser flash photolysis/laser induced fluorescence kinetic spectroscopy. The temperature dependent reaction for the decay of C_2H_3O in the presence of NO_2 is characterized over the measured region by the rate expression, $k_{II}=(1.48\pm0.70)\times10^{-11}\exp(80.7\pm23.4K/T)cm^3molecule^{-1}s^{-1}$. Fluorescence decay rates were determined in the presence to ten collision partners: He, Ar, N_2, O_2, CO, H_2, HCl, CO_2, C_2H_4, and $CH_3OCH=CH_2$. The measured electronic quenching cross-sections vary from 0.01 - 66.5 $Å^2$. A vibrational level dependence was found for the radiative lifetimes. Finally, a general procedure to evaluate the rotational state population distributions of the nascent photofragments from the photodissociation of polyatomic molecules has been implemented with the use of a kinematic distribution function. Numerical evaluations of rotational state population distributions of diatomic photofragments from photodissociation of the general class of triatomic molecules are presented. The calculated rotational state population distributions are compared with the most recent experimental data on OH and SH photofragments to obtain the information on the kinematic aspects of the photodissociating H_2O and H_2S molecules.

I. OBJECTIVES OF THE RESEARCH EFFORT

The objectives of this research effort were:

(1) The development of an experimental program in gas phase photochemistry and unimolecular dissociation dynamics of polyatomic molecules.

(2) To provide a more detailed understanding of the unimolecular dissociation dynamics of free radicals of practical interest.

(3) To extend the established methods of photodissociation dynamics for closed shell species to open-shell species, *i.e.* polyatomic free radicals.

(4) Initiate a research program in mainstream physical chemistry at a minority institution, and provide a strong educational environment for students, both graduate and undergraduate.

II. ACCOMPLISHMENTS OF THE RESEARCH EFFORT

This research effort was initiated June 1, 1989, and we believe that the project reached or at least made significant advances towards the stated goals. We reported at the end of the first year that major equipment had been designed and constructed, the senior personnel had been contracted, and the junior personnel were in the process of being trained. By the end of the second year, we reported that the experimental program was underway and beginning to show signs of productivity. Now at the end of 3.4 years (the term of the contract), we report on the extent of the accomplishments, and how well these results met the stated objectives

In developing our program in gas phase photochemical dynamics of polyatomic molecules, we have done (and continue to do) a body of experimental studies on sulfur monoxide (SO) photoelimination reactions. In our second year report, we noted that preliminary work in this had been accepted for publication in the *Journal of Physical Chemistry*, but that because of the interesting dynamical aspects of the observed reactions, further study was warranted. At this point in time, this work is still not complete, but major advances have been made and experimental studies are continuing. The group of molecules currently under investigation are

Sulfur dioxide {SO_2}, dimethyl sulfoxide {$(CH_3)_2SO$}, and the thionyl halides {SOX_2; where X=F,Cl or Br}. In all of these experiments, the parent molecule is irradiated with an excimer laser (either 193 or 248 nm) and the energy disposal into the nascent SO photofragment is determined, and used as a mechanistic probe. What follows is a brief description of the results found for each of these molecular systems.

SO_2

Due to the large number of studies on the 193 nm photodissociation of sulfur dioxide, we used this system primarily as a test of our laser induced fluorescence (LIF) technique. Our work, however, led us to some interesting discoveries and discrepancies with past work on the 193 nm photodissociation of SO_2. We therefore embarked on a reinvestigation of the photodissociation dynamics of SO_2. We have measured the nascent vibrational, rotational, and spin-state distributions of the $SO(X^3\Sigma)$ fragment in both a bulb and in a pulsed supersonic nozzle. Our vibrational distribution was consistent with past measurements (not by LIF), giving us confidence in our experimental methods. We do find differences in the rotational state distributions obtained in the bulb vs. free jet experiments, which is surprising for the predissociative nature of sulfur dioxide. We have also discovered an interesting spin polarization effect in the nascent SO photofragment, that varies with vibrational level, and appears to have a strong J dependence. We are currently in the process of modelling these effects, as well as looking at the photodissociation at longer wavelengths. These more detailed results on the photodissociation of SO_2 are being prepared for publication in the *Journal of Chemical Physics*.

Cl_2SO

Due to our extremely sensitive and quantum specific capabilities for the detection of $SO(X^3\Sigma)$, we have also begun to study the photodissociation dynamics of thionyl halides, The photodissociation of thionyl chloride (Cl_2SO) is of interest as a model system to study three-body fragmentation processes, which can occur either in concert or stepwise. The photodissociation of this tetratomic molecule at 193 and 248 nm has been studied by laser induced fluorescence spectroscopy of the nascent SO fragment on the $B^3\Sigma^-$-$X^3\Sigma^-$ transition in the region of 237-295 nm. Photolysis of Cl_2SO at 193 nm leads to an inverted vibrational distribution for the nascent $SO(X^3\Sigma^-)$ with a population maximum at $v''=2$. The quantum yield, $\Phi_{SO(X)}^{193\,nm} = 0.73 \pm 0.10$, has

been measured by comparison of the $SO(X^3\Sigma^-)$ produced from SO_2. The results indicate a concerted three-body fragmentation mechanism as the primary dissociation channel. A Franck-Condon/golden rule model elucidates the geometry prior to the fragmentation and suggests a direct dissociation mechanism. The rotational and spin state distributions have been measured from the rovibronically resolved spectra to support our model of the detailed dissociation mechanism. At 248 nm, the nascent vibrational distribution was found to be bimodal. The vibrational state population distribution in $v"=0$-2, which accounts for most ($\sim$94%) of the nascent $SO(X^3\Sigma^-)$ population, was found to be thermal ($T_{vib}=1000\pm200$K), suggesting a stepwise fragmentation process. About 6% of the nascent SO population has been observed in other vibrational levels ($v"=3$-7), and most likely originates from the molecular elimination of Cl_2 from Cl_2SO.

These results provide important evidence of wavelength dependent photolysis channels in polyatomic molecules, and go further in characterizing them in microscopic detail. The original premise of Cl_2SO being a good model for polyatomic photodissociation dynamics studies is borne out.

F_2SO

The vibrational and rotational state distributions and the primary quantum yield of the $SO(X^3\Sigma^-)$ fragment following the laser photolysis of F_2SO at 193 nm have been measured by using laser induced fluorescence spectroscopy on the $SO(B^3\Sigma^- X^3\Sigma^-)$ transition. Molecular elimination of F_2 is the only energetically-allowed channel to produce the SO fragment. The quantum yield measurement, $\Phi_{SO(X)}^{193\,nm} = 0.06 \pm 0.01$, suggests that other photochemical channels, *i.e.*, FSO + F, must be operative as well. The vibrational distribution of the nascent SO(X) fragment has been found to be inverted with a population maximum at $v" = 2$, indicating a rapid dissociation process, and suggests that the nascent F_2 fragment is born with significant vibrational excitation. A Franck-Condon model best fits the observed vibrational state distribution when the SO bond length is similar to that of the ground state F_2SO.

Br_2SO

Photodissociation of Br_2SO following irradiation at 193 and 248 nm has been studied by laser induced fluorescence spectroscopy of the nascent SO fragment. The vibrational

distributions for the nascent SO have been found to be inverted, suggesting a concerted mechanism for the dissociation at both wavelengths. A Franck Condon / Golden Rule model elucidates the geometry prior to the dissociation, suggesting the possibility that photodissociation at both wavelengths occurs via the same excited state of Br_2SO. The rotational and spin state distributions have been measured from rovibronically resolved spectra to support our discussion on the detailed dissociation mechanism. Quantum yield measurements suggest that other electronic states of the SO radical may be directly produced.

$(CH_3)_2SO$

The photodissociation dynamics of the reaction, $(CH_3)_2SO + h\nu(193\ nm) \rightarrow 2CH_3 + SO$, have been examined by laser spectroscopic techniques. Relative vibrational and rotational state energy distributions of the nascent SO photofragment have been determined by using laser induced fluorescence spectroscopy on the $(B^3\Sigma^- X^3\Sigma^-)$ transition. The same technique has also been employed to establish the quantum yield, $\Phi_{193}[SO(X^3\Sigma)] = 1.02 \pm 0.12$. The nascent vibrational state distributions in the ν_1 and ν_2 modes of the methyl radical have been determined by using 2+1 resonance enhanced multiphoton ionization spectroscopy via the $(3p\ ^2A_2'' \leftarrow 2p\ ^2A_2'')$ transition. These measurements were done in collaboration with M. Hawley and H.H. Nelson at the Naval Research Laboratory.

The energy distributions of the nascent fragments are best described by a concerted three-body fragmentation. While some of our data are suggestive of a concerted synchronous dissociation of the two S-C bonds in DMSO,[2] we cannot conclusively determine the synchronicity from our results. Further studies of the photofragment angular distributions following 193 nm irradiation of dimethyl sulfoxide would be helpful in analyzing this aspect of the dissociation dynamics.

Even though the experiments involving $SO(X^3\Sigma)$ remain a tangent from our original proposed research, we believe that these studies are extremely valuable to the Air Force because of the atmospheric importance of these species. Along a similar line, we have studied the reaction dynamics of the vinoxy (C_2H_3O) radical. The primary motivation for this study was that it was a species of interest, and that it provided a nice vehicle for training new graduate

students to use the experimental apparatus. Some of this work has been published in *Chemical Physics Letters.*

C_2H_3O

The temperature (295-374K) and pressure (2.5-100 torr) dependences for the rate constant of the $C_2H_3O + NO_2$ reaction have been measured by laser flash photolysis/laser induced fluorescence kinetic spectroscopy. The temperature dependent reaction for the decay of C_2H_3O in the presence of NO_2 is characterized over the measured region by the rate expression, $k_{II}=(1.48\pm0.70)x10^{-11}exp(80.7\pm23.4K/T)cm^3molecule^{-1}s^{-1}$. This rate expression is found to be independent of pressure. The results can be explained by a reaction mechanism involving the formation of an energized adduct which subsequently decomposes to products, most likely ketene and nitrous acid.

The fast reaction of vinoxy radical + NO_2 has been found to have: 1) No appreciable barrier to reaction; and 2) No apparent pressure dependence over the range of 2.5-100 torr. Our measurements lead us to conclude that the molecule proceeds through an energized collision complex to give C_2H_2O and HONO. While the final products are the same as other alkoxy-NO_2 reactions, the mechanism appears to differ. In order to tell this for sure, more detailed experiments remain to be done. For example, a quantitative analysis, including branching ratios, of the final products of this reaction needs to be characterized. The reaction has important consequences with respect to atmospheric chemistry. Due to the fast rate of this reaction at almost all conditions, we believe that this rate should be considered by kinetic modellers.

State specific radiative lifetimes and electronic quenching cross-sections have been determined for three different vibrational modes of C_2H_3O ($\tilde{B}^2A''$). These experiments were carried out using a two-laser method with laser-induced fluorescence as the detection technique. Ground state vinoxy radicals were produced by 193nm excimer laser photolysis of $CH_3OCH=CH_2$, and were pumped to the B state by a tunable dye laser. Fluorescence decay rates were determined in the presence to ten collision partners: He, Ar, N_2, O_2, CO, H_2, HCl, CO_2, C_2H_4, and $CH_3OCH=CH_2$. The measured electronic quenching cross-sections vary from 0.01 - 66.5 $Å^2$. A vibrational level dependence was found for the radiative lifetimes, which is believed to be due to predissociation. We are now investigating the photodissociation of the vinoxy radical at 308 nm.

Another area that we have been developing is a theoretical treatment of the nascent rotational state population distributions arising from photodissociation reactions. We have developed a kinematic distribution function to accurately reproduce the nascent rotational distributions of OH and SH following the photodissociations of H_2O and H_2S, respectively. This work was published in the *International Journal of Quantum Chemistry*. A second paper on isotope effects in photodissociation dynamics was recently accepted for publication in *Chemical Physics Letters*.

In these works, a general procedure to evaluate the rotational state population distributions of the nascent photofragments from the photodissociation of polyatomic molecules has been implemented with the use of the kinematic distribution function developed by Chen and Pei.[1] Numerical evaluations of rotational state population distributions of diatomic photofragments from photodissociation of the general class of triatomic molecules are presented. The calculated rotational state population distributions are compared with the most recent experimental data on OH and SH photofragments to obtain the information on the kinematic aspects of the photodissociating H_2O and H_2S molecules.

We employ a semi-empirical model that utilizes a kinematic distribution function to calculate the rotational state population distributions of diatomic photofragments from the photodissociation of isotopically variant triatomic molecules. The numerically evaluated rotational distributions of the photofragments, SH and SD, are compared with experimental data on the nascent rotational state population distributions of the diatomic photofragments resulting from the laser photolysis of H_2S ($\lambda_{photolysis}$=193, 222 and 248 nm) and D_2S ($\lambda_{photolysis}$=193 and 222 nm).

In conclusion, the results clearly show that the kinematic distribution function, when used in conjunction with the experimental rotational state population distribution, can provide information about the degree of participation of different adiabatic surfaces in the presence of non-adiabatic coupling among them during a photochemical reaction. Even for the case of hydrogen sulfide photodissociation, where >98% of the available energy is partitioned into translational degrees of freedom, sensitive measurements of the internal energy distribution of the diatomic fragment provide a unique insight into the mechanisms of dissociation. This

---

[1] K. Chen and C. Pei, *Chem. Phys. Lett.* **124**, 365 (1986)

information not only helps unravel a detailed dissociative mechanism, but also gives information about the degree of non-adiabatic coupling between the two surfaces. Finally, the kinematic distribution model provides insight into the wavelength dependent photodissociation of H_2S, but we wish to ***stress*** that the true power of the model lies in systems of greater complexity where *ab initio* potentials are not available. For example, we are currently implementing the model to study the nascent rotational distributions of sulfur monoxide deriving from the 193 nm photodissociation of SO_2.

III. PUBLICATIONS

Xirong Chen, Hongxin Wang, Federico Asmar, Melvin H. Rodriguez, and Brad R. Weiner, "Rotational Distributions of $SO(X^3\Sigma)$ from the 193 nm Photodissociation of SO_2." *Manuscript in preparation*

Katherine I. Barnhard, Min He and Brad R. Weiner, "Fluorescence Lifetimes of C_2H $O(B^2A')$: Evidence for Predissociation." J. Phys. Chem. *To be submitted.*

Hongxin Wang, Xirong Chen, and Brad R. Weiner, "$SO(X^3\Sigma)$ Production from the 193 nm Laser Photolysis of Thionyl Fluoride." Chem. Phys. Lett. *To be submitted.*

Hongxin Wang, Xirong Chen, and Brad R. Weiner, "Laser Photodissociation Dynamics of Thionyl Chloride: Concerted and Stepwise Cleavage of S-Cl Bonds", J. Phys. Chem. *in press.*

Xirong Chen, Hongxin Wang, Brad R. Weiner, Michael Hawley and H.H. Nelson, "Photodissociation of Dimethyl Sulfoxide at 193 nm in the Gas Phase." J. Phys. Chem. *in press* .

Xiaotian Gu, Luis A. Muñoz, Yasuyuki Ishikawa, and Brad R. Weiner, "Isotope Effects and Wavelength Dependence in the Rotational State Distributions of the Diatomic Photofragments, SH and SD, from the Photodissociation of H_2S and D_2S", Chemical Physics Letters, *in press.*

Xirong Chen, Federico Asmar, Hongxin Wang and Brad R. Weiner, "Nascent $SO(X^3\Sigma^-)$ Vibrational Distributions from the Photodissociation of SO_2, $SOCl_2$ and $(CH_3)_2SO$ at 193 nm." J. Phys. Chem. *95*, **1991**, 6415.

Luis A. Muñoz, Y. Ishikawa and Brad R. Weiner, "Kinematic Distribution Function to Calculate Rotational Populations of Photofragments from Photodissociation of Triatomic Molecules." Int. J. Quant. Chem., *S25*, **1991**, 359.

Katherine I. Barnhard, Alejandro Santiago, Min He, Federico Asmar, Brad R. Weiner, "Pressure and Temperature Dependence of the C_2H_3O + NO_2 Reaction." Chemical Physics Letters *178*, **1991**, 150.

IV. PERSONNEL

The following people have participated in this project in addition to the principal investigator.

Senior Personnel

Professor Xirong Chen from the Dalian Institute of Chemical Physics, Dalian, P.R. China, joined our research group in February, 1990.

Junior Personnel

Graduate Students

Federico Asmar (Department of Chemistry)
Katherine I. Barnhard (Department of Chemistry)
Hongxin Wang (Chemical Physics Program)

Undergraduate Students

Luis A. Muñoz (Department of Physics)
Maria E. Nadal (Department of Chemistry)
Miriam Perez (Department of Chemistry)

V. PRESENTATIONS

International

"Dynamics of Sulfur Monoxide Photoelimination Reactions"
Brad R. Weiner
Air Force Office of Scientific Research (AFOSR) Molecular Dynamics Contractor's Meeting, Washington, D.C., 25-27 October 1992.

"The Nascent Vibrational Distribution of SO from the 193 nm Photodissociation of Thionylaniline"
K. Matos, X. Chen and Brad R. Weiner
National Institute of Health MARC-MBRS Symposium, Dorado, Puerto Rico, 21-24 October 1992.

"Photodissociation Dynamics of SO-Containing Molecules"(invited)
Brad R. Weiner
Department of Chemistry, University of Idaho, Moscow, Idaho, 13 October 1992.

"Photodissociation Studies of Sulfur Oxides"
Brad R. Weiner, Hongxin Wang and Xirong Chen
Gordon Research Conference on Atomic and Molecular Interactions, New London, New Hampshire, 20-24 July 1992.

"Fluorescence Lifetimes of the Vinoxy Radical: Evidence for Predissociation".
Katherine I. Barnhard, Min He and Brad R. Weiner
XXth Informal Conference on Photochemistry, Atlanta, Georgia, April 26-May 1, 1992.

"Internal Energy Disposal into the SO Radical Following Photodissociation of $SOCl_2$ and $SOBr_2$".
Hongxin Wang, Xirong Chen and Brad R. Weiner.
203rd National Meeting of the American Chemical Society, San Francisco, California, April 5-10, 1992.

"Vibrational Energy Transfer Studies of Sulfur Monoxide".
Xiaotian Gu, Xirong Chen and Brad R. Weiner
203rd National Meeting of the American Chemical Society, San Francisco, California, April 5-10, 1992.

"Collision-Induced Electronic Quenching of the Vinoxy Radical".
Min He, Katherine I. Barnhard and Brad R. Weiner
203rd National Meeting of the American Chemical Society, San Francisco, California, April 5-10, 1992.

"Internal Energy Distributions of SO from the 193 nm Photodissociation of SO_2 and Dimethyl Sulfoxide (DMSO)."
Federico Asmar, Xirong Chen, Hongxin Wang, and Brad R. Weiner
Second Pan American Chemical Congress, San Juan, Puerto Rico, September 24-29, 1991.

"Gas Phase Reactions of the Vinoxy (C_2H_3O) Radical".
Katherine I. Barnhard, Alejandro Santiago, He Min, and Brad R. Weiner
Second Pan American Chemical Congress, San Juan, Puerto Rico, September 24-29, 1991.

"Internal Energy Distributions of $SO(X^3\Sigma^-)$ from the 193 nm Photodissociation of $SOCl_2$".
Xirong Chen, Hongxin Wang and Brad R. Weiner
202nd National Meeting of the American Chemical Society, New York, NY, August 25-30, 1991.

"Nascent $SO(X^3\Sigma^-)$ Vibrational Distributions from the Photodissociation of SO_2, $SOCl_2$ and $(CH_3)_2SO$ at 193 nm."
Xirong Chen, Hongxin Wang, Federico Asmar, and Brad R. Weiner
Twenty-First International Conference on Free Radicals, Williamstown, Ma., August 4-9, 1991.

"Nascent Rotational Distributions of $SO(X^3\Sigma^-)$ from the 193 nm Photodissociation of SO_2 and Dimethyl Sulfoxide (DMSO)."
Xirong Chen, Federico Asmar, Melvin H. Rodríguez and Brad R. Weiner
201th National Meeting of the American Chemical Society, Atlanta, Ga. April 16, 1991.

"Kinematic Distribution Function to Calculate Rotational Populations of Photofragments from Photodissociation of Triatomic Molecules."
Luis A. Muñoz, Yasuyuki Ishikawa and Brad R. Weiner
Sanibel Symposium on Quantum Chemistry, St. Augustine, Florida, March 11, 1991.

"Fotoquimica y Fotofisica de Dimetilsufoxido (DMSO) a 193nm en Fase Gaseosa."
Federico Asmar, Luis Muñoz, María E. Nadal and Brad R. Weiner
XIX Congreso Latinoamericano de Quimica, Bueños Aires, Argentina, November 1990.

"Probing Chemical Reactions with Lasers." (invited)
Brad R. Weiner
Department of Chemistry, Grinnell College, Grinnell, Iowa, September 19, 1990.

"Photochemistry and Photophysics of Dimethyl Sulfoxide at 193 nm in the Gas Phase."
Federico Asmar, Luis Muñoz, Maria E. Nadal, Xirong Chen and Brad R. Weiner
American Physical Society-Inderdisciplinary Laser Science VI (ILS-VI), Minneapolis, Minnesota, September 18, 1990.

"Gas Phase Reactions of the Vinoxy Radical."
Brad R. Weiner, Katherine I. Barnhard, and Alejandro Santiago
200th National Meeting of the American Chemical Society, Washington, D.C., August 30, 1990.

"Laser Spectroscopic Probing of Chemical Reactions."
Federico Asmar and Brad R. Weiner
Instrument Society of America-Symposium for Innovation in Measurement Science (Student Award Presentation), Geneva, New York, August 9, 1990.

"Photodissociation of Dimethyl Sulfoxide at 193 nm in the Gas Phase."
Luis A. Muñoz, Federico Asmar and Brad R. Weiner
XIX Informal Conference on Photochemistry, Ann Arbor, Michigan, June 22, 1990.

"Photodissociation of Dimethyl Sulfoxide at 193 nm in the Gas Phase."
Federico Asmar, Luis A. Muñoz, Maria E. Nadal, Xirong Chen and Brad R. Weiner,
XIX Informal Conference on Photochemistry, Ann Arbor, Michigan, June 26, 1990.

"Photodissociation Dynamics of Borane Carbonyl at 193 nm."
Brad R. Weiner, L. Pasternack and H.H. Nelson, 1989 Conference of the Dynamics of Molecular Collisions, Asilomar, CA July 16-21, 1989.

Regional

"The Photochemistry of Thionylaniline"
K. Matos, X. Chen and Brad R. Weiner
16th Annual ACS Senior Technical Meeting, Mayagüez, Puerto Rico, 6-7 November 1992.

"Photodissociation Dynamics Studies of Sulfur Oxides"
H. Wang, X. Chen and Brad R. Weiner
16th Annual ACS Senior Technical Meeting, Mayagüez, Puerto Rico, 6-7 November 1992.

"Pulsed Laser Photolysis - Laser Induced Fluorescence Measurements on the Vibrational Relazation of the SO Radical."
Xiaotian Gu, Xirong Chen and Brad R. Weiner
27th Junior Technical Meeting, American Chemical Society, Puerto Rico Section, Gurabo, Puerto Rico, March 7, 1992.

"Energy Disposal in the Photodissociation of Thionyl Halides".
Hongxin Wang, Xirong Chen and Brad R. Weiner
27th Junior Technical Meeting, American Chemical Society, Puerto Rico Section, Gurabo, Puerto Rico, March 7, 1992.

"A Method to Approximate Kinetic Energy of the SO Radical from the Photodissociation of Dimethyl Sulfoxide".
Hongxin Wang, Xirong Chen and Brad R. Weiner.
27th Junior Technical Meeting, American Chemical Society, Puerto Rico Section, Gurabo, Puerto Rico, March 7, 1992.

"Collsion-Induced Electronic Quenching and Fluorescence Lifetimes of $C_2H_3O(B^2A")$".
Katherine I. Barnhard, Min He and Brad R. Weiner
27th Junior Technical Meeting, American Chemical Society, Puerto Rico Section, Gurabo, Puerto Rico, March 7, 1992.

"Photodissociation Dynamics of Thionyl Halides".
Hongxin Wang, Xirong Chen, and Brad R. Weiner
XV Senior Technical Meeting, American Chemical Society, Puerto Rico Section, Ponce, Puerto Rico, November 15, 1991.

"Isotope Effects and Wavelength Dependence in the Rotational State Distributions of Diatomic Photofragments, SH and SD, from the Photodissociation of H_2S and D_2S".
Xiaotian Gu, Luis A. Muñoz, Yasuyuki Ishikawa and Brad R. Weiner
XV Senior Technical Meeting, American Chemical Society, Puerto Rico Section, Ponce, Puerto Rico, November 15, 1991.

"Probing the Photodissociation Dynamics of Small Polyatomic Molecules by Laser Induced Fluorescence".
Brad R. Weiner, Xirong Chen, Hongxin Wang, and Federico Asmar
XV Senior Technical Meeting, American Chemical Society, Puerto Rico Section, Ponce, Puerto Rico, November 15, 1991.

"Nascent Rotational Distributions of $SO(X^3\Sigma^-)$ from the 193 nm Photodissociation of Dimethyl Sulfoxide."
Brenda Reyes, Xirong Chen, Federico Asmar and Brad R. Weiner
26th Junior Technical Meeting, American Chemical Society, Puerto Rico Section, Cayey, Puerto Rico, March 16, 1991.

"Pressure and Temperature Dependence of the $C_2H_3O + NO_2$ Reaction."
Katherine I. Barnhard, Alejandro Santiago, Min He, Federico Asmar, and Brad R. Weiner
26th Junior Technical Meeting, American Chemical Society, Puerto Rico Section, Cayey, Puerto Rico, March 16, 1991.

"The SO Spectrum from Photodissociated SO_2."
Xiaotian Gu, Xirong Chen and Brad R. Weiner
26th Junior Technical Meeting, American Chemical Society, Puerto Rico Section, Cayey, Puerto Rico, March 16, 1991.

"Pressure and Temperature Dependence of the $C_2H_3O + NO_2$ Reaction."
Katherine I. Barnhard, Alejandro Santiago, Min He, Federico Asmar, and Brad R. Weiner
XIV Senior Technical Meeting, American Chemical Society, Puerto Rico Section, Rio Piedras, Puerto Rico, December 8, 1990.

"Nascent Rotational Distributions of CS from the 193nm Photodissociation of CS_2."
Xirong Chen, Melvin H. Rodriguez and Brad R. Weiner
XIV Senior Technical Meeting, American Chemical Society, Puerto Rico Section, Rio Piedras, Puerto Rico, December 8, 1990.

"Kinematic Distribution Function to Calculate Rotational Populations of Photofragments from Polyatomic Photodissociation."
Luis A. Muñoz, Y. Ishikawa, and Brad R. Weiner
XIV Senior Technical Meeting, American Chemical Society, Puerto Rico Section, Rio Piedras, Puerto Rico, December 8, 1990.

"Gas Phase Molecular Reaction Dynamics."
Brad R. Weiner
Joint Annual Conference of Puerto Rico EPSCoR and the American Association for the Advancement of Science, Caribbean Division, Mayaguez, Puerto Rico, September 29, 1990.

"Probing Chemical Reactions with Lasers."
Brad R. Weiner
Department of Chemistry, University of Puerto Rico, Mayaguez, PR, March 19, 1990.

"Photodissociation of Dimethyl Sulfoxide at 193 nm in the Gas Phase."
Luis A. Muñoz, Federico Asmar and Brad R. Weiner
25th Junior Technical Meeting, American Chemical Society, Puerto Rico Section, San German, Puerto Rico, March 17, 1990.

"Laser Induced Fluorescence of DMSO in the Gas Phase."
Maria Elena Nadal, Federico Asmar and Brad R. Weiner
25th Junior Technical Meeting, American Chemical Society, Puerto Rico Section, San German, Puerto Rico, March 17, 1990.

"Photodissociation of Dimethyl Sulfoxide at 193 nm in the Gas Phase."
Luis A. Muñoz, Federico Asmar and Brad R. Weiner
XIII Senior Technical Meeting, American Chemical Society, Puerto Rico Section, Humacao, Puerto Rico, December 2, 1989.

"Photodissociation Dynamics of Small Polyatomic Molecules."
Brad R. Weiner
Department of Chemistry, Catholic University of Puerto Rico, Ponce, Puerto Rico, October 9, 1989.

VI. INTERACTIONS

Collaboration with Drs. H.H. Nelson and M. Hawley at the Chemistry Division, Naval Research Laboratory, Washington, D.C.

VII. SUMMARY

The majority of the objectives inteneded for this contract have been reached. The research effort at the University of Puerto Rico under this contract has produced significant results on the photodissociation dynamics of polyatomic molecules. A series of studies involving SO-containing polyatomic molecules has revealed interesting dynamical effects in the photo-induced production of sulfur monoxide. Several of these molecules warrant further study as model systems for three-body dissociations. A new model has been developed to calculate nascent rotational state distributions from the photodissociation of triatomic molecules. This model is now being applied to complicated systems that are not tractable by other methods.

This contract has gone a long way towards establishing a strong viable research program in gas phase photochemistry at the University of Puerto Rico. The initiation of mainstream physical chemistry research in a minority institution, such as the University of Puerto Rico, provides a unique opportunity to increase underrepresented groups in this area of science. This resource has also led to an improvement in the educational environment for students, both graduate and undergraduate. This is primarily evidenced by students who have passed through this laboratory going on to work in mainstream laboratories i.e. University of California, University of Colorado, for either their graduate or postdoctoral studies.

APPENDICES

AIR FORCE OFFICE OF SCIENTIFIC RESEARCH

FINAL REPORT

for

Contract Number F49620-89-C-0070

PHOTODISSOCIATION STUDIES OF POLYATOMIC FREE RADICALS

Principal Investigator: Brad R. Weiner

Department of Chemistry
University of Puerto Rico
Río Piedras, PR 00931

November 30, 1992

ABSTRACT

An experimental program in gas phase polyatomic photochemistry and photophysics has been established in the Department of Chemistry at the University of Puerto Rico. Real time dynamics of sulfur monoxide photoelimination reactions have been studied by laser induced fluorescence spectroscopy of the nascent SO fragment on the $B^3\Sigma^-$-$X^3\Sigma^-$ transition in the region of 237-295 nm. The group of molecules currently under investigation are Sulfur dioxide {SO_2}, dimethyl sulfoxide {$(CH_3)_2SO$}, and the thionyl halides {SOX_2; where X=F,Cl or Br}. In all of these experiments, the parent molecule is irradiated with an excimer laser (either 193 or 248 nm) and the energy disposal into the nascent SO photofragment is determined, and used as a mechanistic probe. The experiments indicate that the several of these parent molecules undergo three body dissociations. A second set of experiments measures kinetic decay constants of the C_2H_3O, both in the ground state and in the excited state. The temperature (295-374K) and pressure (2.5-100 torr) dependences for the rate constant of the C_2H_3O + NO_2 reaction have been measured by laser flash photolysis/laser induced fluorescence kinetic spectroscopy. The temperature dependent reaction for the decay of C_2H_3O in the presence of NO_2 is characterized over the measured region by the rate expression, $k_{II}=(1.48\pm0.70)\times10^{-11}\exp(80.7\pm23.4K/T)cm^3molecule^{-1}s^{-1}$. Fluorescence decay rates were determined in the presence to ten collision partners: He, Ar, N_2, O_2, CO, H_2, HCl, CO_2, C_2H_4, and $CH_3OCH=CH_2$. The measured electronic quenching cross-sections vary from 0.01 - 66.5 $Å^2$. A vibrational level dependence was found for the radiative lifetimes. Finally, a general procedure to evaluate the rotational state population distributions of the nascent photofragments from the photodissociation of polyatomic molecules has been implemented with the use of a kinematic distribution function. Numerical evaluations of rotational state population distributions of diatomic photofragments from photodissociation of the general class of triatomic molecules are presented. The calculated rotational state population distributions are compared with the most recent experimental data on OH and SH photofragments to obtain the information on the kinematic aspects of the photodissociating H_2O and H_2S molecules.

I. OBJECTIVES OF THE RESEARCH EFFORT

The objectives of this research effort were:

(1) The development of an experimental program in gas phase photochemistry and unimolecular dissociation dynamics of polyatomic molecules.

(2) To provide a more detailed understanding of the unimolecular dissociation dynamics of free radicals of practical interest.

(3) To extend the established methods of photodissociation dynamics for closed shell species to open-shell species, *i.e.* polyatomic free radicals.

(4) Initiate a research program in mainstream physical chemistry at a minority institution, and provide a strong educational environment for students, both graduate and undergraduate.

II. ACCOMPLISHMENTS OF THE RESEARCH EFFORT

This research effort was initiated June 1, 1989, and we believe that the project reached or at least made significant advances towards the stated goals. We reported at the end of the first year that major equipment had been designed and constructed, the senior personnel had been contracted, and the junior personnel were in the process of being trained. By the end of the second year, we reported that the experimental program was underway and beginning to show signs of productivity. Now at the end of 3.4 years (the term of the contract), we report on the extent of the accomplishments, and how well these results met the stated objectives

In developing our program in gas phase photochemical dynamics of polyatomic molecules, we have done (and continue to do) a body of experimental studies on sulfur monoxide (SO) photoelimination reactions. In our second year report, we noted that preliminary work in this had been accepted for publication in the *Journal of Physical Chemistry*, but that because of the interesting dynamical aspects of the observed reactions, further study was warranted. At this point in time, this work is still not complete, but major advances have been made and experimental studies are continuing. The group of molecules currently under investigation are

Sulfur dioxide {SO_2}, dimethyl sulfoxide {$(CH_3)_2SO$}, and the thionyl halides {SOX_2; where X=F,Cl or Br}. In all of these experiments, the parent molecule is irradiated with an excimer laser (either 193 or 248 nm) and the energy disposal into the nascent SO photofragment is determined, and used as a mechanistic probe. What follows is a brief description of the results found for each of these molecular systems.

SO_2

Due to the large number of studies on the 193 nm photodissociation of sulfur dioxide, we used this system primarily as a test of our laser induced fluorescence (LIF) technique. Our work, however, led us to some interesting discoveries and discrepancies with past work on the 193 nm photodissociation of SO_2. We therefore embarked on a reinvestigation of the photodissociation dynamics of SO_2. We have measured the nascent vibrational, rotational, and spin-state distributions of the $SO(X^3\Sigma)$ fragment in both a bulb and in a pulsed supersonic nozzle. Our vibrational distribution was consistent with past measurements (not by LIF), giving us confidence in our experimental methods. We do find differences in the rotational state distributions obtained in the bulb vs. free jet experiments, which is surprising for the predissociative nature of sulfur dioxide. We have also discovered an interesting spin polarization effect in the nascent SO photofragment, that varies with vibrational level, and appears to have a strong J dependence. We are currently in the process of modelling these effects, as well as looking at the photodissociation at longer wavelengths. These more detailed results on the photodissociation of SO_2 are being prepared for publication in the *Journal of Chemical Physics*.

Cl_2SO

Due to our extremely sensitive and quantum specific capabilities for the detection of $SO(X^3\Sigma)$, we have also begun to study the photodissociation dynamics of thionyl halides, The photodissociation of thionyl chloride (Cl_2SO) is of interest as a model system to study three-body fragmentation processes, which can occur either in concert or stepwise. The photodissociation of this tetratomic molecule at 193 and 248 nm has been studied by laser induced fluorescence spectroscopy of the nascent SO fragment on the $B^3\Sigma^-$-$X^3\Sigma^-$ transition in the region of 237-295 nm. Photolysis of Cl_2SO at 193 nm leads to an inverted vibrational distribution for the nascent $SO(X^3\Sigma^-)$ with a population maximum at $v''=2$. The quantum yield, $\Phi^{193\ nm}_{SO(X)} = 0.73\pm0.10$, has

been measured by comparison of the $SO(X^3\Sigma^-)$ produced from SO_2. The results indicate a concerted three-body fragmentation mechanism as the primary dissociation channel. A Franck-Condon/golden rule model elucidates the geometry prior to the fragmentation and suggests a direct dissociation mechanism. The rotational and spin state distributions have been measured from the rovibronically resolved spectra to support our model of the detailed dissociation mechanism. At 248 nm, the nascent vibrational distribution was found to be bimodal. The vibrational state population distribution in $v"=0$-2, which accounts for most ($\sim$94%) of the nascent $SO(X^3\Sigma^-)$ population, was found to be thermal ($T_{vib}=1000\pm200K$), suggesting a stepwise fragmentation process. About 6% of the nascent SO population has been observed in other vibrational levels ($v"=3$-7), and most likely originates from the molecular elimination of Cl_2 from Cl_2SO.

These results provide important evidence of wavelength dependent photolysis channels in polyatomic molecules, and go further in characterizing them in microscopic detail. The original premise of Cl_2SO being a good model for polyatomic photodissociation dynamics studies is borne out.

F_2SO

The vibrational and rotational state distributions and the primary quantum yield of the $SO(X^3\Sigma^-)$ fragment following the laser photolysis of F_2SO at 193 nm have been measured by using laser induced fluorescence spectroscopy on the $SO(B^3\Sigma^- - X^3\Sigma^-)$ transition. Molecular elimination of F_2 is the only energetically-allowed channel to produce the SO fragment. The quantum yield measurement, $\Phi_{SO(X)}^{193\ nm} = 0.06 \pm 0.01$, suggests that other photochemical channels, *i.e.*, FSO + F, must be operative as well. The vibrational distribution of the nascent SO(X) fragment has been found to be inverted with a population maximum at $v" = 2$, indicating a rapid dissociation process, and suggests that the nascent F_2 fragment is born with significant vibrational excitation. A Franck-Condon model best fits the observed vibrational state distribution when the SO bond length is similar to that of the ground state F_2SO.

Br_2SO

Photodissociation of Br_2SO following irradiation at 193 and 248 nm has been studied by laser induced fluorescence spectroscopy of the nascent SO fragment. The vibrational

distributions for the nascent SO have been found to be inverted, suggesting a concerted mechanism for the dissociation at both wavelengths. A Franck Condon / Golden Rule model elucidates the geometry prior to the dissociation, suggesting the possibility that photodissociation at both wavelengths occurs via the same excited state of Br_2SO. The rotational and spin state distributions have been measured from rovibronically resolved spectra to support our discussion on the detailed dissociation mechanism. Quantum yield measurements suggest that other electronic states of the SO radical may be directly produced.

$(CH_3)_2SO$

The photodissociation dynamics of the reaction, $(CH_3)_2SO + h\nu(193\ nm) \rightarrow 2CH_3 + SO$, have been examined by laser spectroscopic techniques. Relative vibrational and rotational state energy distributions of the nascent SO photofragment have been determined by using laser induced fluorescence spectroscopy on the ($B^3\Sigma^- - X^3\Sigma^-$) transition. The same technique has also been employed to establish the quantum yield, $\Phi_{193}[SO(X^3\Sigma)] = 1.02 \pm 0.12$. The nascent vibrational state distributions in the ν_1 and ν_2 modes of the methyl radical have been determined by using 2+1 resonance enhanced multiphoton ionization spectroscopy via the ($3p\ ^2A_2'' \leftarrow 2p\ ^2A_2''$) transition. These measurements were done in collaboration with M. Hawley and H.H. Nelson at the Naval Research Laboratory.

The energy distributions of the nascent fragments are best described by a concerted three-body fragmentation. While some of our data are suggestive of a concerted synchronous dissociation of the two S-C bonds in DMSO,[2] we cannot conclusively determine the synchronicity from our results. Further studies of the photofragment angular distributions following 193 nm irradiation of dimethyl sulfoxide would be helpful in analyzing this aspect of the dissociation dynamics.

Even though the experiments involving $SO(X^3\Sigma)$ remain a tangent from our original proposed research, we believe that these studies are extremely valuable to the Air Force because of the atmospheric importance of these species. Along a similar line, we have studied the reaction dynamics of the vinoxy (C_2H_3O) radical. The primary motivation for this study was that it was a species of interest, and that it provided a nice vehicle for training new graduate

students to use the experimental apparatus. Some of this work has been published in *Chemical Physics Letters.*

C_2H_3O

The temperature (295-374K) and pressure (2.5-100 torr) dependences for the rate constant of the C_2H_3O + NO_2 reaction have been measured by laser flash photolysis/laser induced fluorescence kinetic spectroscopy. The temperature dependent reaction for the decay of C_2H_3O in the presence of NO_2 is characterized over the measured region by the rate expression, $k_{II}=(1.48\pm0.70)x10^{-11}exp(80.7\pm23.4K/T)cm^3molecule^{-1}s^{-1}$. This rate expression is found to be independent of pressure. The results can be explained by a reaction mechanism involving the formation of an energized adduct which subsequently decomposes to products, most likely ketene and nitrous acid.

The fast reaction of vinoxy radical + NO_2 has been found to have: 1) No appreciable barrier to reaction; and 2) No apparent pressure dependence over the range of 2.5-100 torr. Our measurements lead us to conclude that the molecule proceeds through an energized collision complex to give C_2H_2O and HONO. While the final products are the same as other alkoxy-NO_2 reactions, the mechanism appears to differ. In order to tell this for sure, more detailed experiments remain to be done. For example, a quantitative analysis, including branching ratios, of the final products of this reaction needs to be characterized. The reaction has important consequences with respect to atmospheric chemistry. Due to the fast rate of this reaction at almost all conditions, we believe that this rate should be considered by kinetic modellers.

State specific radiative lifetimes and electronic quenching cross-sections have been determined for three different vibrational modes of C_2H_3O ($\tilde{B}^2A''$). These experiments were carried out using a two-laser method with laser-induced fluorescence as the detection technique. Ground state vinoxy radicals were produced by 193nm excimer laser photolysis of $CH_3OCH=CH_2$, and were pumped to the B state by a tunable dye laser. Fluorescence decay rates were determined in the presence to ten collision partners: He, Ar, N_2, O_2, CO. H_2, HCl, CO_2, C_2H_4, and $CH_3OCH=CH_2$. The measured electronic quenching cross-sections vary from 0.01 - 66.5 $Å^2$. A vibrational level dependence was found for the radiative lifetimes, which is believed to be due to predissociation. We are now investigating the photodissociation of the vinoxy radical at 308 nm.

Another area that we have been developing is a theoretical treatment of the nascent rotational state population distributions arising from photodissociation reactions. We have developed a kinematic distribution function to accurately reproduce the nascent rotational distributions of OH and SH following the photodissociations of H_2O and H_2S, respectively. This work was published in the *International Journal of Quantum Chemistry*. A second paper on isotope effects in photodissociation dynamics was recently accepted for publication in *Chemical Physics Letters*.

In these works, a general procedure to evaluate the rotational state population distributions of the nascent photofragments from the photodissociation of polyatomic molecules has been implemented with the use of the kinematic distribution function developed by Chen and Pei.[1] Numerical evaluations of rotational state population distributions of diatomic photofragments from photodissociation of the general class of triatomic molecules are presented. The calculated rotational state population distributions are compared with the most recent experimental data on OH and SH photofragments to obtain the information on the kinematic aspects of the photodissociating H_2O and H_2S molecules.

We employ a semi-empirical model that utilizes a kinematic distribution function to calculate the rotational state population distributions of diatomic photofragments from the photodissociation of isotopically variant triatomic molecules. The numerically evaluated rotational distributions of the photofragments, SH and SD, are compared with experimental data on the nascent rotational state population distributions of the diatomic photofragments resulting from the laser photolysis of H_2S ($\lambda_{photolysis}$=193, 222 and 248 nm) and D_2S ($\lambda_{photolysis}$=193 and 222 nm).

In conclusion, the results clearly show that the kinematic distribution function, when used in conjunction with the experimental rotational state population distribution, can provide information about the degree of participation of different adiabatic surfaces in the presence of non-adiabatic coupling among them during a photochemical reaction. Even for the case of hydrogen sulfide photodissociation, where >98% of the available energy is partitioned into translational degrees of freedom, sensitive measurements of the internal energy distribution of the diatomic fragment provide a unique insight into the mechanisms of dissociation. This

---

[1] K. Chen and C. Pei, *Chem. Phys. Lett.* **124**, 365 (1986)

information not only helps unravel a detailed dissociative mechanism, but also gives information about the degree of non-adiabatic coupling between the two surfaces. Finally, the kinematic distribution model provides insight into the wavelength dependent photodissociation of H_2S, but we wish to ***stress*** that the true power of the model lies in systems of greater complexity where *ab initio* potentials are not available. For example, we are currently implementing the model to study the nascent rotational distributions of sulfur monoxide deriving from the 193 nm photodissociation of SO_2.

III. PUBLICATIONS

Xirong Chen, Hongxin Wang, Federico Asmar, Melvin H. Rodriguez, and Brad R. Weiner, "Rotational Distributions of $SO(X^3\Sigma)$ from the 193 nm Photodissociation of SO_2." *Manuscript in preparation*

Katherine I. Barnhard, Min He and Brad R. Weiner, "Fluorescence Lifetimes of $C_2H_3O(B^2A')$: Evidence for Predissociation." J. Phys. Chem. *To be submitted.*

Hongxin Wang, Xirong Chen, and Brad R. Weiner, "$SO(X^3\Sigma)$ Production from the 193 nm Laser Photolysis of Thionyl Fluoride." Chem. Phys. Lett. *To be submitted.*

Hongxin Wang, Xirong Chen, and Brad R. Weiner, "Laser Photodissociation Dynamics of Thionyl Chloride: Concerted and Stepwise Cleavage of S-Cl Bonds", J. Phys. Chem. *in press.*

Xirong Chen, Hongxin Wang, Brad R. Weiner, Michael Hawley and H.H. Nelson, "Photodissociation of Dimethyl Sulfoxide at 193 nm in the Gas Phase." J. Phys. Chem. *in press* .

Xiaotian Gu, Luis A. Muñoz, Yasuyuki Ishikawa, and Brad R. Weiner, "Isotope Effects and Wavelength Dependence in the Rotational State Distributions of the Diatomic Photofragments, SH and SD, from the Photodissociation of H_2S and D_2S", Chemical Physics Letters, *in press.*

Xirong Chen, Federico Asmar, Hongxin Wang and Brad R. Weiner, "Nascent $SO(X^3\Sigma^-)$ Vibrational Distributions from the Photodissociation of SO_2, $SOCl_2$ and $(CH_3)_2SO$ at 193 nm." J. Phys. Chem. *95*, **1991**, 6415.

Luis A. Muñoz, Y. Ishikawa and Brad R. Weiner, "Kinematic Distribution Function to Calculate Rotational Populations of Photofragments from Photodissociation of Triatomic Molecules." Int. J. Quant. Chem., *S25*, **1991**, 359.

Katherine I. Barnhard, Alejandro Santiago, Min He, Federico Asmar, Brad R. Weiner, "Pressure and Temperature Dependence of the $C_2H_3O + NO_2$ Reaction." Chemical Physics Letters *178*, **1991**, 150.

IV. PERSONNEL

The following people have participated in this project in addition to the principal investigator.

Senior Personnel

Professor Xirong Chen from the Dalian Institute of Chemical Physics, Dalian, P.R. China, joined our research group in February, 1990.

Junior Personnel

Graduate Students

Federico Asmar (Department of Chemistry)
Katherine I. Barnhard (Department of Chemistry)
Hongxin Wang (Chemical Physics Program)

Undergraduate Students

Luis A. Muñoz (Department of Physics)
Maria E. Nadal (Department of Chemistry)
Miriam Perez (Department of Chemistry)

V. PRESENTATIONS

International

"Dynamics of Sulfur Monoxide Photoelimination Reactions"
Brad R. Weiner
Air Force Office of Scientific Research (AFOSR) Molecular Dynamics Contractor's Meeting, Washington, D.C., 25-27 October 1992.

"The Nascent Vibrational Distribution of SO from the 193 nm Photodissociation of Thionylaniline"
K. Matos, X. Chen and Brad R. Weiner
National Institute of Health MARC-MBRS Symposium, Dorado, Puerto Rico, 21-24 October 1992.

"Photodissociation Dynamics of SO-Containing Molecules"(invited)
Brad R. Weiner
Department of Chemistry, University of Idaho, Moscow, Idaho, 13 October 1992.

"Photodissociation Studies of Sulfur Oxides"
Brad R. Weiner, Hongxin Wang and Xirong Chen
Gordon Research Conference on Atomic and Molecular Interactions, New London, New Hampshire, 20-24 July 1992.

"Fluorescence Lifetimes of the Vinoxy Radical: Evidence for Predissociation".
Katherine I. Barnhard, Min He and Brad R. Weiner
XXth Informal Conference on Photochemistry, Atlanta, Georgia, April 26-May 1, 1992.

"Internal Energy Disposal into the SO Radical Following Photodissociation of $SOCl_2$ and $SOBr_2$".
Hongxin Wang, Xirong Chen and Brad R. Weiner.
203rd National Meeting of the American Chemical Society, San Francisco, California, April 5-10, 1992.

"Vibrational Energy Transfer Studies of Sulfur Monoxide".
Xiaotian Gu, Xirong Chen and Brad R. Weiner
203rd National Meeting of the American Chemical Society, San Francisco, California, April 5-10, 1992.

"Collision-Induced Electronic Quenching of the Vinoxy Radical".
Min He, Katherine I. Barnhard and Brad R. Weiner
203rd National Meeting of the American Chemical Society, San Francisco, California, April 5-10, 1992.

"Internal Energy Distributions of SO from the 193 nm Photodissociation of SO_2 and Dimethyl Sulfoxide (DMSO)."
Federico Asmar, Xirong Chen, Hongxin Wang, and Brad R. Weiner
Second Pan American Chemical Congress, San Juan, Puerto Rico, September 24-29, 1991.

"Gas Phase Reactions of the Vinoxy (C_2H_3O) Radical".
Katherine I. Barnhard, Alejandro Santiago, He Min, and Brad R. Weiner
Second Pan American Chemical Congress, San Juan, Puerto Rico, September 24-29, 1991.

"Internal Energy Distributions of $SO(X^3\Sigma^-)$ from the 193 nm Photodissociation of $SOCl_2$".
Xirong Chen, Hongxin Wang and Brad R. Weiner
202nd National Meeting of the American Chemical Society, New York, NY, August 25-30, 1991.

"Nascent SO($X^3\Sigma^-$) Vibrational Distributions from the Photodissociation of SO_2, $SOCl_2$ and $(CH_3)_2SO$ at 193 nm."
Xirong Chen, Hongxin Wang, Federico Asmar, and Brad R. Weiner
Twenty-First International Conference on Free Radicals, Williamstown, Ma., August 4-9, 1991.

"Nascent Rotational Distributions of SO($X^3\Sigma^-$) from the 193 nm Photodissociation of SO_2 and Dimethyl Sulfoxide (DMSO)."
Xirong Chen, Federico Asmar, Melvin H. Rodríguez and Brad R. Weiner
201th National Meeting of the American Chemical Society, Atlanta, Ga. April 16, 1991.

"Kinematic Distribution Function to Calculate Rotational Populations of Photofragments from Photodissociation of Triatomic Molecules."
Luis A. Muñoz, Yasuyuki Ishikawa and Brad R. Weiner
Sanibel Symposium on Quantum Chemistry, St. Augustine, Florida, March 11, 1991.

"Fotoquimica y Fotofisica de Dimetilsufoxido (DMSO) a 193nm en Fase Gaseosa."
Federico Asmar, Luis Muñoz, María E. Nadal and Brad R. Weiner
XIX Congreso Latinoamericano de Quimica, Bueños Aires, Argentina, November 1990.

"Probing Chemical Reactions with Lasers." (invited)
Brad R. Weiner
Department of Chemistry, Grinnell College, Grinnell, Iowa, September 19, 1990.

"Photochemistry and Photophysics of Dimethyl Sulfoxide at 193 nm in the Gas Phase."
Federico Asmar, Luis Muñoz, Maria E. Nadal, Xirong Chen and Brad R. Weiner
American Physical Society-Inderdisciplinary Laser Science VI (ILS-VI), Minneapolis, Minnesota, September 18, 1990.

"Gas Phase Reactions of the Vinoxy Radical."
Brad R. Weiner, Katherine I. Barnhard, and Alejandro Santiago
200th National Meeting of the American Chemical Society, Washington, D.C., August 30, 1990.

"Laser Spectroscopic Probing of Chemical Reactions."
Federico Asmar and Brad R. Weiner
Instrument Society of America-Symposium for Innovation in Measurement Science (Student Award Presentation), Geneva, New York, August 9, 1990.

"Photodissociation of Dimethyl Sulfoxide at 193 nm in the Gas Phase."
Luis A. Muñoz, Federico Asmar and Brad R. Weiner
XIX Informal Conference on Photochemistry, Ann Arbor, Michigan, June 22, 1990.

"Photodissociation of Dimethyl Sulfoxide at 193 nm in the Gas Phase."
Federico Asmar, Luis A. Muñoz, Maria E. Nadal, Xirong Chen and Brad R. Weiner,
XIX Informal Conference on Photochemistry, Ann Arbor, Michigan, June 26, 1990.

"Photodissociation Dynamics of Borane Carbonyl at 193 nm."
Brad R. Weiner, L. Pasternack and H.H. Nelson, 1989 Conference of the Dynamics of Molecular Collisions, Asilomar, CA July 16-21, 1989.

Regional

"The Photochemistry of Thionylaniline"
K. Matos, X. Chen and Brad R. Weiner
16th Annual ACS Senior Technical Meeting, Mayagüez, Puerto Rico, 6-7 November 1992.

"Photodissociation Dynamics Studies of Sulfur Oxides"
H. Wang, X. Chen and Brad R. Weiner
16th Annual ACS Senior Technical Meeting, Mayagüez, Puerto Rico, 6-7 November 1992.

"Pulsed Laser Photolysis - Laser Induced Fluorescence Measurements on the Vibrational Relazation of the SO Radical."
Xiaotian Gu, Xirong Chen and Brad R. Weiner
27th Junior Technical Meeting, American Chemical Society, Puerto Rico Section, Gurabo, Puerto Rico, March 7, 1992.

"Energy Disposal in the Photodissociation of Thionyl Halides".
Hongxin Wang, Xirong Chen and Brad R. Weiner
27th Junior Technical Meeting, American Chemical Society, Puerto Rico Section, Gurabo, Puerto Rico, March 7, 1992.

"A Method to Approximate Kinetic Energy of the SO Radical from the Photodissociation of Dimethyl Sulfoxide".
Hongxin Wang, Xirong Chen and Brad R. Weiner.
27th Junior Technical Meeting, American Chemical Society, Puerto Rico Section, Gurabo, Puerto Rico, March 7, 1992.

"Collsion-Induced Electronic Quenching and Fluorescence Lifetimes of $C_2H_3O(B^2A")$".
Katherine I. Barnhard, Min He and Brad R. Weiner
27th Junior Technical Meeting, American Chemical Society, Puerto Rico Section, Gurabo, Puerto Rico, March 7, 1992.

"Photodissociation Dynamics of Thionyl Halides".
Hongxin Wang, Xirong Chen, and Brad R. Weiner
XV Senior Technical Meeting, American Chemical Society, Puerto Rico Section, Ponce, Puerto Rico, November 15, 1991.

"Isotope Effects and Wavelength Dependence in the Rotational State Distributions of Diatomic Photofragments, SH and SD, from the Photodissociation of H_2S and D_2S".
Xiaotian Gu, Luis A. Muñoz, Yasuyuki Ishikawa and Brad R. Weiner
XV Senior Technical Meeting, American Chemical Society, Puerto Rico Section, Ponce, Puerto Rico, November 15, 1991.

"Probing the Photodissociation Dynamics of Small Polyatomic Molecules by Laser Induced Fluorescence".
Brad R. Weiner, Xirong Chen, Hongxin Wang, and Federico Asmar
XV Senior Technical Meeting, American Chemical Society, Puerto Rico Section, Ponce, Puerto Rico, November 15, 1991.

"Nascent Rotational Distributions of $SO(X^3\Sigma^-)$ from the 193 nm Photodissociation of Dimethyl Sulfoxide."
Brenda Reyes, Xirong Chen, Federico Asmar and Brad R. Weiner
26th Junior Technical Meeting, American Chemical Society, Puerto Rico Section, Cayey, Puerto Rico, March 16, 1991.

"Pressure and Temperature Dependence of the $C_2H_3O + NO_2$ Reaction."
Katherine I. Barnhard, Alejandro Santiago, Min He, Federico Asmar, and Brad R. Weiner
26th Junior Technical Meeting, American Chemical Society, Puerto Rico Section, Cayey, Puerto Rico, March 16, 1991.

"The SO Spectrum from Photodissociated SO_2."
Xiaotian Gu, Xirong Chen and Brad R. Weiner
26th Junior Technical Meeting, American Chemical Society, Puerto Rico Section, Cayey, Puerto Rico, March 16, 1991.

"Pressure and Temperature Dependence of the $C_2H_3O + NO_2$ Reaction."
Katherine I. Barnhard, Alejandro Santiago, Min He, Federico Asmar, and Brad R. Weiner
XIV Senior Technical Meeting, American Chemical Society, Puerto Rico Section, Rio Piedras, Puerto Rico, December 8, 1990.

"Nascent Rotational Distributions of CS from the 193nm Photodissociation of CS_2."
Xirong Chen, Melvin H. Rodriguez and Brad R. Weiner
XIV Senior Technical Meeting, American Chemical Society, Puerto Rico Section, Rio Piedras, Puerto Rico, December 8, 1990.

"Kinematic Distribution Function to Calculate Rotational Populations of Photofragments from Polyatomic Photodissociation."
Luis A. Muñoz, Y. Ishikawa, and Brad R. Weiner
XIV Senior Technical Meeting, American Chemical Society, Puerto Rico Section, Rio Piedras, Puerto Rico, December 8, 1990.

"Gas Phase Molecular Reaction Dynamics."
Brad R. Weiner
Joint Annual Conference of Puerto Rico EPSCoR and the American Association for the Advancement of Science, Caribbean Division, Mayaguez, Puerto Rico, September 29, 1990.

"Probing Chemical Reactions with Lasers."
Brad R. Weiner
Department of Chemistry, University of Puerto Rico, Mayaguez, PR, March 19, 1990.

"Photodissociation of Dimethyl Sulfoxide at 193 nm in the Gas Phase."
Luis A. Muñoz, Federico Asmar and Brad R. Weiner
25th Junior Technical Meeting, American Chemical Society, Puerto Rico Section, San German, Puerto Rico, March 17, 1990.

"Laser Induced Fluorescence of DMSO in the Gas Phase."
Maria Elena Nadal, Federico Asmar and Brad R. Weiner
25th Junior Technical Meeting, American Chemical Society, Puerto Rico Section, San German, Puerto Rico, March 17, 1990.

"Photodissociation of Dimethyl Sulfoxide at 193 nm in the Gas Phase."
Luis A. Muñoz, Federico Asmar and Brad R. Weiner
XIII Senior Technical Meeting, American Chemical Society, Puerto Rico Section, Humacao, Puerto Rico, December 2, 1989.

"Photodissociation Dynamics of Small Polyatomic Molecules."
Brad R. Weiner
Department of Chemistry, Catholic University of Puerto Rico, Ponce, Puerto Rico, October 9, 1989.

VI. INTERACTIONS

Collaboration with Drs. H.H. Nelson and M. Hawley at the Chemistry Division, Naval Research Laboratory, Washington, D.C.

VII. SUMMARY

The majority of the objectives inteneded for this contract have been reached. The research effort at the University of Puerto Rico under this contract has produced significant results on the photodissociation dynamics of polyatomic molecules. A series of studies involving SO-containing polyatomic molecules has revealed interesting dynamical effects in the photo-induced production of sulfur monoxide. Several of these molecules warrant further study as model systems for three-body dissociations. A new model has been developed to calculate nascent rotational state distributions from the photodissociation of triatomic molecules. This model is now being applied to complicated systems that are not tractable by other methods.

This contract has gone a long way towards establishing a strong viable research program in gas phase photochemistry at the University of Puerto Rico. The initiation of mainstream physical chemistry research in a minority institution, such as the University of Puerto Rico, provides a unique opportunity to increase underrepresented groups in this area of science. This resource has also led to an improvement in the educational environment for students, both graduate and undergraduate. This is primarily evidenced by students who have passed through this laboratory going on to work in mainstream laboratories i.e. University of California, University of Colorado, for either their graduate or postdoctoral studies.

APPENDICES

Pressure and temperature dependence of the $C_2H_3O+NO_2$ reaction

Katherine I. Barnhard, Alejandro Santiago, Min He, Federico Asmar and Brad R. Weiner [1]
Department of Chemistry, University of Puerto Rico, Rio Piedras, PR 00931, USA

Received 17 December 1990

The temperature (295–374 K) and pressure (2.5–100 Torr) dependences for the rate constant of the $C_2H_3O+NO_2$ reaction have been measured by laser flash photolysis/laser-induced fluorescence kinetic spectroscopy. The temperature-dependent reaction for the decay of C_2H_3O in the presence of NO_2 is characterized over the measured region by the rate expression $k_{II} = (1.48\pm0.70)\times10^{-11}\exp(80.7\pm23.4\ K/T)$ cm^3 molecule^{-1} s^{-1}. This rate expression is found to be independent of pressure. The results can be explained by a reaction mechanism involving the formation of an energized adduct which subsequently decomposes to products, most likely ketene and nitrous acid.

1. Introduction

Alkoxy radicals (RO) are important chemical intermediates in both combustion [1] and atmospheric [2] systems. The radicals can arise from a variety of hydrocarbon oxidation reactions, and can also be formed in various near-UV photolyses and photosensitized decompositions of ethers [3]. While a base of indirect kinetic data has been reported for chemical reactions of the simpler alkoxy radicals (e.g. methoxy, ethoxy) [4], no such information exists for the vinoxy radical. The vinoxy radical, C_2H_3O, is readily formed in the following oxidations of unsaturated hydrocarbons:

$$O(^3P)+C_2H_4\rightarrow C_2H_3O+\text{products [5]}, \quad (1)$$

$$OH+C_2H_2\rightarrow C_2H_3O+\text{products [6]}, \quad (2)$$

$$OH+C_2H_4O\rightarrow C_2H_3O+\text{products [7]}. \quad (3)$$

While alkoxy radicals have been shown to react slowly with trace atmospheric gases, such as hydrocarbons [8], they undergo fast reactions with NO_2. Direct kinetic measurements of $RO+NO_2$ ($R=CH_3$, C_2H_5, and i-C_3H_7) have been reported as a function of temperature and pressure [9]. In these studies, the association reaction to form $RONO_2$ is believed to be the predominate pathway, but atom-transfer channels could not be ruled out. The reaction dynamics of the vinoxy radical provides an interesting case for study. Although technically an alkoxy radical, vinoxy more closely resembles an alkyl radical (formyl methyl), with the unpaired electron localized on the terminal carbon rather than on the oxygen atom of the molecule. Previous direct kinetic studies of the vinoxy radical with O_2 and NO have found pressure-dependent reactions with small, i.e. negligible, activation barriers [10]. In both cases, the primary product of the reaction was predicted to be a collisionally stabilized adduct with radical molecule addition occurring at the terminal carbon.

We report here a direct measurement of the temperature and pressure dependence of the gas-phase kinetics of the $C_2H_3O+NO_2$ reaction using a two-laser, pump–probe technique, laser flash photolysis/laser-induced fluorescence kinetic spectroscopy. In brief, the vinoxy radicals are produced by excimer-laser photolysis of methyl vinyl ether (MVE) at 193 nm, and are detected by laser-induced fluorescence (LIF) on the B–$\tilde{X}$ transition near 337 nm [11]. Bimolecular rate constants are obtained by monitoring the vinoxy radical disappearance as a function of NO_2 concentration in real time under pseudo-first-order conditions.

[1] To whom correspondence should be addressed.

0009-2614/91/$ 03.50

tems gated integrator (model SR250), and then digitized and sent to a computer (Northgate 286) for display, storage, and analysis. Temporal profiles of the vinoxy radical were recorded by scanning the delay time in between the two lasers with a digital delay pulse generator (Stanford Research Systems, model DG535). Data were typically collected at 30 Hz, and 10 laser shots were averaged for each temporal point. LIF excitation spectra were taken in a similar manner. At a fixed delay time between photolysis and probe lasers, the frequency of the dye laser was scanned while collecting the total fluorescence signal at the photomultiplier tube. The signal was processed, digitized and stored in the same manner as described above.

Experiments were conducted to measure the stable photoproducts following the 193 nm irradiation of MVE/NO_2 mixtures (1:10). These experiments were performed by placing these mixtures (total pressure = 50 Torr) in a 10 cm long infrared cell fitted with CaF_2 windows and measuring the FT-IR (Nicolet 740) spectrum prior to and after the 193 nm laser irradiation. UV irradiation times were varied from 1000–20000 laser shots.

The gases were purchased from the following suppliers and used without further purification: methyl vinyl ether (Matheson, 99%), nitrogen dioxide (Matheson, 99.5%) and N_2 (General Gases, 99.99%).

3. Results

Prior to beginning the kinetics experiments, we verified the production of the vinoxy radical following 193 nm photolysis of methyl vinyl ether by recording the LIF excitation spectra from 335–350 nm. Our result agrees with the excitation spectrum reported in ref. [11]. From this spectrum, we chose the most intense bands at 337.0 (100) and 342.1 (001) nm to use for our kinetic studies. A typical kinetic decay of the vinoxy radical in the presence of NO_2 is shown in fig. 2a. In the absence of reactant gas, the rate of disappearance of C_2H_3O is consistent with the diffusion of the radical out of the probe-laser beam. No difference was observed in the kinetic decay data measured by using other spectroscopic probe lines.

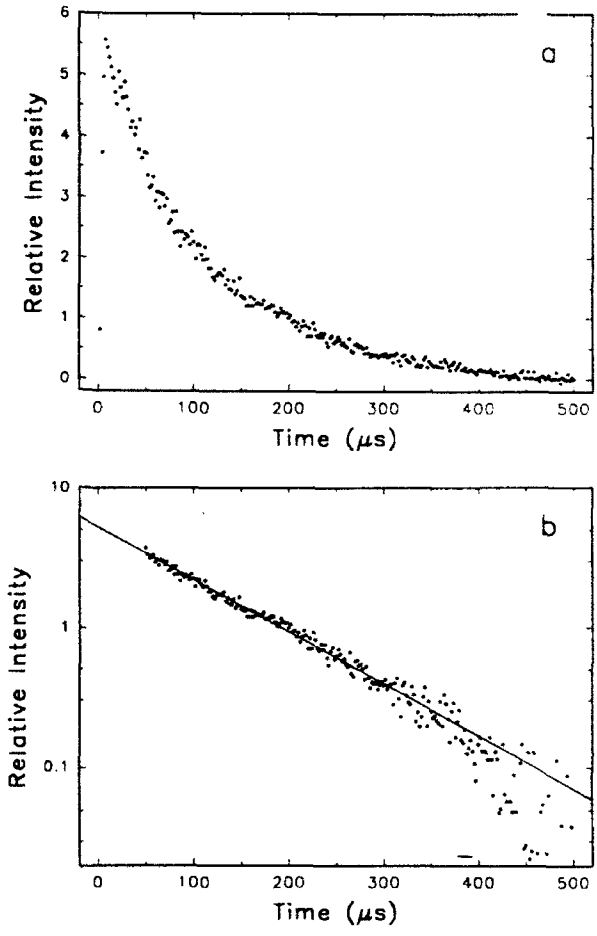

Fig. 2. (a) A typical temporal profile obtained under the following conditions: $P_{MVE} = 0.0036$, $P_{NO_2} = 0.0055$, P_{total} (balance N_2) = 10.06 Torr, and $T = 308$ K. (b) The logarithm of the relative intensity versus time of decay profile shown in (a). The line is a linear least-squares fit to the data.

In order to obtain second-order rate constants, k_{II}, for the $C_2H_3O + NO_2$ reaction, the pseudo-first-order rate constants, obtained from a linear least-squares fit to the slope of the logarithm of the decay (see fig. 2b), are plotted as a function of NO_2 pressure. Linear fits to the logarithmic decays were taken over 3–4 reaction lifetimes beginning at a delay time corresponding to at least 3000 gas kinetic collisions. This is to ensure that the vinoxy radical, which is initially prepared with significant internal energy from the UV photolysis, is allowed to reach thermal equilibrium. A typical plot of the pseudo-first-order rate

4. Discussion

Consistent with previous kinetic work on the vinoxy radical [10], two reaction pathways can be postulated,

$$C_2H_3O+NO_2 \rightarrow O_2NCH_2CHO\,, \qquad (4a)$$

$$C_2H_3O+NO_2 \rightarrow CH_2CO+HONO\,. \qquad (4b)$$

The first pathway, (4a), leads to the production of a pressure-dependent, stabilized addition product, nitroacetaldehyde ($\Delta H_{RXN4a} = -58$ kcal/mol), while the second process, (4b), corresponds to an H-atom transfer pathway ($\Delta H_{RXN4b} = -44$ kcal/mol) [#1]. Reaction (4b) can proceed either by a direct abstraction mechanism, or by formation of an energized adduct, which can subsequently rearrange and decompose. For the case of either pathway, we assume that if an adduct is formed, addition of NO_2 occurs at the carbon position, because in its ground-state configuration, vinoxy is predicted to be more like a formylmethyl ($\cdot CH_2-CH=O$) radical than an ethenyloxy ($CH_2=CH-O\cdot$) radical [13]. The slightly negative temperature dependence of this reaction is indicative of a negligible activation barrier for the reaction. The result is consistent with previous findings on the temperature-dependent reactions of vinoxy with O_2 and NO [10], and is often observed in radical–radical reactions [14]. These effects have been explained previously by having the reaction proceed through a bound complex separated from the final products by a small potential barrier. Depending on the magnitude of this potential barrier, the observed reaction rate can vary with respect to the "capture ratio" [15]. If the barrier from the bound state to the products is small enough, and the initial reactants are sufficiently energized, the reaction can be observed to have a negative temperature dependence. A similar type of mechanism, as shown in scheme 1, can be envisioned here. Nitrogen dioxide adds on the carbon-centered radical of the ground-state vinoxy molecule. The fate of this energized adduct, when it encounters the potential surface at the transition state between the reactants and the products, has at least two possible deactivation pathways (see scheme 1). These two routes are also consistent with the previously shown vinoxy radical pathways, (4a) and (4b).

The two pathways can be differentiated by measuring the effects of total pressure on the reaction. The apparent lack of a pressure dependence for the $C_2H_3O+NO_2$ reaction indicates that the formation of a stabilized nitroacetaldehyde is unlikely. This result is further substantiated by the fact that this molecule has never been isolated (to the best of our knowledge). It must be noted, however, that it is possible that for a system of this molecular size, which

[#1] Thermochemical values are either taken directly from the tables, or estimated by group additivity methods [12].

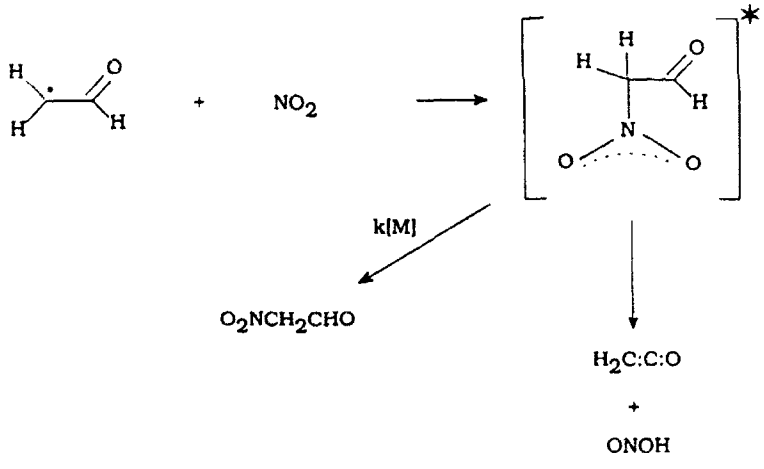

Scheme 1.

M. Yamaguchi, T. Momose and T. Shida, J. Chem. Phys. 93 (1990) 4211.
[14] R. Atkinson, D.L. Baulch, R.A. Cox, R.F. Hampson Jr., J.A. Kerr and J. Troe, J. Phys. Chem. Ref. Data 18 (1989) 881.
[15] L.F. Phillips, J. Phys. Chem. 94 (1990) 7482.
[16] W.F. Arendale and W.H. Fletcher, J. Chem. Phys. 26 (1957) 793.
[17] D.J. Nesbitt, H. Petek, M.F. Foltz, S.V. Filseth, D.J. Bamford and C.B. Moore, J. Chem. Phys. 83 (1985) 223.
[18] J.K. Crandall, S.A. Sojka and J.B. Kamin, J. Org. Chem. 39 (1974) 2172;
P. Michaud and C. Ouellet, Can. J. Chem. 49 (1971) 294, 303.

Kinematic Distribution Function to Calculate Rotational Populations of Photofragments from Photodissociation of Triatomic Molecules

LUIS A. MUÑOZ, YASUYUKI ISHIKAWA,* and BRAD R. WEINER*

Department of Chemistry and Chemical Physics Program, University of Puerto Rico, Río Piedras, Puerto Rico 00931

Abstract

A general procedure to evaluate the rotational state population distributions of the nascent photofragments from the photodissociation of polyatomic molecules has been implemented with the use of the kinematic distribution function developed by Chen and Pei [Chem. Phys. Lett. **124**, 365 (1986)]. Numerical evaluations of rotational state population distributions of diatomic photofragments from photodissociation of the general class of triatomic molecules are presented. The calculated rotational state population distributions are compared with the most recent experimental data on OH and SH photofragments to obtain the information on the kinematic aspects of the photodissociating H_2O and H_2S molecules.

Introduction

Since the pioneering work on the photodissociation of NaI by Terenin [1], there have been many important technological advances in the experimental studies on photodissociation dynamics [2]. The major advances in recent experimental studies on polyatomic photodissociation dynamics are primarily due to the development and applications of molecular beams and lasers [3]. In typical experiments, the information obtained has been on the quantum state population, velocity, and angular distributions of the products. The quantum state distributions of the nascent photofragments may be measured directly by a variety of experimental techniques, e.g., laser-induced fluorescence (LIF) spectroscopy [4], Doppler spectroscopy [5], infrared (IR) absorption spectroscopy [6], and coherent anti-Stokes Raman scattering (CARS) spectroscopy [7]. By using these techniques and others, the translational, vibrational, and rotational state populations of the nascent photofragments from polyatomic photodissociations have been reported in high accuracy for a number of molecular systems [2].

Photodissociation reactions often yield nascent products with rotational excitation [8]. The fragment rotational, vibrational, and angular distributions are affected by the constraints of angular momentum and energy conservation. Consequently, the experimentally measured rotational state population distributions of the photofrag-

* To whom correspondence should be addressed.

International Journal of Quantum Chemistry: Quantum Chemistry Symposium 25, 359–370 (1991)

CCC 0020-7608/91/010359-12$04.00

ments contain valuable information on the dynamic constraints imposed on the final-state interactions of the photodissociation. Rotational state population distributions of diatomic photofragments are typically measured by laser detection methods [4–7]. These measurements can reveal detailed information about the angular dependence of the excited-state potential energy surfaces. With these detailed experimental findings, a major task is to develop a theory that relates parameters of the molecular system to the experimentally measured quantities and extract the nature of how the potential energy surfaces govern the dynamics of the interaction between the fragments. Several approaches, varying from time-dependent, quantum dynamical models employing *ab initio* potential energy surfaces to simple impulsive models, have been used to model the experimental observables [9]. The approach presented here is the theoretical evaluation of the rotational state population distributions of the photofragments.

The photodissociations of H_2O and H_2S have been studied extensively, both experimentally [10,11] and theoretically [12,13]. For the most part, it is generally accepted that H_2O dissociates via a single electronic state, i.e., direct dissociation, while the most recent work on H_2S suggests that at least two states are involved during the photofragmentation process [11,13]. One of the remaining questions in these case studies is the nature of the two excited states that participate in the dissociative pathways for H_2S.

In the work reported here, we compare the rotational state population distributions of the diatomic photofragments obtained by the numerical evaluation of the kinematic distribution functions with the most recent experimental results on the nascent OH [10] and SH [11] photofragments to study the dynamic constraints on the recoil of the photofragments, and deduce the dissociative mechanisms of the H_2O and H_2S molecules. The photodissociation of H_2O represents a logical starting point for studies of this type because it is the best understood case of triatomic photodissociation.

Chen and Pei have previously analyzed the experimental nascent diatomic rotational state populations from the photodissociation of NO_2 [14] and H_2S [15] by using the kinematic distribution approach to reveal a dissociation mechanism. Their results on H_2S were consistent with experimental data existing at that time [16], but more complete results on the nascent SH rotational state population distribution are now available, and they suggest a reworking of the calculation.

In the next section, we outline a general procedure to evaluate the rotational state population distribution of the diatomic photofragments in terms of the kinematic distribution function developed by Chen and Pei [17]. In the third section, the results on H_2O and H_2S are presented and the kinematic aspects of the photodissociation processes are discussed.

Numerical Evaluation of the Kinematic Distribution Function

In scattering processes, the total energy and angular momentum are conserved, and thus dynamic constraints are of primary importance in experimental studies. Schulten and Gordon [18], and Elsum and Gordon [19] have studied the kinematic

contributions to the angular momentum distributions for reactive molecular scattering. They have derived analytic expressions for the reactant-product angular momentum coupling coefficients, which are applicable for all reactive scattering calculations. Based on Schulten and Gordon's study [18], Chen and Pei [17] have recently developed an approach to study the kinematic aspects of the photodissociation processes for diatomic and triatomic molecules. In the following, we outline the kinematic distribution function approach of Chen and Pei to show how the dynamic constraints on the recoil of a photofragment may be derived from its rotational state population distribution computed by using the kinematic distribution function [17].

The photodissociation process of a triatomic molecule is usually represented in two separate steps,

$$ABC + h\nu \rightarrow ABC^* \rightarrow AB + C \tag{1}$$

where ABC^* represents the photoactivated species. The first step represents the absorption process, while the fragmentation of the excited species into products AB and C occurs in the second step. The diatomic photofragment AB acquires a rotational state population distribution from the recoil interaction with the departing atom C. We assume that the atom C recoils with wavenumber k, and that its wave function may be approximated by a plane wave, $\exp(ikZ)$ [17,18]. The plane wave may be expanded in terms of the spherical wave basis functions,

$$e^{ikZ} = \sum_l \hat{l} |l0, \hat{k}\rangle \tag{2}$$

where,

$$|lm, \hat{k}\rangle = (4\pi)^{1/2} i^l j_l(kr) Y_{lm}(\hat{k}) . \tag{3}$$

Here $\hat{l} = (2l + 1)^{1/2}$, and $j_l(kr)$ is a spherical Bessel function.

With the use of the addition theorem of Schulten and Gordon [18], the density matrix of the dissociating state may be expressed in terms of the basis, $|l_1 m_1 \mathbf{r}_{AB}\rangle$, which represents the rotational motion of the diatomic photofragment AB and the basis $|l_2 m_2 \mathbf{r}_0\rangle$, which corresponds to the orbital angular momentum of the system AB and C,

$$\begin{aligned}\sum_l \hat{l}^2 |l0, \hat{k}\rangle\langle l0, \hat{k}| = 16\pi^2 \sum_{\substack{l_1 l_2 l_3 l_4 \\ m_1 m_2 m_3 m_4}} (-1)^{l_1+l_2+l_3+l_4} \hat{l}^4 \\ \times \begin{pmatrix} l_1 & l_2 & l \\ m_1 & m_2 & 0 \end{pmatrix} \begin{pmatrix} l_3 & l_4 & l \\ m_3 & m_4 & 0 \end{pmatrix} \times F^l_{l_1 l_2}(x) F^l_{l_3 l_4}(x) \\ \times |l_1 m_1, \hat{r}_{AB}\rangle\langle l_3 m_3, \hat{r}_{AB}| \otimes |l_2 m_2, \hat{r}_0\rangle\langle l_4 m_4, \hat{r}_0| \end{aligned} \tag{4}$$

The kinematic distribution function $P(l_1)$,

$$P(l_1) = \sum_{l l_2} \hat{l}^2 |F^l_{l_1 l_2}(x)|^2 , \tag{5}$$

which describes the rotational state population distribution of photofragment AB, may be obtained by projecting the density matrix onto the state [17]

$$\sum_{l_6 m_5 m_6} |l_5 m_5, \hat{r}_{AB}\rangle\langle l_5 m_5, \hat{r}_{AB}| \circledast |l_6 m_6, \hat{r}_0\rangle\langle l_6 m_6, \hat{r}_0| \,. \tag{6}$$

In Eq. 4. $F^l_{l_1 l_2}(x)$ is the so-called Schulten-Gordon coefficient that represents the radial-rotational coupling, and is given by [18]

$$\begin{aligned} F^l_{l_1 l_2}(x) = {} & \tfrac{1}{2}\pi^{1/2}(-1)^{l+l_1+l_2/2}\hat{l}_1\hat{l}_2\begin{pmatrix} l & l_1 & l_2 \\ 0 & 0 & 0 \end{pmatrix} \\ & \times \frac{\Gamma\left(\frac{l+3}{2}\right)\Gamma\left(\frac{l_1+l_2}{2}\right)}{\Gamma\left(\frac{l}{2}\right)\Gamma(l_2+\frac{3}{2})\Gamma\left(\frac{l_1-l_2+3}{2}\right)} x^{l_2} \\ & \times {}_2F_1\left(\frac{l_1+l_2}{2}, \frac{l_2-l_1-1}{2}; \quad l_2+\frac{3}{2}; \quad x^2\right) \end{aligned} \tag{7}$$

for $x < 1$.

For x larger than unity, the following symmetry property is invoked to calculate the coupling coefficients [18],

$$F^l_{l_1 l_2}(x) = (\text{sign } x)^l F^l_{l_2 l_1}(x^{-1}) \tag{8}$$

Here, ${}_2F_1$ is the hypergeometric function. Γ is the gamma function, and $(:::)$ is a $3-j$ symbol. The experimentally measured rotational state population distributions are usually normalized to unity, whereas the kinematic distribution function (cf. Eq. 5), in general, is not normalized,

$$\sum_{l_1} P(l_1) = c(\neq 1) \tag{9}$$

Thus, it remains to divide the kinematic distribution function by the constant c to compare it with the experimental rotational state population distributions.

Results and Discussion

The molecular configuration on which the kinematic model is based is shown schematically in Figure 1. The distance from the C atom to the AB center of mass is α, and β is the distance from the AB center of mass to the intersection of the extension of the AB bond axis and the direction ($\hat{\mathbf{k}}$) of the C atom leaving the molecule. The parameter x in the kinematic distribution function (cf. Eq. 5) represents the ratio α/β. This ratio indicates the direction in which the C atom is leaving the molecule, and hence, the recoil imparted to the AB photofragment as a result of the dissociation of the C atom. Two cases are shown in Figure 1 for different recoil directions of the $\hat{\mathbf{k}}$ vector. It can be seen how the distance β changes as a function of the direction of $\hat{\mathbf{k}}$, which in turn causes x to vary.

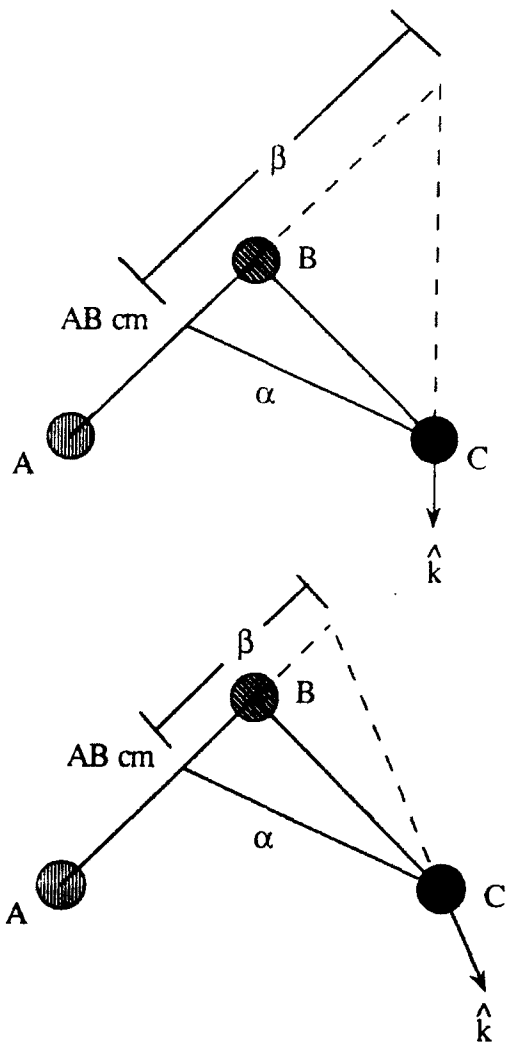

Figure 1. A schematic representation of the photodissociating *ABC* molecule depicting two different cases of the departing *C* atom leaving along unit vector $\hat{\mathbf{k}}$. The kinematic distribution function is based on the parameter $x = \alpha/\beta$. For further explanation, see text.

In principle, x can be calculated from the excited state geometry and recoil direction. In practice, however, this information is not always available, and x is treated as a parameter along with the total angular momentum l_{max} of the system. The dependence of the kinematic distribution function on these two variables is shown in Figure 2. The effect on the calculated rotational state population of increasing l_{max} for a fixed x becomes apparent in Figure 2(a). With increasing l_{max}, the higher values of l_i are populated to a greater extent, while the lower values of l_i decrease in population.

Figure 2(b) shows the rotational state distribution for the case of varying x at a fixed l_{max}. We have used the convention of Chen and Pei [15] to refer to this

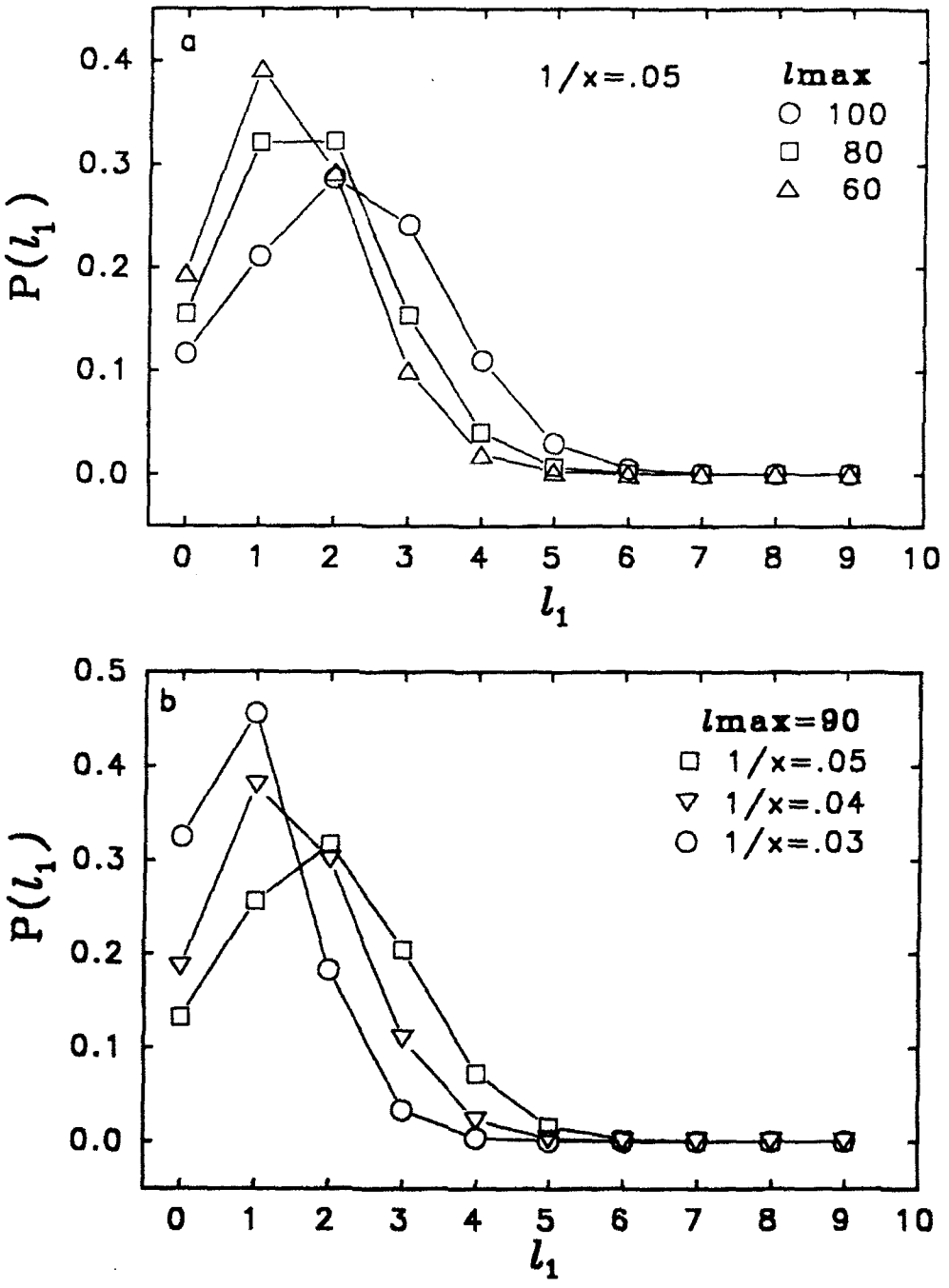

Figure 2. (a) Variation of the rotational state distribution with l_{max} for a fixed $x(1/x = 0.05)$. (b) Variation of the rotational state distribution as a function of $1/x$ for $l_{max} = 100$.

TABLE I. Calculated values used in the best fit of the experimental data for the photodissociation of H_2O at 157 nm. The values were calculated by using Eq. 5 for $x = 17.54$.

l_1	$l_{max} = 90$ $P(l_1)$	$l_{max} = 150$ $P(l_1)$
0	1.11×10^{-1}	4.69×10^{-2}
1	2.01×10^{-1}	9.56×10^{-2}
2	2.73×10^{-1}	1.32×10^{-1}
3	2.45×10^{-1}	1.45×10^{-1}
4	1.23×10^{-1}	1.49×10^{-1}
5	3.77×10^{-2}	1.65×10^{-1}
6	7.89×10^{-3}	1.40×10^{-1}
7	1.22×10^{-3}	8.10×10^{-2}
8	1.48×10^{-4}	3.34×10^{-2}
9	1.49×10^{-5}	1.04×10^{-2}
10	1.26×10^{-6}	2.53×10^{-3}

parameter in terms of $1/x$. For the cases of large $1/x$ (i.e., small α and large β), the higher values of l_1 are more populated, and therefore the lower values of l_1 have less population. For the opposite case (i.e., small $1/x$), the reverse is true. By comparison with the molecular configuration (cf. Fig. 1), one can see that small values of $1/x$ indicate that the recoil exerted by the C atom will be closer to the center of mass of the AB photofragment, thereby making it more difficult to populate

TABLE II. Calculated values used in the best fit of the experimental data for the photodissociation of H_2S at 193 nm. The values were calculated by using Eq. 10 with $x_1 = 33.0$ and $x_2 = 11.1$.

l_1	$l_{max} = 80$ $P(l_1)$
0	2.27×10^{-1}
1	2.88×10^{-1}
2	1.49×10^{-1}
3	9.84×10^{-2}
4	9.94×10^{-2}
5	7.76×10^{-2}
6	4.02×10^{-2}
7	1.47×10^{-2}
8	4.09×10^{-3}
9	9.20×10^{-4}
10	1.74×10^{-4}

higher l_1 values. Conversely, large values of $1/x$ correspond to a force being exerted away from the AB center of mass and result in a larger recoil imparted to the diatomic fragment.

The photodissociation of H_2O is generally accepted as the best known case of a direct dissociation, i.e., the molecule is excited from the ground state to an upper repulsive state by the absorption of a photon to yield an atom and a diatomic fragment [10]. Since the dissociation is instantaneous, the geometry of the ground state is retained, and thus for this kinematic model, H_2O represents an excellent test case. By holding the molecular configuration constant (i.e., ground state configuration) and varying l_{max}, the model described above should reproduce the experimental data. Our calculated best fits to the experimentally determined rotational state population are shown in Figure 3(a) (H_2O at 300 K) and 3(b) (H_2O at 10 K). In both cases, the value of x was fixed at 17.54 ($1/x = 0.057$) corresponding to the equilibrium ground state geometry of H_2O (HOH bond angle = 105.2°, H—OH bond length = 0.96 Å), with the H atom leaving along the bond axis.

As can be seen from Figures 3(a), 3(b), the calculated rotational state populations come close to reproducing the reported experimental distribution. Essentially, the only difference between the two cases shown is the total angular momentum content of the parent H_2O molecule at 300 K and at 10 K, and therefore the calculated best fits should have different l_{max} values. This is reflected in our data, where we fit the 300 K H_2O data with an $l_{max} = 150$ and the 10-K H_2O data with an $l_{max} = 90$ (cf. Figs. 3a,b).

The calculated rotational state populations (Table I) do not accurately reproduce the population of the higher rotational angular momentum states. However, our results agree almost quantitatively with previous calculations based on a Franck-Condon model for photodissociation [12]. The origin of the discrepancy between the calculated and experimental rotational state distributions is not immediately obvious, but it is possible that it arises from the selection of a single, most probable geometry as the only dissociating state.

Chen and Pei applied their kinematic distribution function to the photodissociation of H_2S at 193 nm [15]. At the time, the available experimental data on the nascent SH rotational state populations was limited [16]. Since the appearance of the work of Chen and Pei, a flurry of studies on the photodissociation dynamics of H_2S has been carried out by a variety of experimental techniques. Weiner et al. employed LIF in a pulsed supersonic jet to measure nascent SH rotational state populations, spin-orbit state population ratios, and Λ-doublet state populations following the excimer laser photodissociation of H_2S at 193, 222, and 248 nm [11]. Wittig and co-workers used a Doppler profile technique to observe vibrational excitation of SH up to $v'' = 8$ at 193 nm [20]. Kleinermanns et al., using emission spectroscopy of the dissociating H_2S at 193 nm, presented evidence that suggested a correlation between the bending and stretching vibrational excitation as the dissociating triatomic molecule progressed along the reaction coordinate [21]. Emission spectroscopic studies by Person et al. [22] and Brudzynski et al. [23] come to similar conclusions. The combination of all these studies has shed quite a bit of light on the subject, but a global understanding of the dissociation (as exists for

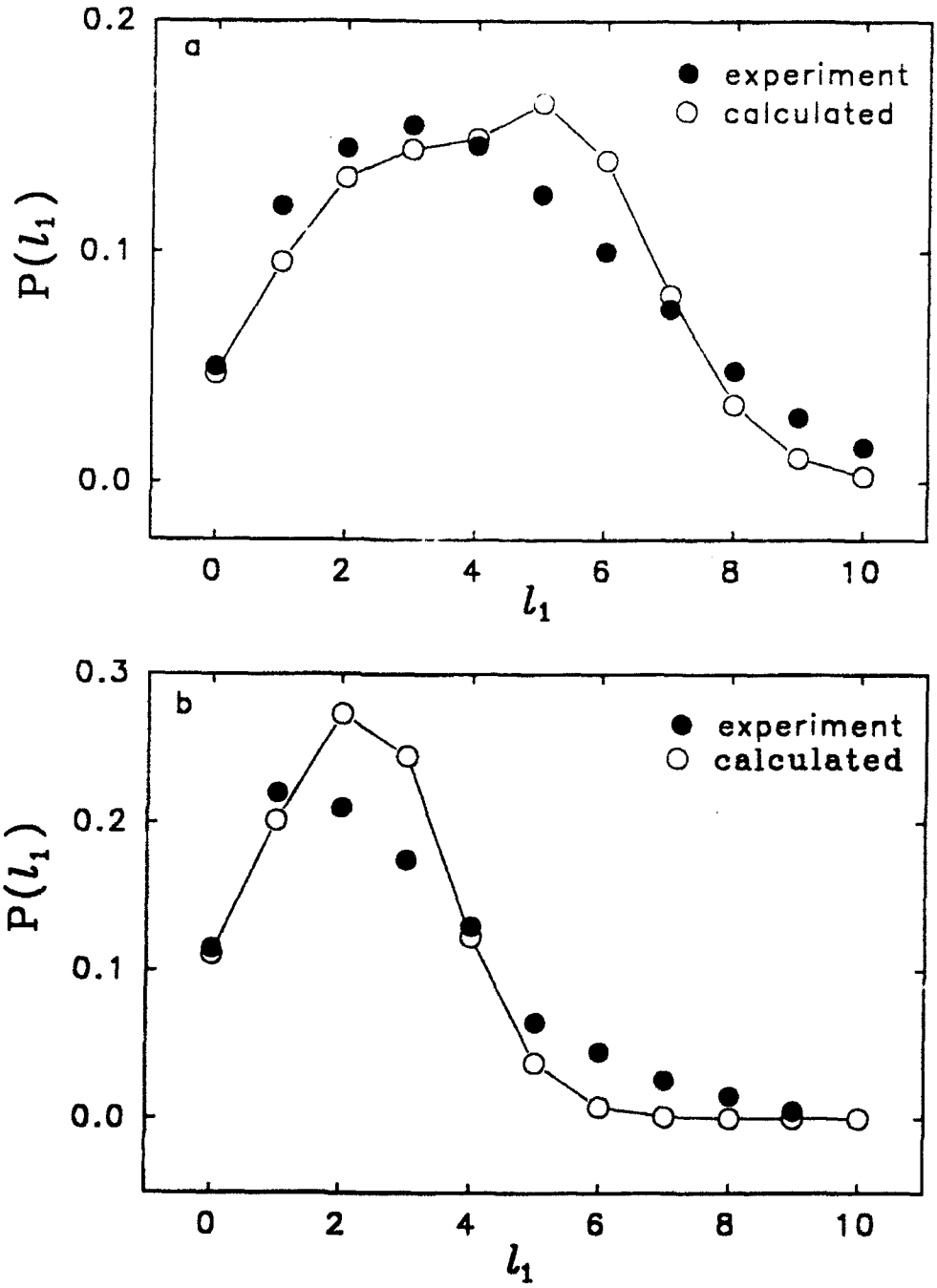

Figure 3. Comparison of the calculated best fit (○) and experimental (●) rotational state distribution of the OH($^2\Pi$) photofragment from the 157 nm photodissociation of (a) H_2O at 300 K; and (b) H_2O at 10 K. The experimental data is from Reference 10. The line connecting the calculated data points is only to serve as a guide to the reader. For more details about the calculated best fit data, see text.

H_2O) remains elusive. None of the explanations given in these references could account for all the detailed experimental findings.

The anomalous rotational state population distribution obtained experimentally suggests more than one dissociation channel [12]. A recent study by Weide et al. has provided new insight into the problem [13]. These workers have calculated the two lowest excited singlet states for a fixed bond angle of 92° for C_{2v} and C_s symmetries. For the C_{2v} case, the two excited states are $^1B_1$ and $^1A_2$. State correlation diagrams show that dissociation to ground state photofragments can only occur from the $^1A_2$ state, but that the $^1A_2$-$^1A_1$ transition is electronically forbidden, yet vibronically allowed [24]. On the other hand, the $^1B_1$ state does not correlate to the ground-state photofragments, but the $^1B_1$-$^1A_1$ transition is electric-dipole allowed. The accepted mechanistic pathway has been to photoexcite the $^1B_1$ state followed by predissociation on the $^1A_2$ surface [24].

Weide et al. have proposed the innovation that perhaps elongation of the H—SH bond occurs upon excitation, making the two excited states C_s symmetry, and thus both states belong to $^1A''$ symmetry, and therefore undergo an avoided crossing [13(c)]. In C_s symmetry, both states have electric-dipole allowed transitions from the ground state. At 193 nm, the two states are populated in a 3:1 ratio according to the multiconfigurational self-contained field (SCF) calculations performed by these workers. The change in bond length is reflected in the structure of the 195 nm absorption band in H_2S, which had previously been attributed to the bending vibration [25].

The proposed model of Weide et al. [13(c)] accounts for almost all of the observed features of the photodissociation process. However, it still fails to explain the high end of the rotational state distributions detected in Reference 11. We believe this arises because the only way to achieve any population of photofragments containing significant angular momentum is via the change of geometry of the parent molecule prior to dissociation, i.e., a change in bond angle and bond length between the ground and excited states.

Based on this result, we have modified our kinematic distribution function to include two dissociation channels. This requires modification of the total kinematic distribution (cf. Eq. 5) to be the linear combination of the kinematic distribution functions for two different dissociation geometries.

$$P(l_1) = \omega_1 P_{x_1,l_{max}}(l_1) + \omega_2 P_{x_2,l_{max}}(l_1), \tag{10}$$

where x_1 and x_2 correspond, respectively, to two different dissociation geometries. Our reasoning here was that part of the excitation leads to a bound state that can undergo nuclear rearrangement before making a nonadiabatic jump to the dissociative surface. Our initial attempts to fit the experimental data were done by using the ground state geometry for the repulsive state, a branching ratio of $\omega_1:\omega_2 = 3:1$ between the two states and then, parametrizing the geometry of the bound $^1A''$ state (x_2) and the l_{max}. In this case, we are defining $1/x_1 = 0.03$, corresponding to the ground-state equilibrium geometry of H_2S with dissociation along the bond angle. This x_1 value cannot provide the photofragments with high rotational angular momentum because the recoil is close to the AB center of mass. The second dissociation

geometry must correspond to a case where the recoil is directed away from the diatomic center of mass in order to provide the necessary torque to produce photofragments with significant rotational angular momentum. The analysis corroborates that a significant channel dependency in the rotational state distribution of the SH fragment exists, i.e., diatomic fragments with low J arise from channel 1, while channel 2 must give rise to the rotational states with higher J. By using the 3:1 ratio, we could not adequately fit the experimental data. The best fit to the experimental data, shown in Figure 4, is achieved with $1/x_2 = 0.09$, $l_{max} = 80$, and a branching ratio, $\omega_1:\omega_2$ = 1:1. The calculated rotational state populations are tabulated in Table II.

Our result is in qualitative agreement with Weide et al. in that the experimental observables are better explained by two dissociation channels. The quantitative difference in the assigned branching ratio of these two pathways remains small given the approximations used. It should be noted that the 193 nm photofragmentation of H_2S has been considered to be an intermediate case between direct and indirect photodissociation. The results here demonstrate that it is more likely half direct and half indirect.

In conclusion, our results demonstrate the power of the kinematic distribution function to accurately reproduce experimental rotational state distributions, and elucidate the details of photofragmentation mechanisms. Furthermore, the model

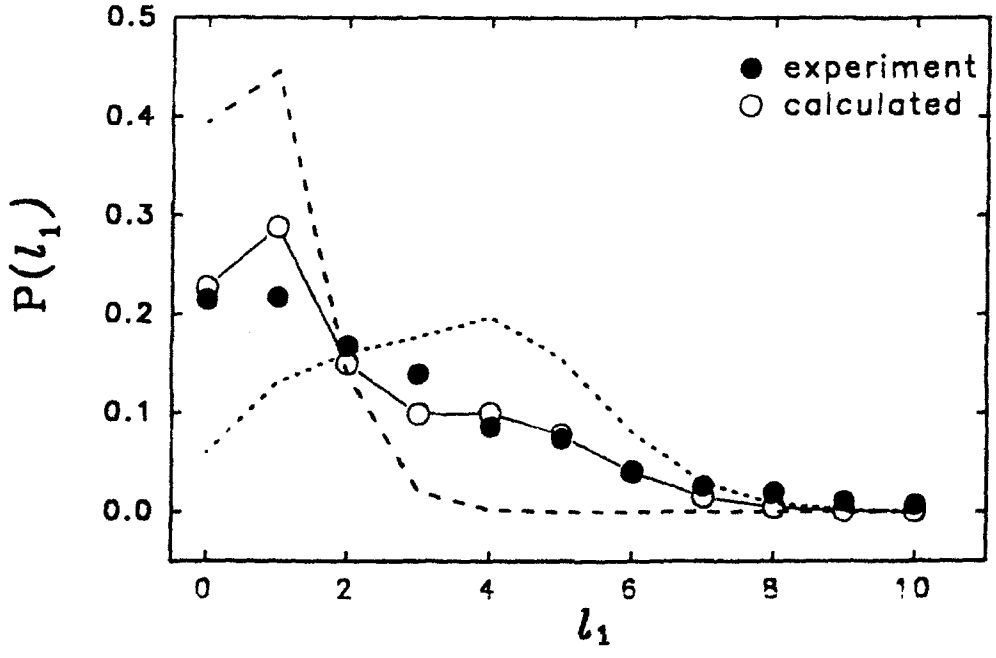

Figure 4. Comparison of the calculated best fit (○) and experimental (●) rotational state distribution of the SH($^2\Pi$) photofragment from the 193 nm photodissociation of H_2S. The experimental data is from Reference 11. The best fit data was calculated by using Eq. 10. Broken and dotted lines represent the calculated rotational state populations (normalized to unity) for channels 1 and 2, respectively. For further explanation about the calculations, see text.

provides a valuable method of determining excited state geometries. We expect this model will have continued use in the arsenal of tools used to elaborate the photodissociation dynamics of polyatomic molecules.

Acknowledgments

We would like to acknowledge the generous support of this project by the Air Force Office of Scientific Research (Contract No. F49620-89-C0070) and NSF-EPSCoR (Grant No. R11-8610677).

Bibliography

[1] A. Terenin, J. Phys. **37**, 98 (1926).
[2] See, for example, W. M. Jackson and H. Okabe, Adv. Photochem. **13**, 1 (1986) and references therein.
[3] See, for example, R. D. Levine and R. B. Bernstein, *Molecular Reaction Dynamics and Chemical Reactivity* (Oxford University Press, New York, 1987), pp 81–102.
[4] A. Baronavski, in *Lasers as Reactants and Probes in Chemistry*, W. M. Jackson and A. B. Harvey, Eds. (Howard University Press, Washington, D.C., 1985).
[5] P. L. Houston, J. Phys. Chem. **91**, 5388 (1987).
[6] B. R. Weiner, L. Pasternack, H. H. Nelson, K. A. Prather, and R. N. Rosenfeld, J. Phys. Chem. **94**, 4138 (1990).
[7] H. B. Levene, J. C. Nieh, and J. J. Valentini, J. Chem. Phys. **87**, 2583 (1987).
[8] R. Bersohn, J. Phys. Chem. **88**, 5145 (1984).
[9] (a) G. E. Busch and K. R. Wilson, J. Chem. Phys. **56**, 3626, 3638, 3655 (1972); (b) K. C. Kulander and E. J. Heller, J. Chem. Phys. **69**, 2439 (1978); (c) M. D. Morse and K. F. Freed, J. Chem. Phys. **78**, 6066 (1983); (d) G. G. Balint-Kurti and M. Shapiro, in *Photodissociation and Photoionization*, K. P. Lawley, Ed. (Wiley-Interscience, New York, 1985), p. 403; (e) V. Z. Kresin and W. A. Lester, *Adv. Photochem.* **13**, 95 (1986); (f) R. Kosloff, J. Phys. Chem. **92**, 2087 (1988); (g) P. K. Swaminathan, C. D. Stodden, and D. A. Micha, J. Chem. Phys. **90**, 5501 (1989).
[10] P. Andresen and R. Schinke, in *Molecular Photodissociation Dynamics*, M. N. R. Ashfold and J. E. Baggott, Eds. (Royal Society of Chemistry, London, 1987), pp. 61–113.
[11] B. R. Weiner, H. B. Levene, J. J. Valentini, and A. P. Baronavski, J. Chem. Phys. **90**, 1403 (1989).
[12] D. Häusler, P. Andresen, and R. Schinke, J. Chem. Phys. **87**, 3949 (1987).
[13] (a) K. C. Kulander, Chem. Phys. Lett. **103**, 373 (1984); (b) R. N. Dixon, C. C. Marston, and G. G. Balint-Kurti, J. Chem. Phys. **93**, 6520 (1990); (c) K. Weide, V. Staemmler, and R. Schinke, J. Chem. Phys. **93**, 861 (1990).
[14] K. Chen and C. Pei, Chem. Phys. Lett. **137**, 361 (1987).
[15] K. Chen and C. Pei, Chem. Phys. Lett. **134**, 259 (1987).
[16] W. G. Hawkins and P. L. Houston, J. Chem. Phys. **73**, 297 (1980); **76**, 729 (1982).
[17] K. Chen and C. Pei, Chem. Phys. Lett. **124**, 365 (1986).
[18] K. Schulten and R. G. Gordon, J. Chem. Phys. **64**, 2918 (1976).
[19] I. R. Elsum and R. G. Gordon, J. Chem. Phys. **76**, 3009 (1982).
[20] Z. Xu, B. Koplitz, and C. Wittig, J. Chem. Phys. **87**, 1062 (1987).
[21] K. Kleinermanns, E. Linnebach, and R. Suntz, J. Phys. Chem. **91**, 5543 (1987).
[22] M. D. Person, K. Q. Lao, B. J. Eckholm, and L. J. Butler, J. Chem. Phys. **91**, 812 (1989).
[23] R. J. Brudzynski, R. J. Sension, and B. Hudson, Chem. Phys. Lett. **165**, 487 (1989).
[24] G. N. A. van Veen, K. A. Mohamed, T. Baller, and A. E. DeVries, Chem. Phys. **74**, 263 (1983).
[25] S. D. Thompson, D. G. Carroll, F. Watson, M. O'Donnell, and S. P. McGlynn, J. Chem. Phys. **45**, 1367 (1966).

Received March 27, 1991

Reprinted from The Journal of Physical Chemistry, 1991, 95.

Nascent SO($X^3\Sigma^-$) Vibrational Distributions from the Photodissociation of SO_2, $SOCl_2$, and $(CH_3)_2SO$ at 193 nm

Xirong Chen, Federico Asmar, Hongxin Wang, and Brad R. Weiner*

Department of Chemistry, University of Puerto Rico, Río Piedras, Puerto Rico 00931
(Received: May 29, 1991; In Final Form: June 28, 1991)

Nascent vibrational state distributions of SO($X^3\Sigma^-$) have been measured by laser-induced fluorescence spectroscopy following the 193-nm photodissociations of SO_2, $SOCl_2$, and $(CH_3)_2SO$ in the gas phase. All three of the distributions are found to be inverted, indicating strong dynamical effects in the photodissociation processes. A Franck–Condon/golden rule model is used to propose mechanisms to account for the experimental vibrational distributions.

Introduction

The detailed mechanisms of photodissociation processes can be revealed by measurement of the nascent vibrational state distributions of one or more of the photofragments following photoactivation of a polyatomic molecule.[1] Information about the nature of the excited species immediately prior to the fragmentations can be obtained from this data. In the case of multiple bond dissociations in polyatomics, nascent vibrational state distributions can help elucidate whether photofragmentation occurs stepwise or in concert.[1]

We report in this Letter the measurement of nascent vibrational state distributions of the SO($X^3\Sigma^-$) fragment obtained in the 193-nm photodissociations of sulfur dioxide (SO_2), thionyl chloride ($SOCl_2$), and dimethyl sulfoxide ($(CH_3)_2SO$). The nascent vibrational distributions were measured by laser-induced fluorescence (LIF) spectroscopy of SO($A^3\Pi$–$X^3\Sigma^-$) transition in the wavelength region of 255–295 nm.

Experimental Section

The experiment employs a typical two-laser, pump–probe apparatus, which has been described previously.[2] Briefly, low pressures (0.01–0.05 Torr) of SO_2, $SOCl_2$, or $(CH_3)_2SO$ are flowed through a reaction chamber comprised of a four-way stainless steel cross fitted with scattered-light-reducing, brass extension arms on two opposite sides. Gas inlets are located on the extension arms, and the gas outlet is on the four-way cross. The reaction cell is pumped by a 2-in. diffusion pump, and the entire chamber and vacuum system can be evacuated to 10^{-4} Torr, routinely. Cell pressures are measured at the exit of the cell by a capacitance manometer.

Reactant gases are photolyzed with the 193-nm output (10–50 mJ/cm^2) of an excimer laser (Lambda Physik LPX205i) operating on the ArF transition. Nascent SO photofragments are monitored by LIF on the (A–X) transition in the 255–295-nm region of the spectrum. The probe laser light in this region was generated by frequency doubling (β-BaB_2O_4 crystal) the output of a Lambda Physik FL3002 tunable dye laser (dye is Coumarin 503 or Coumarin 540A), which is pumped by a Lambda Physik LPX205i excimer laser at 308 nm. The lasers are collinearly counterpropagated along the extension arm axis to maximize the overlap region in the center of the reaction chamber.

Fluorescence is viewed at 90° relative to the laser beam axis by a high gain photomultiplier tube (Hamamatsu R943-02) through a long-pass filter (Schott WG295). The output of the photomultiplier tube is processed and averaged by a gated inte-

* To whom correspondence should be addressed.

(1) Bersohn, R. In *Molecular Photodissociation Dynamics*; Ashfold, M. N. R., Baggott, J. E., Eds.; Royal Society of Chemistry: London, 1987; pp 1–30.

(2) Barnhard, K. I.; Santiago, A.; He, M.; Asmar, F.; Weiner, B. R. *Chem. Phys. Lett.* **1991**, *178*, 150.

0022-3654/91/2095-6415$02.50/0

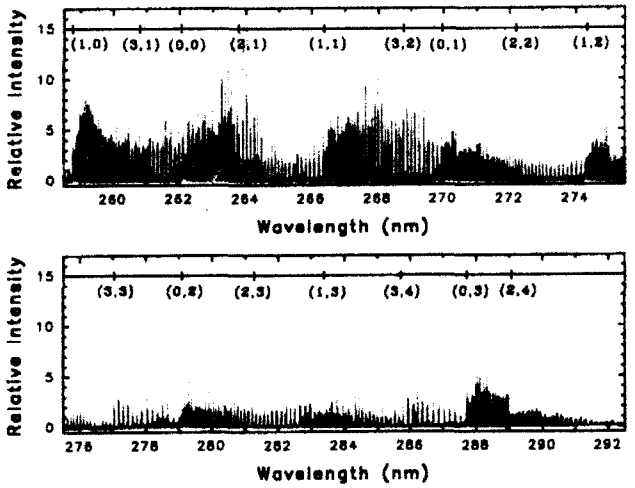

Figure 1. LIF spectrum of nascent $SO(X^3\Sigma^-)$ from the 193-nm photodissociation of 0.03 Torr of $SOCl_2$. The delay between the pump and probe lasers was 200 ns. The origins of the vibrational bands are assigned from the constants of refs 3 and 4.

grator (SRS Model SR250), digitized (SRS Model 245), and sent to a microcomputer for display, storage, and analysis. The delay time (100–400 ns) between the two lasers was controlled with a digital delay pulse generator (SRS, Model DG535). For a fixed delay time between photolysis and probe lasers, the frequency-doubled output of the dye laser was scanned while collecting the total fluorescence signal to obtain a nascent excitation spectrum. Data were typically collected at 30–40 Hz. To extract the LIF signal due to SO from the scattered laser light and the laser-induced fluorescence from the parent molecule, and also to correct the signal for the dye tuning curve, the following procedure is used. The probe laser is fired at the appropriate time delay of the experiment, i.e., *after* the photolysis laser, to give an integrated LIF signal, A. The probe laser is now fired for the same number of shots 1 μs *before* the photolysis laser. This second integrated signal, B, contains primarily fluorescence from the parent molecule and is proportional to the dye laser power. In order to get the integrated LIF signal due solely to SO(A–X) and normalized for dye laser power, we subtract B from A and divide this value by B, i.e., $(A - B)/B$. Typical scan times for the data reported here were about 2 nm/h. For these long scans, the SO laser-induced fluorescence signal was also corrected for photolysis laser power.

SO_2 (Matheson, 99.9%) was used without further purification. $SOCl_2$ (Fluka, 99%) and $(CH_3)_2SO$ (MCB Reagents, 99.9%) were subjected to repeated freeze–pump–thaw cycles prior to use.

Results and Discussion

Figure 1 shows the LIF excitation spectrum of $SO(A^3\Pi–X^3\Sigma^-)$ following the 193-nm photodissociation of $SOCl_2$ at 298 K. This spectrum was obtained under nascent conditions (P_{tot} = 0.03 Torr; probe laser delay = 200 ns), and corresponding nascent SO excitation spectra under similar conditions can also be obtained from the 193-nm photodissociations of SO_2 and $(CH_3)_2SO$. The spectra are in good agreement with the previous assignments of Colin[3] and of Clyne and co-workers.[4]

In order to measure accurate vibrational state populations from these spectra, we integrate the area under the bands corresponding to the $(0,v'')$ and $(1,v'')$ transitions, where v'' = 0, 1, 2, 3, and 4 of the (A–X) system. These series of bands were chosen to minimize the overlap of other bands and to avoid excited-state lifetime perturbations.[5] The integrated area of each of these vibrational bands is corrected for Franck–Condon factors (from ref 4) and normalized. The results are presented in Figures 2 and

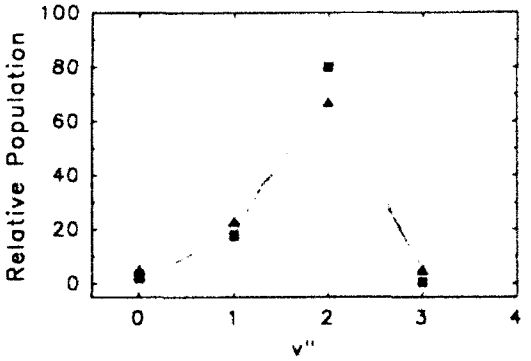

Figure 2. Comparison of the nascent vibrational state distributions of $SO(X^3\Sigma^-,v'')$ following 193-nm photodissociation of SO_2, obtained from this work (■), from ref 6 (▽), and from ref 7 (▲). The calculated best fit to our data from eq 1 is shown as (□). For further explanation, see text.

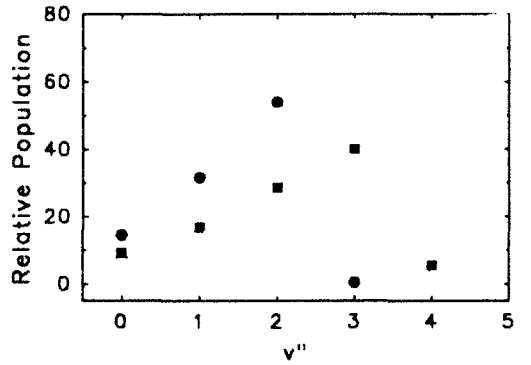

Figure 3. Nascent vibrational state distributions of $SO(X^3\Sigma^-,v'')$ from the 193-nm photodissociations of $SOCl_2$ (■, □) and $(CH_3)_2SO$ (●, ○). The filled symbols represent the experimentally measured distributions, and the open symbols are calculated best fits using eq 1. For further explanation, see text.

3. Figure 2 shows a comparison of the nascent vibrational distributions of $SO(X^3\Sigma^-)$ resulting from the 193-nm photodissociation of SO_2. The figure shows that despite three different experimental techniques used, i.e., infrared absorption spectroscopy,[6] photofragment time-of-flight mass spectroscopy,[7] and LIF (this work), the results are surprisingly consistent. The major difference is that we find no population in $SO(X^3\Sigma^-,v''=3)$,[8] while the other two studies find ≤5%. We also found no evidence for population in $v'' = 5$, as was reported by Kanamori et al.,[6] but because of the small Franck–Condon factors for the $(v',5)$ transitions in this spectral region, we are not very sensitive to this vibrational level.

The 193-nm photodissociation of SO_2 has received considerable attention over the past 15 years.[6,7,9–13] It is generally accepted now that the photodissociation proceeds from the $\tilde{C}^1B_2$ state to produce $O(^3P)$ and $SO(X^3\Sigma^-)$, formed with an inverted population distribution peaked at $v'' = 2$. Berry has shown that inverted

(3) (a) Colin, R. *J. Chem. Soc., Faraday Trans. 2* **1982**, *78*, 1139. (b) Colin, R. *Can. J. Phys.* **1969**, *47*, 979.

(4) (a) Clyne, M. A. A.; McDermid, I. S. *J. Chem. Soc., Faraday Trans. 2* **1979**, *75*, 505. (b) Clyne, M. A. A.; Tennyson, P. H. *J. Chem. Soc., Faraday Trans. 2* **1986**, *82*, 1315.

(5) Lo, G.; Beaman, R.; Setser, D. W. *Chem. Phys. Lett.* **1988**, *149*, 384.

(6) Kanamori, H.; Butler, J. E.; Kawaguchi, K.; Yamada, C.; Hirota, E. *J. Chem. Phys.* **1985**, *83*, 611.

(7) Felder, P.; Effenhauser, C. S.; Haas, B. M.; Huber, J. R. *Chem. Phys. Lett.* **1988**, *148*, 417.

(8) By increasing the pressure of SO_2 in the reaction chamber to non-nascent conditions, we have been able to observe a trace of $SO(X^3\Sigma^-,v''=3)$. We estimate the amount at ≤5%.

(9) Freedman, A.; Yang, S.-C.; Bersohn, R. *J. Chem. Phys.* **1979**, *70*, 5313.

(10) Kawasaki, M.; Kasatani, K.; Sato, H. *Chem. Phys.* **1982**, *73*, 377.

(11) Kim, H.-R. Ph.D. Dissertation, Cornell University, Ithaca, NY, May 1984.

(12) Bower, R. D.; Hawkins, W. G.; Houston, P. L.; Jones, R. W.; Kim, H.-R.; Marinelli, W. J.; Sivakumar, N. In *Advances in Laser Spectroscopy*; Garetz, B. A., Lombardi, J. R., Eds.; John Wiley and Sons: New York, 1987; pp 132–135.

(13) Ebata, T.; Nakazawa, O.; Ito, M. *Chem. Phys. Lett.* **1988**, *143*, 31.

vibrational population distributions occurring in chemical reactions can be approximated by a Franck–Condon/golden rule model,[14] shown in eq 1. This model calculates the probability, $P(f)$, of

$$P(f) \sim (2\pi/\hbar)|\langle i|f\rangle|^2\rho(E) \quad (1)$$

forming SO in vibrational state $|f\rangle$, where $|i\rangle$ is the initial "dressed oscillator" state, corresponding to SO in SO_2, and $\rho(E)$ is the final density of states.[14] Morse oscillator functions are used for $|f\rangle$ and $|i\rangle$. We have investigated the application of (1) for the $\tilde{C}^1B_2$ state of SO_2 going to $SO(X^3\Sigma^-,v'')$. We find our best fit (see Figure 2) corresponds to a "dressed" SO oscillator with a bond length of 1.56 Å, with a vibrational frequency $\nu = 900$ cm^{-1}. This is in close agreement with the 1.56-Å bond length and $\nu = 960$ cm^{-1} of the $\tilde{C}$ state of SO_2 reported by Hoy and Brand.[15] The slight discrepancies between the experimental data and the calculated fit may arise from the final state interactions, which have previously been observed.[6,13]

The excellent agreement between the previous studies and the work reported here gives credence to the use of LIF of the SO(A–X) transition as a viable technique for measuring relative vibrational state populations. With this result in mind, as well as the sensitivity and ease of application of laser-induced fluorescence to gas-phase reactions, we applied this technique to the investigation of the 193-nm photodissociation dynamics of SO-containing polyatomics. Figure 3 shows the nascent $SO(X^3\Sigma^-)$ vibrational state distributions obtained from the 193-nm photodissociation of $SOCl_2$ and $(CH_3)_2SO$. Both distributions are clearly inverted, indicating strong dynamical effects in their respective photodissociation mechanisms.

Kawasaki et al. used photofragment time-of-flight spectroscopy to investigate the photodissociation dynamics of $SOCl_2$ at 193 nm.[16] They found evidence for two SO-producing channels:[17]

$$SOCl_2 + h\nu\ (193\ nm) \rightarrow 2Cl + SO \qquad \Delta H_{RXN} = 108\ kcal/mol \quad (2)$$

$$\rightarrow Cl_2 + SO \qquad \Delta H_{RXN} = 52\ kcal/mol \quad (3)$$

Hirota and co-workers employed 193-nm photolysis of $SOCl_2$ as a source for infrared diode laser absorption studies of the $SO(a^1\Delta)$ state, which lies ~18 kcal/mol above the ground state, $SO(X^3\Sigma^-)$.[18] They measured a quantum yield of 0.20 for $SO(a^1\Delta)$ production, which they found populated up to $v'' = 5$. One possibility is that the production of $SO(a^1\Delta)$ is consistent with the molecular elimination channel, (3), while the ground state of SO is produced via channel 2. In this work, $SO(X^3\Sigma^-)$, with vibrational population up to $v'' = 4$ and peaked at $v'' = 3$, has been observed. This less energetic vibrational state distribution is consistent with the lower energy available ($E_{avl} = 40$ kcal/mol) of the radical dissociation pathway, (2).

If we assume that $SO(X^3\Sigma^-)$ is produced by channel 2, then we need to ask, does $SOCl_2$ dissociate in a stepwise or concerted fashion? Kawasaki et al. claim that at 193 nm both the stepwise and concerted (three-body) dissociations are operative. By using the Franck–Condon/golden rule model described above (cf. eq 1), we find that the optimal "dressed" SO bond length of the dissociating state is 1.57 Å and $\nu = 1050$ cm^{-1}. This bond length could correspond to an excited-state geometry of $SOCl_2$ or to the ClSO radical. More information about the molecular geometries of these species is required to identify the moiety that produces $SO(X^3\Sigma^-)$.

The detection of SO production from the 193-nm photodissociation of dimethyl sulfoxide is the first observation of the gas-phase photochemistry of this molecule. Two energetically feasible ground-state SO-producing channels are available:[19]

$$(CH_3)_2SO + h\nu\ (193\ nm) \rightarrow 2CH_3 + SO \qquad \Delta H_{RXN} = 113.2\ kcal/mol \quad (4)$$

$$\rightarrow C_2H_6 + SO \qquad \Delta H_{RXN} = 24.8\ kcal/mol \quad (5)$$

Our vibrational distribution results are more consistent with the lower available energy ($E_{avl} = 34.8$ kcal/mol), radical dissociation channel, (4). Furthermore, we have tried, without success, to observe the production of ethane as a final product by infrared absorption spectroscopy and concluded that channel 5 was negligible.

Assuming that SO production proceeds by channel 4, we are again faced with the stepwise vs concerted reaction question. The SO bond length in ground-state $(CH_3)_2SO$ is 1.49 Å[20] as compared to the equilibrium value of 1.48 Å in $SO(X^3\Sigma^-)$. Direct dissociation from $(CH_3)_2SO$, in its ground-state equilibrium geometry to $SO(X\ ^3\Sigma^-)$, would not rationalize our inverted vibrational population distribution. Clearly, the SO bond must be lengthening either in excited-state $(CH_3)_2SO$ prior to dissociation or as CH_3SO in a stepwise dissociation to $SO(X^3\Sigma^-)$. Gollnick and Strauss reported indirect evidence for

$$(CH_3)_2SO \rightarrow CH_3 + CH_3SO \quad (6)$$

as the primary process for $(CH_3)_2SO$ photolysis at 254 nm in solution.[21] On the basis of their result, we favor that the SO bond elongation occurs in CH_3SO prior to dissociating to $SO(X^3\Sigma^-)$. Our Franck–Condon/golden rule model best fits (cf. Figure 3) the experimental data for a bond length of 1.55 Å and a vibrational frequency of 950 cm^{-1}. No detailed spectroscopic and/or geometric data have been reported for CH_3SO to verify this hypothesis.

In conclusion, we have demonstrated that SO(A–X) LIF is a valuable technique for studying the dynamics of SO-producing chemical reactions. The intriguing dynamical effects that dominate the photodissociation mechanisms discussed above warrant more detailed studies. An expansion of the data shown in Figure 1 reveals that it is possible to get detailed rotational state population distributions from the LIF excitation spectra. Complete descriptions of the nascent rotational and spin state populations reveal much about the nature of the photodissociating state(s), as well as final state interactions. These results will be reported in upcoming publications.

Acknowledgments are made to the Air Force Office of Scientific Research (Contract F49620-89-C0070) and NSF-EPSCoR (Grant R11-8610677) for their generous support of this project.

(14) Berry, M. J. *Chem. Phys. Lett.* **1974**, *29*, 323, 329.
(15) Hoy, A. R.; Brand, J. C. D. *Mol. Phys.* **1978**, *36*, 1409.
(16) Kawasaki, M.; Kasatani, K.; Sato, H.; Shinohara, H.; Nishi, N.; Ohtoshi, H.; Tanaka, I. *Chem. Phys.* **1984**, *91*, 285.
(17) Thermochemical values are taken from ref 1.
(18) Kanamori, H.; Tiemann, E.; Hirota, E. *J. Chem. Phys.* **1988**, *89*, 621.
(19) ΔH_f° values are taken as follows: (a) SO and CH_3 from: Benson, S. W. *Thermochemical Kinetics*, 2nd ed.; Wiley-Interscience: New York, 1976; pp 288–299. (b) CH_3SO from: Benson, S. W. *Chem. Rev.* **1978**, *78*, 23–25. (c) $(CH_3)_2SO$ from: ref 21 and references therein.
(20) Dreizler, H.; Dendl, G. *Z. Naturforsch.* **1964**, *19A*, 512.
(21) Gollnick, K.; Strauss, H. U. *Pure Appl. Chem.* **1973**, *33*, 217.

ISOTOPE EFFECTS AND WAVELENGTH DEPENDENCE IN THE ROTATIONAL STATE DISTRIBUTIONS OF THE DIATOMIC PHOTOFRAGMENTS, SH and SD, FROM THE PHOTODISSOCIATION OF H_2S AND D_2S

Xiaotian Gu, Luis A. Muñoz, Yasuyuki Ishikawa* and Brad R. Weiner*

Department of Chemistry and the Chemical Physics Program
University of Puerto Rico, Río Piedras, Puerto Rico 00931 USA

Abstract

We employ a semi-empirical model that utilizes a kinematic distribution function to calculate the rotational state population distributions of diatomic photofragments from the photodissociation of isotopically variant triatomic molecules. The numerically evaluated rotational distributions of the photofragments, SH and SD, are compared with experimental data on the nascent rotational state population distributions of the diatomic photofragments resulting from the laser photolysis of H_2S ($\lambda_{photolysis}$=193, 222 and 248 nm) and D_2S ($\lambda_{photolysis}$=193 and 222 nm).

* To whom correspondence should be addressed.

1. Introduction

Triatomic molecules have served as benchmark systems in both experimental and theoretical studies of photodissociation dynamics.[1] Among them, H_2S is one of the most intensively studied systems by both experiment[2,3,4,5,6,7,8,9,10,11,12] and theory[13,14,15,16,17,18,19]. H_2S is appealing from an experimental point of view because: (1) its first absorption band extends from *ca.* 270-180 nm which is readily accessible by high intensity excimer lasers; and (2) both of the resulting photofragments can be probed directly with quantum state specificity by modern spectroscopic methods. Furthermore, the triatomic dihydride is theoretically quite tractable by means of accurate *ab-initio* calculations[15,16,17,19]. In contrast to the older studies, some of the more recent theoretical works[15,16,17,18,19] strongly suggest that H_2S does not dissociate via a single excited electronic state, but instead involves two adiabatic surfaces with substantial nonadiabatic coupling between them.

Our goal in this study is to examine the nature of the coupled state photodissociation mechanism, by using a kinematic distribution function to numerically evaluate rotational state population distributions of the photofragments, SH and SD, and then compare them with experimentally measured nascent distributions. While thorough *ab-initio* results have been reported for the photodissociation of H_2S [19], we choose to employ our semi-empirical method here to demonstrate the validity of the model. The advantages of this model lie in its capability to be extended to systems of greater complexity with respect to potential energy surfaces. In a coupled state photodissociation mechanism, the vibrational levels of the bound excited electronic state are affected by the continuum of a repulsive state of the same symmetry which does not cross the bound excited state. The spectroscopic features may vary, depending on the coupling strength, and the relative size of the transition dipole moments involved. In principle, isotope effects may serve as a probe of the strength of nonadiabatic coupling, since effects due to isotopic substitution on the electronic state are a clear manifestation of the breakdown of the adiabaticity. Furthermore, by accessing different parts of the potential energy surfaces with different photolysis wavelengths, information about the specificity of the coupling can be obtained. In a previous study[18], we have employed the kinematic distribution function [20] to calculate the rotational state population distributions of the photofragments, OH and SH, from

the photodissociation of H_2O and H_2S at 193 nm, respectively. In this letter, we present the kinematic distribution function as a theoretical tool to examine the isotope effects and photolysis wavelength dependence of the rotational state population distributions of diatomic photofragments, SH and SD, from the laser photodissociation of H_2S and D_2S.

2. The Kinematic Distribution Function

In a pioneering work on angular momentum coupling in reactive collisions, Schulten and Gordon[21] have derived analytic expressions for the reactant-product angular momentum coupling coefficients that are applicable for all reactive scattering calculations. Based on Schulten and Gordon's study[21], Chen and Pei[20] initiated a study of the dynamical aspects of the photodissociation processes for di- and tri-atomic molecules by using the kinematic distribution function. *In scattering processes, the total energy and angular momentum are* conserved, and therefore, dynamic constraints are of primary importance in experimental and theoretical studies. The dynamic constraints on the recoil of a photofragment may be derived from its rotational state population distribution computed by using the kinematic distribution function[20].

The kinematic distribution function, $P(\ell_1)$[20],

$$P(\ell_1) = \sum_{\ell_2} \ell^2 |F^{\ell}_{\ell_1\ell_2}(x)|^2 \qquad (1)$$

where $\ell = (2\ell+1)^{1/2}$, describes the rotational state population distribution of a diatomic photofragment. In equation 1, $F^{\ell}_{\ell_1\ell_2}(x)$ is the so-called Schulten-Gordon coefficient (*a la* Chen and Pei[20]) which represents the radial-rotational coupling, and is given by,

$$F^{\ell}_{\ell_1\ell_2}(x) = \frac{1}{2}\pi^{\frac{1}{2}}(-1)^{\frac{\ell+\ell_1+\ell_2}{2}}\ell_1\ell_2\begin{pmatrix}\ell & \ell_1 & \ell_2\\ 0 & 0 & 0\end{pmatrix} \times \frac{\Gamma[\frac{\ell+3}{2}]\,\Gamma[\frac{\ell_1+\ell_2}{2}]}{\Gamma[\frac{\ell}{2}]\,\Gamma[\ell_2+\frac{3}{2}]\,\Gamma[\frac{\ell_1-\ell_2+3}{2}]} x^{\ell_2} \times {}_2F_1\left(\frac{\ell_1+\ell_2}{2}, \frac{\ell_2-\ell_1-1}{2}; \ell_2+\frac{3}{2}; x^2\right) \qquad (2)$$

for $x < 1$

For x larger than unity, the following symmetry property is invoked to calculate the coupling coefficients,[21]

$$F^{\ell}_{\ell_1\ell_2}(x) = (sign\ x)^{\ell} F^{\ell}_{\ell_2\ell_1}(x^{-1}) \tag{3}$$

In equation 2, ${}_2F_1$ is the hypergeometric function, Γ is the gamma function, and $(:::)$ is a 3-j symbol. The variable $x = \alpha/\beta$ in the kinematic distribution function may be inferred from Fig. 1, where the molecular configuration of H_2S (on which the kinematic model is based) is shown schematically. The distance from the hydrogen (deuterium) atom to the SH (SD) center-of-mass is α. β is the distance from the SH (SD) center-of-mass to the intersection of the extension of the SH (SD) bond axis and the direction (**k**) of the hydrogen (deuterium) atom leaving the molecule. The ratio $x = \alpha/\beta$ indicates the direction in which the hydrogen (deuterium) atom is leaving the molecule, and hence, the recoil imparted to the SH (SD) fragment as a result of the dissociation of the hydrogen atom. From Fig. 1, it can be seen how the distance β changes as a function of the direction of **k**, which in turn causes x to vary. In principle, x can be calculated from the excited state geometry and recoil direction. In practice however, all the necessary information is not always available, and x is treated as a parameter along with ℓ_{max}, the maximum value of the total angular momentum, ℓ, of the system to fit the calculated $P(\ell_1)$ with experimental data. The total angular momentum, ℓ, is assumed to be non-zero in the present approach. The diatomic photofragment acquires a rotational state population distribution from the recoil interaction with the departing atom. We assume that the atom recoils with wavenumber k, and that its wave function may be approximated by a plane wave, exp(ikZ)[14,21]. The plane wave may be expanded in terms of the spherical wave basis functions,

$$e^{ikz} = \sum_{\ell} \ell \,|\ell 0, \hat{k}\rangle \tag{4}$$

where,

$$|\ell m, \hat{k}\rangle = (4\pi)^{\frac{1}{2}} i^{\ell} j_{\ell}(kr)\ Y_{\ell m}(\hat{k}) \tag{5}$$

Here $\hat{\ell} = (2\ell+1)^{1/2}$, and $j_\ell(kr)$ is a spherical Bessel function. This is in contrast to, *e.g.* the wave packet dynamic studies, in which one almost always assumes for computational simplicity, zero total angular momentum, such that the rotational angular momentum, ℓ_1, of the diatomic fragment SH, exactly cancels the orbital angular momentum, ℓ_2, of H with respect to SH. This simplification invariably causes an artificial, rapid oscillation in the computed rotational state distributions.[19] The maximum value of ℓ_1 of SH, allowed by the available energy and the rotational constant is *ca.* 45 at 193 nm. The maximum values of ℓ, ℓ_1, and ℓ_2 are confined by the triangular condition of angular momentum algebra. In our kinematic distribution approach, all the ℓ values up to ℓ_{max} must be summed in equation (1). The strong repulsive potential and the fragmentation of H nearly along the S-H bond suggests a wide range of ℓ_2. Thus, the triangular condition of angular momentum algebra implies a relatively large value of maximum ℓ. The dependence of the kinematic distribution function on these two variables was studied in detail in the previous work[18].

The experimentally measured rotational state population distributions are usually normalized to unity, whereas the kinematic distribution function (*cf.* equation 1), in general, is not normalized,

$$\sum_{\ell_1} P(\ell_1) = c \quad (\neq 1) \tag{6}$$

Thus, it remains to divide the kinematic distribution function by the constant, c, to compare it with the experimentally determined nascent rotational state population distributions.

3. Results and discussion

For the photodissociation of H_2S in its first absorption band, electronic structure calculations indicate the presence of two electronic states[15-19]. The rotational state population distribution obtained experimentally for the 193 nm photodissociation of H_2S and D_2S can be understood in light of these results. This is in contrast to the photodissociation of the water molecule in the first continuum, where the fragmentation proceeds via one dissociative potential energy surface.[22] In a previous study on the photodissociation of H_2S at 193 nm, we modified our kinematic distribution function to include the two dissociation channels[18], because the experimental rotational state population distribution could not be accounted for by a single

pathway. This requires modification of the total kinematic distribution to be the superposition of the kinematic distribution functions for the two dissociation channels[18].

$$P(\ell_1) = \omega_1 P_{x_1,\ell_{max}}(\ell_1) + \omega_2 P_{x_2,\ell_{max}}(\ell_1) \qquad (7)$$

where x_1 and x_2 correspond to different dissociation geometries in the two distinct channels, and ω_1 and ω_2 correspond to the fractional participation of each of the respective channels, such that $\omega_1 + \omega_2 = 1$. In a recent study on the photodissociation of NO_2, Chen and Pei analyzed the anomalous rotational state population distributions of NO photofragments in terms of a kinematic distribution function of the type given in Eq. (7), and successfully revealed a predissociative mechanism of the $^2B_2$ excited state of NO_2[23].

In Figure 2, the calculated rotational state population distribution of the SH fragment is compared with the experimental data[6] for the nascent diatomic fragment from photodissociation of H_2S at 193 nm. We have chosen to use the experimental data of reference [6], as opposed to the more recent data on rotational state distributions of SH following the 193 nm photodissociation of H_2S [12], because of the availability of information at other wavelengths. In this way, the comparison of the data at different wavelengths will be internally consistent.[24] We fit the experimental data by using the value of x_1 determined by the ground state geometry for the repulsive state (hereafter channel 1), and then parameterizing the geometry, x_2, of the bound state (hereafter channel 2) and the ℓ_{max}. In this case, we are defining $1/x_1 = 0.03$ with dissociation along the bond angle, which adequately reproduces the lower end of the rotational state population distribution. The best fit to the high end of the experimental data, shown in figure 2, is achieved with $1/x_2 = 0.09$, $\ell_{max} = 80$ and the branching ratio, $\omega_1:\omega_2 = 0.5:0.5$. Recent *ab initio* calculations by Heumann *et al.* require up to $\ell_1 = 25$ to obtain converged results in their wave packet dynamics calculations [19]. They assumed that the total angular momentum is zero, *i.e.* $-\ell_1 = \ell_2$. In our kinematic distribution approach, this would require that the summation over the total angular momentum, ℓ, in equation (1) be up to $|\ell_1 + \ell_2| = 50$. The value, $\ell_{max} = 80$, that is required to fit the rotational state distribution in our calculations, is higher than their value. Note that we do not see the rapid oscillations in our computed product distributions, which are commonly observed in wave packet dynamics calculations of diatomic

rotational state distributions resulting from photodissociation of polyatomic molecules.

Recent theoretical studies by Dixon, Marston and Balint-Kurti[15] and by Schinke and coworkers[16,17,19] have provided a great deal of insight into the problem. These theoretical calculations have clearly shown that the photodissociation of H_2S in the first absorption band proceeds via two electronic states, which are $^1B_1$ and $^1A_2$ symmetry in the C_{2v} point group. In the C_s point group, *i.e.* the two S-H bond distances are not equal, both of these two electronic states have $^1A''$ symmetry, and the two potential energy surfaces are not allowed to cross. Because of this avoided crossing, the lower adiabatic potential energy surface is now dissociative, while the upper one is bound. A substantial nonadiabatic coupling between them is expected to exist.

The previous theoretical models [15,16,17,19] are consistent with almost all of the observed features of the photodissociation process. The importance of these lie in their ability to rationalize the observed vibrational structure in the absorption spectra[25,26], the emission spectroscopy of the dissociating molecules[5,7,8], the energy distribution into vibrational, rotational and translational degrees of freedom of the photofragments[3,4,6,11,12], and the degree of anisotropy in the angular distribution of the birthing photodissociation products[3,11,12]. In our earlier study[18], we have used the kinematic distribution function to accurately model SH rotational state populations, and to show that there must be a significant dependence on the angle of the dissociating triatomic leading to rotational motion of the diatomic photofragments[18]. The only way to achieve any population of photofragments containing significant rotational angular momentum is via the change of geometry of the parent H_2S molecule prior to dissociation, *i.e.* a change in bond angle as well as bond length. As shown here, the rotational state population distribution for the high end ($\ell_1 \geq 6$) is due primarily to P_{x_2} dissociation. The chronology of channel 2 dissociation can be viewed as photoexcitation to the bound $^1A''$ surface where the molecule undergoes conformational reorganization on the timescale of a few vibrational periods, and subsequently couples with the continuum of the $^1A''$ dissociative surface. The results of a recent study by Schinke and coworkers supports this view [17,19]. Their *ab-initio* results clearly demonstrate that the nonadiabatic coupling between the two states increases dramatically as the bending angle increases, and that this angular dependence can have significant effects on the rotational motion of the recoiling molecule.

In Figure 3, the calculated rotational state population distribution of the SH fragment is compared with the experimental data[6] for the diatomic fragment from photodissociation of H_2S at 222 nm. With all the parameters (except the branching ratio) fixed as in the 193 nm case, the calculated rotational state population distributions with $\omega_1:\omega_2=0.33:0.67$ gives excellent agreement with the experimental data. The parameters can be fixed because the parent triatom always contains the same average angular momentum prior to photolysis, and the orbital angular momentum gain is assumed to be the same for photoactivation at all wavelengths.

van Veen, *et al.*, [3] have reported lower limit excited state lifetimes of $\leq 10^{-14}$ and 1.8 x 10^{-14} s for photoactivated H_2S at 193 and 222 nm, respectively. These lifetimes, on the order of a few vibrational periods, have been verified by Xie, *et al.* [12], and are consistent with our calculated results here. In the 193 nm case, the shorter lifetime of the photoactivated H_2S implies greater direct excitation to the dissociative state, and less average time spent in the bound $^1A''$ state. Recently, Schinke and coworkers show that 193 nm excitation results in *ca.* 100% in the bound excited state.[19] If this is so, then our results can be interpreted as strong overlap in the Franck-Condon region, leading to dissociation in less than a vibrational period. Channel 2 would correspond to dissociation after several vibrational periods. For the 222 nm case, a larger contribution due to channel 2 is found. This correlates with the longer lifetime observed in reference [3]. Consistent with this explanation, is the increased proportion of vibrational excitation (0.078 vs. 0.04) with respect to the available energy in the 222 nm versus 193 nm photodissociation.

The experimental data available for still longer wavelengths, *i.e.* 248 nm, appear, at first glance, to be contradictory. van Veen, *et al.*[3] have measured significantly less vibrational excitation (0.017) with respect to the available energy, but at the same time a longer lifetime (3.3×10^{-14}s) for the H_2S photoactivated at 248 nm. The longer lifetime seems to imply, based on the arguments thus far presented, that there is an even greater participation from channel 2. However, it is possible that at 248 nm, excitation may be primarily due to the dissociative state, and that the increased lifetime arises due to the proximity of a small barrier caused by the avoided crossing.[16,17] Our results are consistent with this explanation. By comparing the experimental and calculated rotational state distributions, and keeping all the parameters except the branching ratio fixed, we obtain a best fit for $\omega_1:\omega_2=0.67:0.33$.

Isotopic substitution may provide additional support for the degree of non-adiabatic coupling. Figures 4 and 5 compare the calculated and experimental rotational state population distribution of the SD fragment from D_2S photodissociation at 193 and 222 nm, respectively. The channel 1 component dominates the rotational state distributions for low ℓ_1, and thus, to get reasonable fits, a value of $1/x_1=0.029$ was used for D_2S. This differs from the ground state configuration value of $1/x_1=0.058$, which corresponds to a bond angle change of less than 2°. The maximum total angular momentum has been changed by a factor of $\sim\sqrt{2}$ to $\ell_{max}=110$, to compensate for the doubling of the mass. By fixing $1/x_1=0.029$ and $\ell_{max}=110$, we obtain a best fit for the higher ℓ_1 experimental data by using $1/x_2=0.105$, and $\omega_1:\omega_2$ = 0.33:0.67 and 0.07:0.93 for the 193 and 222 nm photodissociations of D_2S, respectively.

As in the H_2S case, an increase in the participation of channel 2 is observed for a longer photolysis wavelength in the D_2S photodissociation. The branching ratios we obtain, most likely represent the degree of initial photoexcitation into the two excited states (*i.e.* the differences in the Franck-Condon factors associated with the transitions to the two excited state surfaces). The dramatic increase in channel 2 participation in the 222 nm photodissociation of D_2S suggests that a much longer lifetime of the photoactivated species is involved. This should be reflected by increased vibrational structure in the D_2S absorption spectrum, but is not observed. One possible explanation is that there may not be a significant increase in lifetime, because the non-adiabatic coupling is indeed larger for D_2S than for H_2S. This could arise from the presence of lower frequency modes in the isotopically substituted species. It would be an interesting experiment for those groups that do photofragment anisotropy studies, to measure the lifetime of the D_2S following photoactivation at 222 nm.

In conclusion, the results presented here clearly show that the kinematic distribution function, when used in conjunction with the experimental rotational state population distribution, can provide information about the degree of participation of different adiabatic surfaces in the presence of non-adiabatic coupling among them during a photochemical reaction. Even for the case of hydrogen sulfide photodissociation, where >98% of the available energy is partitioned into translational degrees of freedom, sensitive measurements of the internal energy distribution of the diatomic fragment provide a unique insight into the mechanisms of dissociation. This information not only helps unravel a detailed dissociative mechanism, but also gives information

about the degree of non-adiabatic coupling between the two surfaces. Finally, the kinematic distribution model here provides insight into the wavelength dependent photodissociation of H_2S, but we wish to ***stress*** that the true power of the model lies in systems of greater complexity where *ab initio* potentials are not available. For example, we are currently implementing the model to study the nascent rotational distributions of sulfur monoxide deriving from the 193 nm photodissociation of SO_2.

4. Acknowledgements

We would like to acknowledge the generous support of this project by the Air Force Office of Scientific Research(Contract No. F49620-89-C0070). NSF (through the Puerto Rico EPSCoR) and NASA (through the Capability Enhancement Grant) also provided partial support..

5. Figure Captions

Figure 1: A schematic representation of the photodissociating $H_2S(D_2S)$ molecule. The H(D) is depicted leaving along the unit vector, **k**. the kinematic distribution function is based on the parameter $x=\alpha/\beta$. For more details, see text.

Figure 2: Comparison of the calculated best fit (○) and experimental (●) rotational state distribution of the $SH(^2\Pi)$ photofragment from the 193 nm photodissociation of H_2S. More details about the calculated best fit data are given in the Results and Discussion section.

Figure 3: Comparison of the calculated best fit (○) and experimental (●) rotational state distribution of the $SH(^2\Pi)$ photofragment from the 222 nm photodissociation of H_2S. For more details about the calculated best fit data, see text.

Figure 4: Comparison of the calculated best fit (○) and experimental (●) rotational state distribution of the $SD(^2\Pi)$ photofragment from the 193 nm photodissociation of D_2S. More details about the calculated best fit data are given in the Results and Discussion section.

Figure 5: Comparison of the calculated best fit (○) and experimental (●) rotational state distribution of the $SD(^2\Pi)$ photofragment from the 222 nm photodissociation of D_2S. For more details about the calculated best fit data, see text.

6. References

1. R. Bersohn, *J. Phys. Chem.* **88** (1984) 5145.
2. W.G. Hawkins and P.L. Houston, *J. Chem. Phys.* **73** (1980) 297; **76** (1982) 729.
3. G.N.A. van Veen, K.A. Mohamed, T. Baller and A.E. de Vries, *Chem. Phys.* **74** (1983) 263.
4. Z. Xu, B. Koplitz and C. Wittig, *J. Chem. Phys.* **87** (1987) 1062.
5. K. Kleinermanns, E. Linnebach and R. Suntz, *J. Phys. Chem.* **91** (1987) 5543.
6. B.R. Weiner, H.B. Levene, J.J. Valentini and A.P. Baronavski, *J. Chem. Phys.* **90** (1989) 1403.
7. M.D. Person, K.Q. Lao, B.J. Eckholm and L.J. Butler, *J. Chem. Phys.* **91** (1989) 812.
8. R.J. Brudzynski, R.J. Sension and B. Hudson, *Chem. Phys. Lett.* **165** (1989) 487.
9. X. Xie, L. Schneider, H. Wallmeier, R. Boettner, K.H. Welge and M.N.R. Ashfold, *J. Chem. Phys.* **92** (1990) 1608.
10. L.J. Butler, *Chem. Phys. Lett.* **182** (1991) 393.
11. R.E. Continetti, B.A. Balko, and Y.T. Lee, *Chem. Phys. Lett.* **182** (1991) 400.
12. M.N.R. Ashfold, L. Schneider and K.H. Welge, *Faraday Discuss. Chem. Soc.* **91**, (1991) 812.
13. K.C. Kulander, *Chem. Phys. Lett.* **103** (1984) 373.
14. K. Chen and C. Pei, *Chem. Phys. Lett.* **134** (1987) 259.
15. R.N. Dixon, C.C. Marston and G.G. Balint-Kurti, *J. Chem. Phys.* **93** (1990) 6520.
16. K. Weide, V. Staemmler and R. Schinke, *J. Chem. Phys.* **93** (1990) 861.
17. B. Heumann, R. Düren and R. Schinke, *Chem. Phys. Lett.* **180**, 1991, 593.
18. L. Muñoz, Y. Ishikawa and B.R. Weiner, *Int. J. Quantum. Chem.* **S25** , 1991, 359.
19. B. Heumann, K. Weide, R. Düren and R. Schinke, *J. Chem. Phys.* **98** (1993) 5508.
20. K. Chen and C. Pei, *Chem. Phys. Lett.* **124** (1986) 365.
21. K. Schulten and R.G. Gordon, *J. Chem. Phys.* **64** (1976) 2918..
22. P. Andresen and R. Schinke in *Molecular Photodissociation Dynamics*, Eds. M.N.R. Ashfold and J.E. Baggott, Royal Society of Chemistry, London, 1987, pp. 61-113.
23. K. Chen and C. Pei, *Chem. Phys. Lett.* **137** (1987) 361.
24. We recognize that we are underestimating the nascent population in the higher rotational levels as shown in reference 12. Use of the rotational state distribution reported in reference 12 leads to a slightly larger value of ω_2, but the conclusions we reach remain unchanged.

25. H.-T. Wang, W.S. Felps, and S.P. McGlynn, *J. Chem. Phys. 67 (1977) 2614.*

26. L.C. Lee, X. Wang, and M. Suto, *J. Chem. Phys.* **86** (1987) 4353.

Figure .

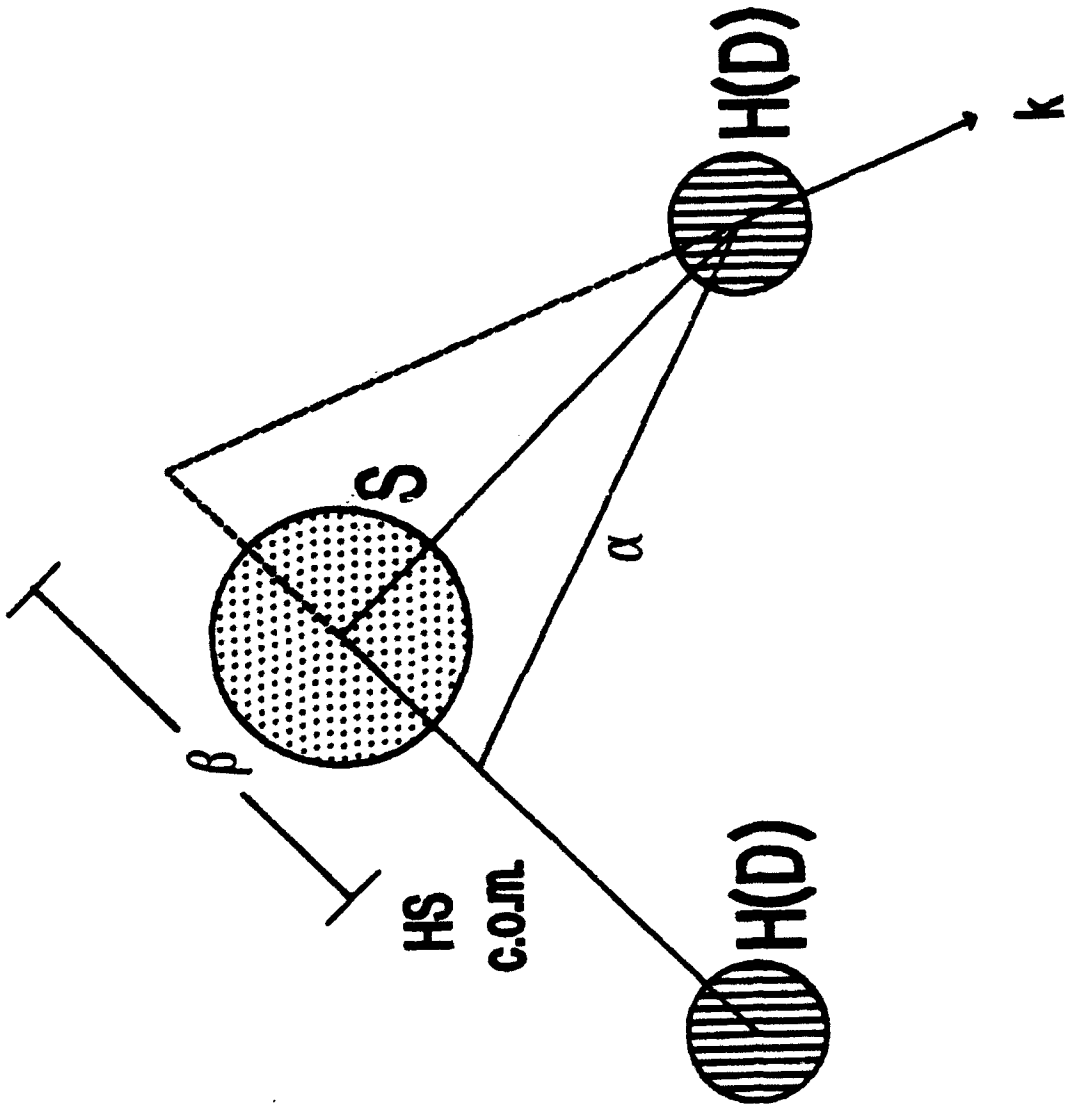

Figure 1

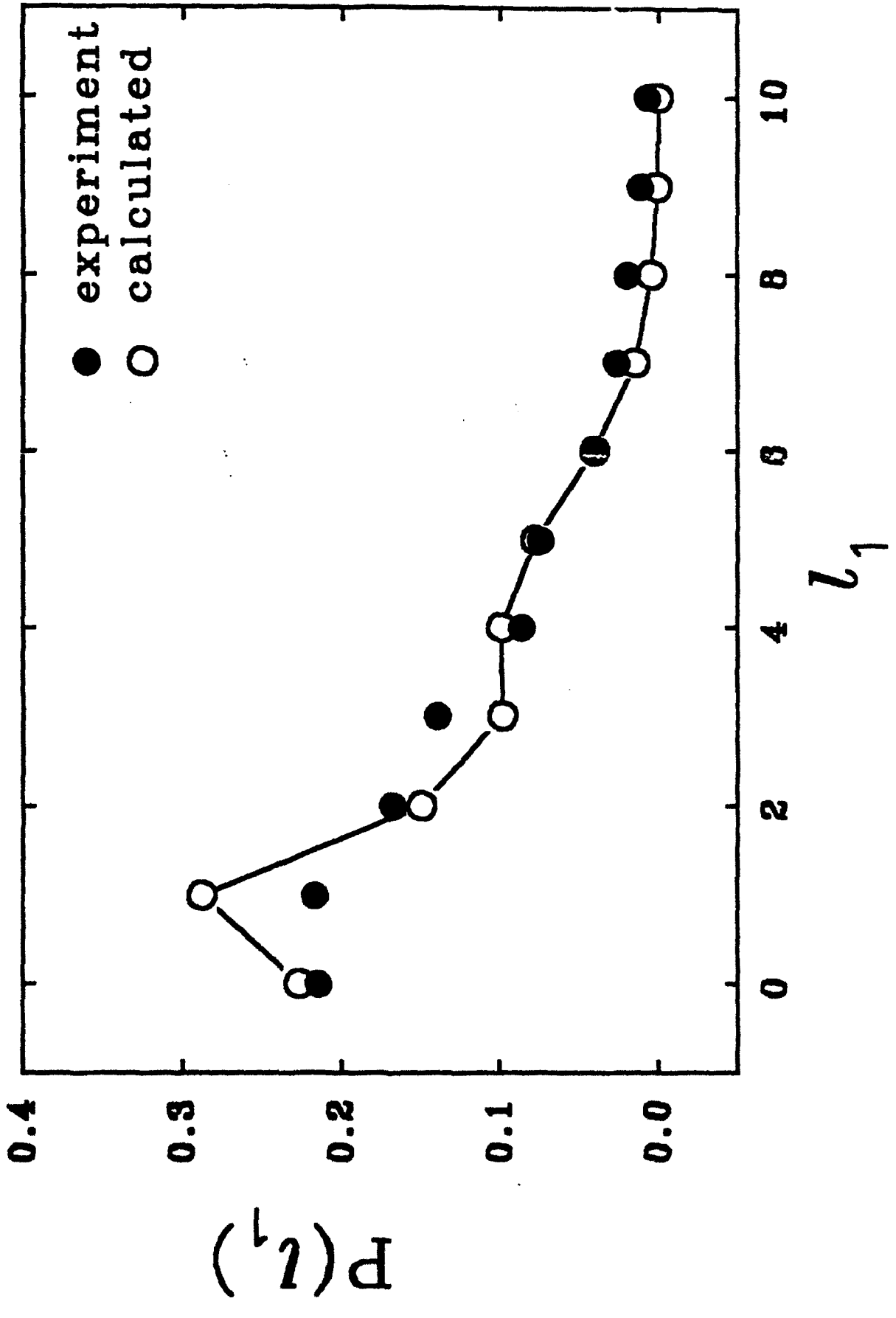

Figure 3

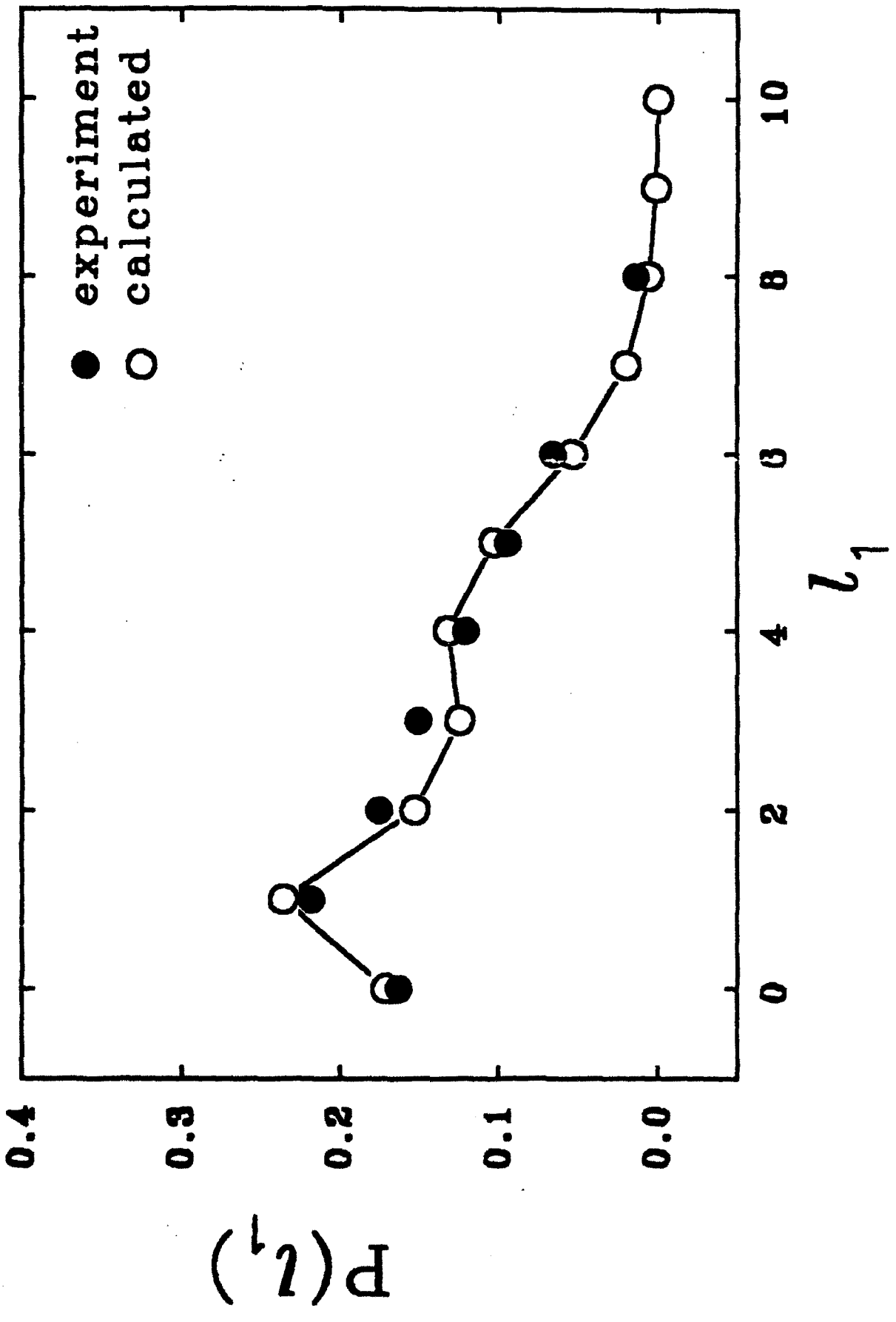

Figure 4

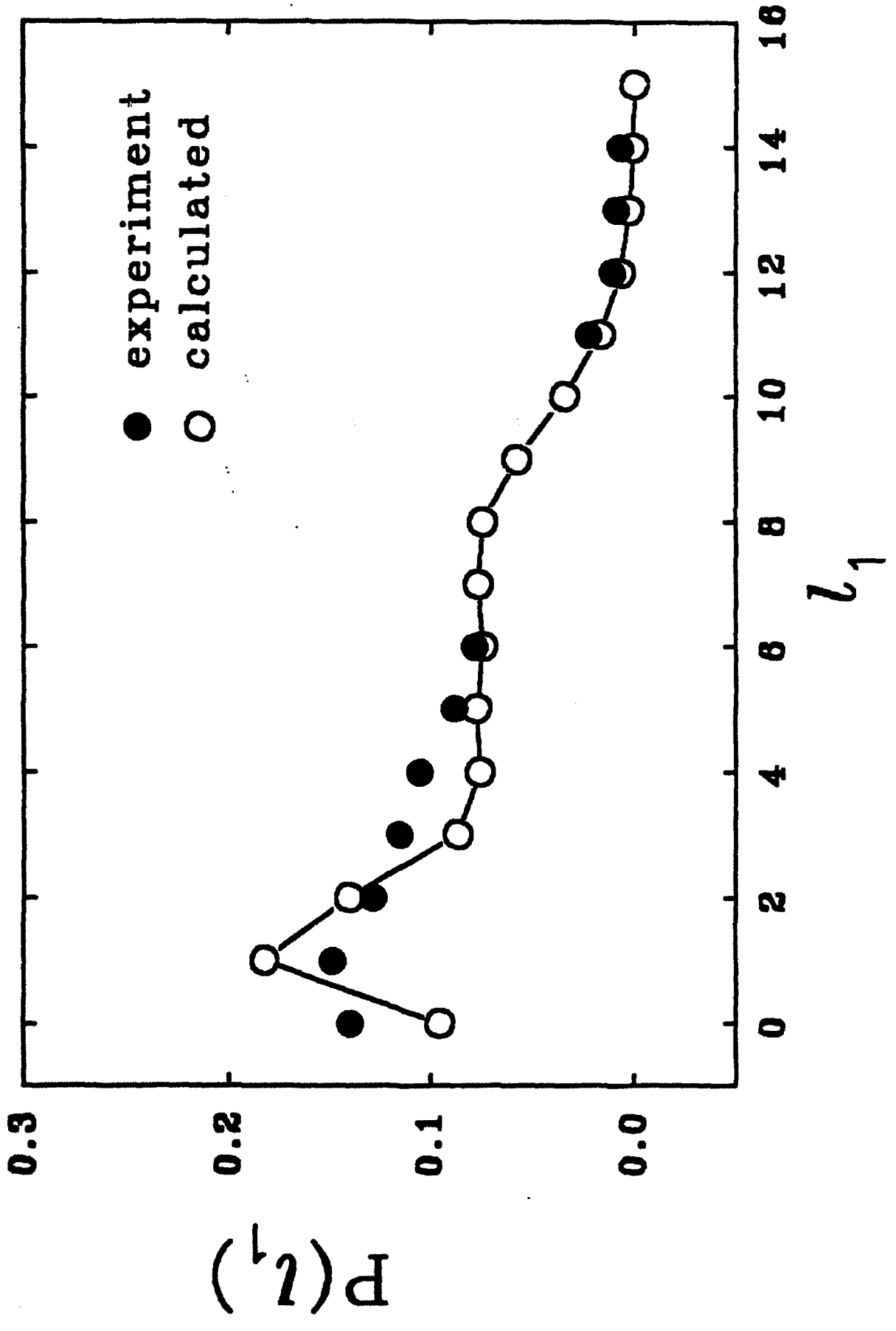

Figure 5

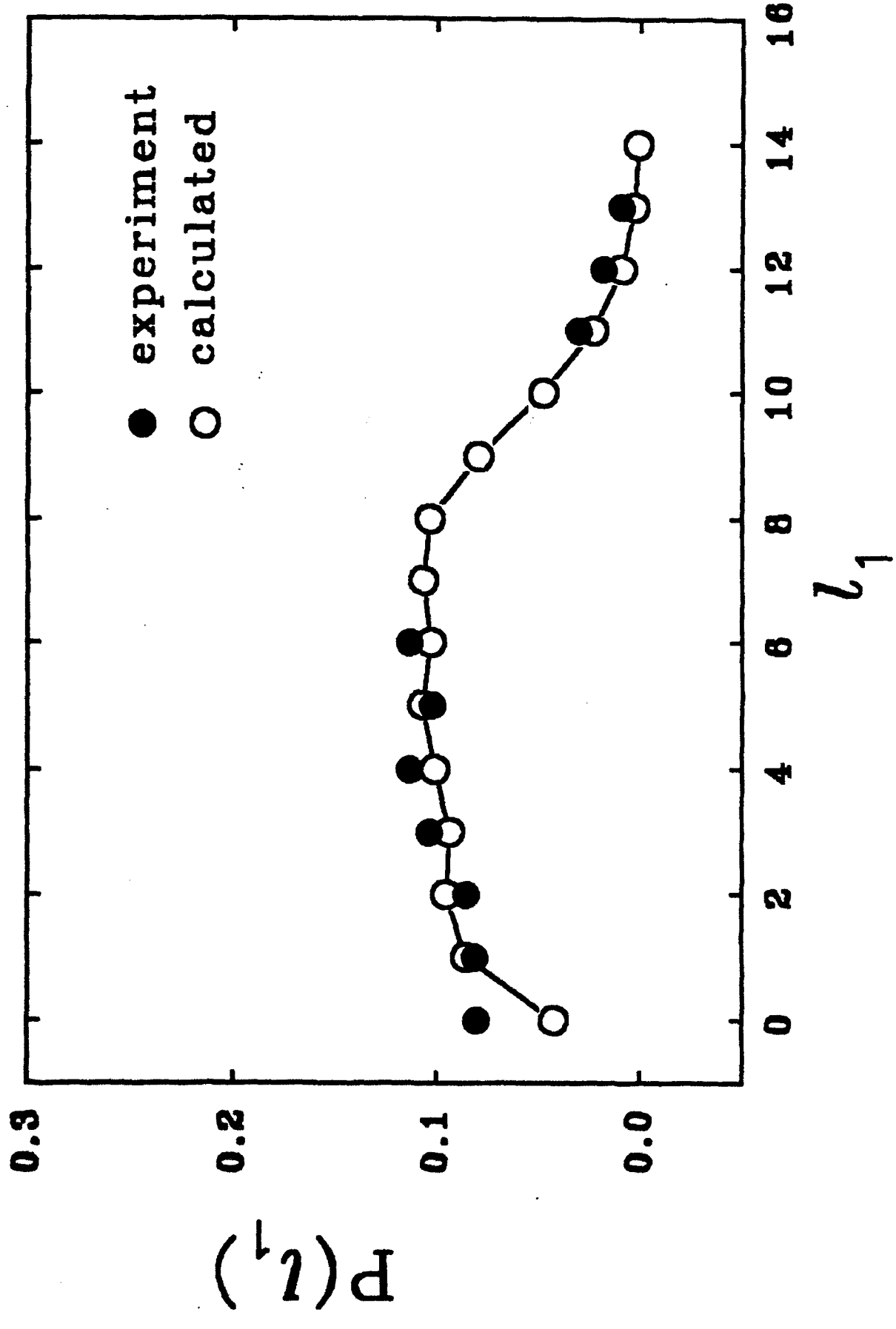

J. Phys. Chem
in press

LASER PHOTODISSOCIATION DYNAMICS OF THIONYL CHLORIDE: CONCERTED AND STEPWISE CLEAVAGE OF S-Cl BONDS

Hongxin Wang, Xirong Chen and Brad R. Weiner*

Department of Chemistry and Chemical Physics Program
University of Puerto Rico
Box 23346 UPR Station
Río Piedras, PR 00931

Abstract

The photodissociation of thionyl chloride (Cl_2SO) is of interest as a model system to study three-body fragmentation processes, which can occur either in concert or stepwise. The photodissociation of this tetratomic molecule at 193 and 248 nm has been studied by laser induced fluorescence spectroscopy of the nascent SO fragment on the $B^3\Sigma^-$-$X^3\Sigma^-$ transition in the region of 237-295 nm. Photolysis of Cl_2SO at 193 nm leads to an inverted vibrational distribution for the nascent $SO(X^3\Sigma^-)$ with a population maximum at $v''=2$. The quantum yield, $\Phi_{SO(X)}^{193\,nm} = 0.73 \pm 0.10$, has been measured by comparison of the $SO(X^3\Sigma^-)$ produced from SO_2. The results indicate a concerted three-body fragmentation mechanism as the primary dissociation channel. A Franck-Condon/golden rule model elucidates the geometry prior to the fragmentation and suggests a direct dissociation mechanism. The rotational and spin state distributions have been measured from the rovibronically resolved spectra to support our model of the detailed dissociation mechanism. At 248 nm, the nascent vibrational distribution was found to be bimodal. The vibrational state population distribution in $v''=0$-2, which accounts for most ($\sim$94%) of the nascent $SO(X^3\Sigma^-)$ population, was found to be thermal ($T_{vib}=1000\pm200$K), suggesting a stepwise fragmentation process. About 6% of the nascent SO population has been observed in other vibrational levels ($v''=3$-7), and most likely originates from the molecular elimination of Cl_2 from Cl_2SO.

* To whom correspondence should be addressed.

LASER PHOTODISSOCIATION DYNAMICS OF THIONYL CHLORIDE: CONCERTED AND STEPWISE CLEAVAGE OF S-Cl BONDS

Introduction

Real time descriptions of chemical processes have drawn a great deal of attention recently in dynamical studies of various chemical reactions, particularly in photodissociation reactions[1]. Photodissociation of molecules can be separated, in principle, into two major processes[2]. The first step is the electronic excitation of the parent molecule through the absorption of a photon, in which the initial conditions for the nuclear motion in the excited electronic state are defined[2]. The second step refers to the spontaneous decay of the parent molecule in the excited state into the nascent products and is known as the final state interaction[2]. For a photodissociation process producing three fragments, the concepts of concertedness and/or synchronicity need to be considered. A stepwise reaction is defined as one which occurs in two kinetically distinct steps via a long-lived intermediate, while a concerted reaction is one which proceeds in a single kinetic step[3]. Some concerted reactions can be synchronous, *i.e.* where all the bond breaking events take place with exactly the same rate and in phase[4]. In a multiple bond-breaking photodissociative event, such as ABCD → AB + C + D, if the bonds in the parent molecule fragment within a given time, the process is considered to be in concert, otherwise it is stepwise[5]. This defined time can be determined for the molecule itself[5]. For the limiting case of a concerted dissociation, where ABCD fragments into AB + C + D synchronously, the spatial angular distribution of the fragments would be narrow. In the opposite case, a stepwise dissociation, where D was to dissociate first while ABC rotates freely

about its center of mass prior to its dissociation, an isotropic spatial angular distribution of fragment C would result. Therefore, the rotational period of the ABC intermediate provides an accepted criterion for distinguishing between a concerted and a stepwise process[5]. This can be elucidated experimentally by measuring the spatial anisotropy of the fragments.

The tetratomic molecule, thionyl chloride (Cl_2SO), offers an excellent test case for three-fragment photodissociation studies[6,7,8]. Several previous studies have examined various aspects of the electronic structure of and photodissociation dynamics of Cl_2SO[6,7,8,9]. The ground state molecular structure has been determined by Suzuki *et al.* by using microwave spectroscopy[9]. The UV absorption spectrum of Cl_2SO shows an origin near 300 nm with two absorption maxima at 194 nm ($\sigma = 1.3 \times 10^{-17}$ cm^2) and 244 nm ($\sigma = 7.1 \times 10^{-18}$ cm^2)[10]. These absorption maxima have been assigned previously to $n_{Cl} \rightarrow \sigma_{S\text{-}Cl}^*$ and $n_S \rightarrow \sigma_{S\text{-}Cl}^*$ type electronic transitions, respectively, by comparison with molecular orbital calculations[6,11]. The vacuum UV absorption spectrum and photochemistry of Cl_2SO between 116 and 135 nm has also been studied by Okabe[12]. Flash photolysis of this tetratomic molecule was first investigated in the far UV region by Donovan *et al.* by using transient absorption spectroscopy[13]. Kawasaki *et al.* used photofragment time-of-flight spectroscopy to investigate the excimer laser photodissociation process of thionyl chloride[6]. They found evidence for two distinct SO-producing channels in the 193 nm photolysis of Cl_2SO: three body fragmentation to give two Cl atoms and molecular elimination of Cl_2. Emission spectra in the region of 220-340 were observed and assigned to SO(B→X) and Cl_2(B→X) transitions following the 248 nm irradiation of Cl_2SO[6]. These spectra most likely arise from secondary 248 nm excitation of the nascent SO and Cl_2

fragments. No information about SOCl was reported. Baum *et al.* have studied the photodissociation of Cl_2SO at both 193 and 248 nm, once again by using photofragment time-of-flight translational spectroscopy and probing at *m/e* = 35, 48, 70 and 83 corresponding to Cl, SO, Cl_2 and SOCl, respectively[8]. Their experiments lead to the following branching ratios for the ultraviolet photodissociation[8].

		PRODUCTION YIELD[8]		
$Cl_2SO + h\nu$	ΔH_{rxn} (kcal/mol)	At 248 nm	At 193 nm	
→ SOCl + Cl	57.3	96.5%	17%	(1)
→ SO + Cl_2	51.3	3.5%	3%	(2)
→ SO + Cl + Cl	108 .5	---	80%	(3)

A schematic energy diagram based on the previously reported data[8,14] was developed and is shown as Fig. 1. In the photodissociation of Cl_2SO at 248 nm, channels (1) and (2), with a branching ratio of 30:1, are the only operative reactions[8]. In the molecular elimination channel, the nascent products of $SO(b^1\Sigma^+)$ and $SO(X^3\Sigma^-)$ were found to have a ratio of 9:1. No three body dissociation, (3), has been observed[8], even though it is energetically feasible following absorption of a 248 nm photon (115 kcal/mol)[8,14]. An energy barrier may exist to prevent such a photochemical process from proceeding directly. At 193 nm, Baum *et al.* found that about 17% of the photoactivated Cl_2SO molecules undergo single bond fission, (1), and less than 3% proceed via the molecular elimination channel, (2). Following the homolytic cleavage (1), there may be further fragmentation of SOCl into SO and Cl, either through a

unimolecular decay or via a secondary photodissociation. Both of these possibilities were ruled out by experiments of Baum *et al.*[8]. The possibility of further fragmentation of Cl_2 into two Cl atoms was eliminated as well[8]. The authors thus concluded that the remaining 80% of photoactivated Cl_2SO undergoes a three-body dissociation (3).

Hirota and coworkers employed 193 nm photolysis of Cl_2SO as a source for infrared diode laser absorption studies of $SO(a^1\Delta)$, which lies 18 kcal/mole above the ground state $SO(X^3\Sigma^-)$.[15] They found a branching ratio of 1:4 for $SO(a^1\Delta)$ to $SO(X^3\Sigma^-)$. The $SO(a^1\Delta)$ radicals were produced with significant vibrational (up to $v''=5$) and rotational (up to $N''=40$) excitation. Stuart *et al.* have investigated the saturation of SO(A-X) excitation following the photodissociation of Cl_2SO with both narrow and broad band KrF laser emission[16]. They measured SO(A-X) absorption saturation fluence, and determined the efficiency of $SO(A^3\Pi)$ excitation with possible applications to an ultraviolet energy storage laser. No photodissociation mechanism of Cl_2SO was discussed in their report.

Investigation of the energy disposal into the rovibronic states of the nascent fragment or fragments from the photodissociation of molecules can reveal the detailed dissociation mechanisms[7,17]. In the case of multiple bond breaking in a polyatomic molecule, this can help distinguish whether the process occurs in a concerted or in a stepwise manner[7,17]. While the previous experiments have addressed the branching ratio from Cl_2SO photolysis based on photofragment translational spectroscopy, the internal state distributions of the nascent fragments are almost unknown. A nascent vibrational distribution of $SO(X^3\Sigma^-,v'')$ from the photolysis of Cl_2SO at 193 nm was recently described by us in a letter[7]. However, no rotational state distributions of the nascent $SO(X^3\Sigma^-)$ have been previously reported and no detailed dissociation

mechanism, related to the energy disposal into the internal states of the nascent fragments, has been addressed. We report here our measurements on the nascent vibrational, rotational and spin state distributions and the quantum yield of the nascent $SO(X^3\Sigma^-)$ following excimer laser photolysis of Cl_2SO at 193 and 248 nm. The $SO(X^3\Sigma^-, v''=0\text{-}7)$ was observed directly by using laser induced fluorescence (LIF) spectroscopy on the $B^3\Sigma^- X^3\Sigma^-$ transition. These data provide valuble insight towards a more complete understanding of the 193 and 248 nm photodissociation of thionyl chloride.

Experimental

The experiments were performed in a standard laser pump-probe apparatus, which has been described in detail previously[7,18]. Briefly, the purified sample, either neat or in buffer gas, was flowed through a glass four-way cross which serves as the reaction chamber. The glass cross is extended with glass arms at each side, along the laser axis, to reduce the scattered light. Gas inlets are located on the extension arms while the outlet to the vacuum is located near the reaction zone. Heterogeneous decomposition of Cl_2SO was minimized by using only glass, polyethylene and stainless steel components for the reaction cell and the inlet system[8]. The system was passivated for about 0.5 hours before the experiment. The reaction cell was pumped to a vacuum of 10^{-3} Torr by a mechanical pump and the pressure of the chamber was measured at the exit by a capacitance manometer.

In our experiments, the reactant vapor, Cl_2SO, was photolyzed with either the 193 nm (25-30 mJ/cm^2) or 248 nm output (60-70 mJ/cm^2) of an excimer laser

(Lambda Physik LPX205i), operating on the ArF and KrF transitions, respectively. Nascent SO radicals were monitored by laser induced fluorescence (LIF) spectroscopy on the $B^3\Sigma^- - X^3\Sigma^-$ transition in the 237-295 nm region of the spectrum. The probe laser in this region was generated by frequency doubling (β-BaB_2O_4 crystal) the output of a Lambda Physik FL3002 tunable dye laser (dyes used: Coumarin 460, Coumarin 480, Coumarin 503 and Coumarin 540A), which was pumped by a Lambda Physik LPX205i excimer laser operated at 308 nm. The two lasers were collinearly counterpropagated along the extension arm axis to maximize the overlap region in the center of the reaction cell. Laser induced fluorescence was viewed at 90° relative to the laser beam axis by a high gain photomultiplier tube through longpass filters (Schott WG295, WG305). The output of the photomultiplier tube was processed and averaged by a gated integrator (Stanford Research System (SRS); model SR250), digitized (SRS; model 245) and sent to a personal computer for screen display, data storage and analysis. The delay time between the two lasers was controlled with a digital delay pulse generator (SRS; model DG535) and was fixed between 300-2000 ns while the frequency-doubled output of the dye laser was scanned to collect the total fluorescence signal to obtain a nascent LIF excitation spectrum. The photolysis laser was operated at a repetition rate of 40 Hz and each data point represents the average of 10 laser shots. The LIF intensity was found to be linear as a function of dye laser power, and the signals, taken over a large wavelength region, were normalized to the dye laser power.

Commercial thionyl chloride (Fluka, ≥99.5%) was purified by doubly distilling under vacuum which leads to a colorless liquid. The sample was prepared on a vacuum line containing only glass and stainless steel. To remove possible SO_2

impurities[6,8], the sample was continuously pumped at 0°C for several minutes before a day's experiments. The residual SO_2 in a gas phase sample during the experiments was found to be less than 1% by using laser induced fluorescence monitoring of SO_2. Sulfur dioxide (Air Products, 99.8%) was used directly as supplied, as a calibrant and as an actinometer in the quantum yield experiments. Helium (General Gases, 99.9%) was used directly, without further purification.

Results

1. Vibrational State Distribution of Nascent SO($X^3\Sigma^-$)

The vibrational state population distributions of the nascent SO($X^3\Sigma$, v'') resulting from the photodissociation of Cl_2SO at 193 and 248 nm have been determined by using LIF excitation spectroscopy on the SO($B^3\Sigma^-$-$X^3\Sigma^-$) transition in the region of 237-295 nm (see Fig. 2). The vibrational bands terminating on the $v' = 1$ level of the B state, (1, v''=0-7), were used to determine the nascent vibrational population. Assignment of these bands was accomplished by using Colin's spectroscopic data[19]. The measured integrated band areas under this spectrum were analyzed and normalized for Franck-Condon factors of the SO($B^3\Sigma^-$-$X^3\Sigma^-$) transition to obtain the relative vibrational state populations of SO($X^3\Sigma^-$,v'' =0-7)[20]. While some discrepancy about the accuracy of the Franck-Condon factors in the SO($B^3\Sigma^-$-$X^3\Sigma^-$) transition exists for higher vibrational levels ($v'>6$) of the upper electronic state, the calculations for $v' \leq 6$ have been shown to be reliable through agreement with values obtained from Morse potential curves.[20] In the 193 nm photodissociation of thionyl chloride, the LIF excitation spectrum was obtained under collision-free conditions

(0.020 Torr Cl_2SO, 400 ns probe delay). For the 248 nm photodissociation experiments, a 1 μs delay time was the minimum possible due to the strong scattered light and secondary fluorescence from the pump laser. Helium (*ca.* 1 Torr) was blown onto the reaction cell windows to minimize deposit build-up that would subsequently reduce the amount of UV laser light passing into the cell. Consequently, each SO radical undergoes *ca.* 10 gas phase collisions prior to detection. While these collisions may affect the nascent rotational state distributions (see below), the vibrational state population distributions are virtually unperturbed. This result has been confirmed by recent studies of the vibrational relaxation of sulfur monoxide in this laboratory, which shows approximately 10^4 gas phase collisions in helium are required to completely thermalize the SO vibrational state distribution.[21]

In the case of 193 nm photolysis, the vibrational state distribution of the nascent $SO(X^3\Sigma^-)$ has previously been reported by this laboratory[7]. In those experiments, the nascent $SO(X^3\Sigma^-)$ photofragment was probed by LIF spectroscopy on the $A^3\Pi$-$X^3\Sigma^-$ electronic transition[7]. In the present experiments, the B-X transition as opposed to the A-X transition was monitored to improve our sensitivity for the higher vibrational levels due to the larger Franck-Condon factors[20]. The nascent vibrational state population of the $SO(X^3\Sigma^-)$ following the 193 nm photolysis (see Table I and Fig. 3) has been observed up to $v'' = 6$ and the distribution has been found to be inverted with a population maximum of $35 \pm 6\%$ at $v'' = 2$. However, the nascent population may peak in the adjacent state of $v'' = 1$ ($30 \pm 8\%$). This observation is different from the result previously reported by Chen *et al.*[7], where an inverted nascent vibrational distribution with a population maximum at $v'' = 3$ was observed. The discrepancy in the measurements might be due to the weakness of the

A-X transition and the spectral overlap between the A-X and the B-X transitions. It may also have resulted from decomposition and/or SO_2 impurities in the Cl_2SO sample in the previous study.

Following the 248 nm UV irradiation of Cl_2SO, a bimodal vibrational state distribution has been found for the nascent $SO(X^3\Sigma^-)$ fragment, as shown in Table I and Fig. 4. In this case, the majority of the nascent $SO(X^3\Sigma^-)$ population (94%) was found in $v''=0$-2, while the remaining 6% populated $v''=3$-7 with a second peak at $v''=5$. The signal intensity in several vibrational states, *e.g.* (1,1) and (1,5) transition band, have been measured as a function of the photolysis laser fluence and, in all cases, was found to be linear, suggesting a single photon process in the production of all the nascent $SO(X^3\Sigma^-)$ fragments. The nascent population in the first three vibrational levels ($v''=0$-2) of the $SO(X^3\Sigma^-)$ radicals can be fit to a Boltzmann distribution:

$$P(v'') \propto \exp[-E_{vib}/K_B T_{vib}], \qquad (4)$$

where E_{vib} is the vibrational energy of the corresponding levels. The vibrational temperature, T_{vib}, was found to be 1000 ± 200K.

2. *Rotational State Distribution of Nascent $SO(X^3\Sigma^-)$*

The $SO(B^3\Sigma^- - X^3\Sigma^-)$ LIF spectra, (*e.g.* Fig. 5 and Fig. 6), have been used for the measurement of rotational state population distributions following the 193 nm photolysis of Cl_2SO. Only six branches, namely P_{11}, P_{22}, P_{33}, R_{11}, R_{22}, R_{33}, are strongly allowed for the SO(B-X) transition[19,22,23]. P_{22} and R_{22} were resolved for $N>10$ and 15, respectively (*e.g.*, see Fig. 6), for our maximum spectral resolution (*ca.* 0.25 cm^{-1}). The assignment of these partially resolved spectra was made by calculating the

transition frequencies based on Colin's spectroscopic constants[19]. The experimental spectra were calibrated by adjusting the bandheads to the literature values. The agreement between calculated rotational line positions and the experimental positions was within 1 cm^{-1}.

The population of a single rovibrational state P(v", N") is related to the observed intensity of the LIF rovibronic transition, I(v', N' - v", N"), by[22]:

$$P(v", N") = I(v', N' - v", N") \cdot g(J") / S(N', N") \quad (5)$$

where S(N', N") is the Hönl-London factor[24] and g(J") is the rotational degeneracy, (2J" + 1). The nascent rotational state population for the vibrational bands of (1, n), where n = 1-3, could be directly obtained from P_{22} and/or R_{22} (*cf.* Fig. 6), because these two branches are nearly resolved for the higher rotational levels, N > 10. By mapping our observed rotational state distribution on a Boltzmann plot, *i.e.* ln[P/g(J")] vs. E_r(N"), we can obtain a linear least square fit, with a slope of $-1/kT_{rot}$, from which rotational temperatures, T_{rot}, for the nascent SO($X^3\Sigma^-$) result. All the observed rotational state distributions for the nascent SO(X, $v"$ = 1-3) from the photodissociation of Cl_2SO at 193 nm can be described by a Boltzmann distribution (Fig. 7). The rotational temperatures of the nascent SO($X^3\Sigma^-$) for $v"$ = 1-3 were obtained and listed as follows:

$v"$	1	2	3
T_{rot}	1800 ± 400 K	1400 ± 300 K	1300 ± 300 K

The rotational state population of the nascent SO($X^3\Sigma^-$) in the lower rotational levels, *i.e.*, N < 10, cannot be obtained directly from the spectrum because the corresponding spectral lines were not resolved. This problem was addressed by spectral simulation. A Boltzmann rotational state distribution with a trial temperature

and a Gaussian profile (FWHM = 0.25 cm^{-1}) for the spectral lines were assumed to simulate the observed LIF spectra. The spectral simulation, using the temperature obtained from the Boltzmann plot of the rotational state distribution at the higher rotational levels, yields a close resemblance to the LIF spectrum of the complete vibrational band, as shown in Fig. 5.

Rotational state distributions of SO(X, $v''=4,5$) were difficult to obtain due to strong overlap of the rovibronic lines in the (1, 4) and (1, 5) vibrational bands. The nascent rotational state distribution for $v''=0$ was also not measured because the signal-to-noise ratio was too small to give reliable data. For the photodissociation of Cl_2SO at 248 nm, no nascent rotational state population distribution for the SO($X^3\Sigma^-$) has been measured because the radicals encounter *ca.* 10 gas phase collisions (20 mTorr Cl_2SO; 1 Torr He; 1 μs delay) prior to detection and the corresponding rotational state distributions were, at least partially, relaxed.

3. *Spin State Distributions of Nascent SO($X^3\Sigma^-$)*

For the nascent SO($X^3\Sigma^-$) resulting from the photodissociation of Cl_2SO at 193 nm, the spin state distribution has been examined. Kanamori *et al.* found a spin polarization ratio $F_1:F_2:F_3$ = 3:1:3 for the nascent SO(X, $v''=1$) from the photodissociation of SO_2, indicating a preference for spin parallel or anti-parallel, vs. spin perpendicular configurations[25]. In our experiments, we can resolve F_1, F_2, F_3 at high N (>30) levels, but cannot resolve F_1 and F_3 for $10 \leq N < 30$. For N = 30-47, we found $F_1 = F_3$ and therefore assumed $F_1 = F_3$ for N = 10-30, where the two components cannot be resolved. The population in F_2 was directly obtained from resolved spectral lines, which allows us to compare the spin states $F_1 = F_3$ vs. F_2. As an example, the

result for $SO(X^3\Sigma^-, v''=1)$ is shown as Fig. 8. Unlike in the case of SO_2[25], the ratios for the nascent spin state distribution, F_1/F_2, were found to be close to unity. For $v''=2$, the spin state distribution could be similarly obtained. For $v''=3$-5, however, because of the overlap of the rovibronic transitions with different rotational quantum numbers, the ratios can only be obtained approximately by comparing the intensities of the spectral peaks containing F_1 and F_3 with those containing F_2 and normalizing them to the Hönl-London factors. These spin state distribution ratios (F_1/F_2) were averaged over all the rotational states in a single vibrational level. The F_1/F_2 ratios obtained for the nascent $SO(X^3\Sigma^-)$ from photolysis of Cl_2SO at 193 nm have been found to be 1.0 ± 0.4 for $v''=1$; 1.1 ± 0.3 for $v''=2$; 0.9 ± 0.4 for $v''=3$; 0.9 ± 0.4 for $v''=4$ and 1.2 ± 0.5 for $v''=5$ (errors are 2σ). The spin state distribution ratio cannot be measured in the vibrational state of $v''=0$ because the signal-to-noise ratio is too small to give a reliable result. In the case of the photodissociation of Cl_2SO at 248 nm, no spin state distribution for $SO(X^3\Sigma^-)$ was measured since the SO radical produced was no longer nascent (0.020 Torr Cl_2SO; 1 Torr He; and 1 μs delay) and the spin state distribution could be relaxed.

4. *Quantum Yield of Nascent SO($X^3\Sigma^-$)*

The measurement of the quantum yield of SO($X^3\Sigma^-$) production may provide insight into the photodissociation mechanism of Cl_2SO, particularly in light of the fact that other electronic states of SO are energetically allowed. In our experiments, the LIF signal of a given rovibronic transition corresponding to SO($X^3\Sigma^-$, $v''=1$) vibrational state was used to measure the quantum yield. We use $v''=1$ because this is the state where there is significant nascent population for the case of the photodissociation of Cl_2SO at both 193 and 248 nm, and for the photodissociation of SO_2 at 193 nm, as well. The LIF signal intensity was found to be linear with respect to the concentration of SO($X^3\Sigma^-$) radical by varying the pressure of sample gas, Cl_2SO or SO_2, around 0.020 Torr. One Torr of helium was added as buffer gas and a 2 μs delay between the photolysis and probe lasers was used to insure the rotational and spin state relaxation. We recorded the LIF signal intensities originating from SO($X^3\Sigma^-$) from the photodissociating Cl_2SO and SO_2, respectively, under identical conditions except for photolysis laser fluence (25 mJ/cm^2 at 193 nm and 65 mJ/cm^2 at 248 nm). The LIF signal intensity was the average of 2000 points and the data we used for the quantum yield calculation was the average of 10 signals. The quantum yield, ψ, of the SO($X^3\Sigma^-$) was derived as follows:

$$\psi \propto I_{SO(X)} / [\, \sigma \cdot P(v'') \cdot P_{Laser} \,], \qquad (6)$$

where the σ is the absorption cross section of the parent molecule at the corresponding photolysis wavelength, $P(v'')$ is the fractional nascent population in the vibrational state of SO($X^3\Sigma^-$, $v''=1$) and P_{Laser} is the fluence of the photolysis laser. Because the SO($X^3\Sigma^-$) production is greater than 99.5% from the photolysis of SO_2 at 193 nm[15], we assume it to be unity. By comparing ψ value from the photolysis of

Cl_2SO at both 193 and 248 nm with the ψ value from the photolysis of SO_2 at 193 nm, relative quantum yields, Φ, of $SO(X^3\Sigma^-)$ from Cl_2SO were obtained.

$$\Phi^{Cl2SO}_{193\,nm} = \psi^{Cl2SO}_{193\,nm} / \psi^{SO2}_{193\,nm} = 0.73 \pm 0.10,$$

$$\Phi^{Cl2SO}_{248\,nm} = \psi^{Cl2SO}_{248\,nm} / \psi^{SO2}_{193\,nm} = 0.13 \pm 0.07,$$

The errors are statistical, based on the multiple measurements. The large error of the quantum yield measurement in the case of 248 nm photolysis most likely arise from the change of the photolysis laser source and/or the change of the related optical components.

Discussion

1. 193 nm PHOTODISSOCIATION

According to Strauss and Houston[5], a concerted dissociation is defined as one in which all the bond-breaking events occur on a timescale shorter than a rotational period of the possible reaction intermediate, which in turn, allows anisotropic effects to be observed experimentally. By measuring the internal state distributions of the fragment(s), information about whether or not a photodissociation process occurs in concert may be directly revealed. For example, in a concerted process, the vibrational state distributions of the fragment(s) may reflect characteristics of the Franck-Condon excitation, since the final state interactions are weak due to the rapid cleavage of all the bonds. In this case, the distribution of the fragment(s) may be inverted or non-statistical, while in a stepwise dissociation, a thermalized distribution of the product states may be expected since a long-lived intermediate may allow the statistical distribution and/or disposal of the excess energy.

In our experiments, rotational state distributions of the nascent SO can be characterized by a single temperature, suggesting that there is one major dissociation channel responsible for the production of ground state sulfur monoxide. The uniform spin state distributions (F_1/F_2 = 0.9-1.2, error = ± 0.4) for SO($X^3\Sigma^-$, v'' = 1-5) are also consistent with this hypothesis. The inverted vibrational distribution of SO($X^3\Sigma^-$) that results from the Cl_2SO dissociation indicates that both Cl-S bonds break within a short enough time so as to minimize final state interactions. Since no spectroscopic data is available for OSCl, the rotational period of SOCl is taken as 3×10^{-12} seconds assuming rotational constant B = 1 cm^{-1} (typical order for nonlinear triatomic molecules) and N ~ 10. The vibrational periods of OSCl, corresponding to the three vibrational modes, are estimated from the data available for SSCl to approximate the possible intermediate in our experiment[26]. These vibrational periods are estimated to be 5×10^{-14}, 5.6×10^{-14} and 9.8×10^{-14} s, respectively. The order of these timescales are assumed to be true for OSCl. From this estimate, the intermediate, OSCl, would vibrate over 50 times in one rotational period. In the case that the nascent SO($X^3\Sigma^-$) was produced via a stable OSCl intermediate that lives longer than a rotational period, the intramolecular vibrational energy randomization during the lifetime of the intermediate would produce a thermalized, *i.e.* non-inverted, distribution. Thus the existence of a stable OSCl intermediate is not likely in the photochemical pathway for the production of nascent SO($X^3\Sigma^-$) following irradiation at 193 nm. The major channel, which produces the nascent SO($X^3\Sigma^-$) in the photodissociation of Cl_2SO at 193 nm, most likely proceeds via a concerted dissociation mechanism in which one S-Cl bond may break first, but the second one must cleave within one rotational period of the assumed reaction intermediate, OSCl.

To further address the major dissociation channel, the energy disposal into the fragments was analyzed. The energy disposal into the vibrational degree of freedom of the $SO(X^3\Sigma^-)$ fragment was evaluated as the sum of the energy partitioned into each vibrational level: $E_{vib} = \Sigma c_v(E_v-E_o)$, where c_v is the fractional population in v'' state obtained from Fig. 3 and E_v and E_o are the energy of the given vibrational level v'' and the zero point energy of the electronic state respectively. The average vibrational energy, E_{vib}, for $SO(X^3\Sigma^-)$ from the photodissociation of Cl_2SO at 193 nm was calculated to be 7.2 ± 1.2 kcal/mol. The rotational energy at each vibrational level was estimated by $E_r(v'') = kT_r(v'')$, where T_{rot} is the rotational temperature in the given vibrational state and the other variables are the same as given above. The average rotational energy, E_{rot}, for the $SO(X^3\Sigma^-)$ was estimated by $\Sigma(K_B T_{rot} \bullet c_v)/\Sigma c_v$, and calculated to be 3.1 ± 0.9 kcal/mol. The average internal energy disposal into the nascent $SO(X^3\Sigma^-)$ was found to be 10.3 ± 2.1 kcal/mol.

The upper limit of the translational energy of the nascent $SO(X^3\Sigma^-)$ fragment was found to be 11 ± 2 kcal/mol by assuming that the observed spectral linewidth of a single rovibronic transition is its Doppler width. This assumption is at best an upper limit since the observed spectral linewidths are close to the probe laser bandwidth. The average translational energy can be calculated based on the kinetic energy of the nascent $SO(X^3\Sigma^-)$. Assuming three-body dissociation geometry, the following equations were used to calculate the total kinetic energy,

$$m_{SO} \bullet v_{SO} = 2m_{Cl} \bullet v_{Cl} \bullet \cos(\alpha/2) \quad (7)$$

$$E_{trans}^{SO+2Cl} = \tfrac{1}{2} \bullet (m_{SO} \bullet v_{SO}^2 + 2m_{Cl} \bullet v_{Cl}^2) \quad (8)$$

where m represents the mass, v is the velocity and α is the angle of Cl-S-Cl ($\sim 97°$)[31]. Based on these equations, $v_{Cl} = 1.03 \bullet v_{SO}$ and $E_{trans}^{SO+2Cl} = 2.56 \bullet E_{trans}^{SO}$ were obtained.

The calculation yields an upper limit value of $E_{trans}^{SO+2Cl} < 28$ kcal/mol. This value is consistent with the result of Baum *et al.* of 26±3 kcal/mol (peak value) for the photofragment translational energy of SO+2Cl following 193 nm photolysis of Cl_2SO[8]. It is important to note that if the two chlorine atoms dissociate in sequential steps, but in less than a rotational period of ClSO, then the average translational energy release to the photofragments can be either greater than or less than the value obtained here, depending on the dynamics of each of the processes. The overall energy disposal into the various modes of the nascent fragments is summarized in Table II.

The total energy disposal into the three fragments $SO(X^3\Sigma^-)$ + 2Cl is found to be 38.3±5 kcal/mol if a three body dissociation is assumed, and E_{trans}^{SO+2Cl} = 28 kcal/mol (upper limit) was used. This value is in close agreement with the total available energy of 39.7 kcal/mol for $Cl_2SO + h\nu \rightarrow SO(X^3\Sigma^-) + Cl + Cl$ at 193 nm[8]. This energy balance analysis supports our hypothesis that the SO in its ground state, $X^3\Sigma^-$, is most likely produced via a concerted three-body dissociation, **(3)**. The production yield of the nascent $SO(X^3\Sigma^-)$ from the 193 nm photolysis of Cl_2SO, which was found to be 73±10% in our experiments, is consistent with Baum *et al.*'s conclusion of 80% proceeding by the three body dissociation, **(3)**[8]. These results suggest that most of the nascent $SO(X^3\Sigma^-)$ population following the 193 nm irradiation on Cl_2SO must be produced via the concerted three body dissociation channel, **(3)**, rather than the molecular elimination of Cl_2 **(2)**.

We have concluded thus far that the concerted three-body fragmentation, $Cl_2SO \rightarrow SO + Cl + Cl$, is the major dissociation channel for Cl_2SO photolysis at 193 nm to produce $SO(X^3\Sigma^-)$. This brings the question, does the dissociation take place on the

potential surface of an initially excited repulsive state or is it a predissociation where the molecule crosses from a bound excited state potential to a repulsive surface[2]? Modelling the nascent vibrational distribution may be useful in providing insight into this question, if we can predict the Cl_2SO geometry immediately prior to dissociation[7,27].

Several research groups have applied a Franck-Condon/golden rule treatment to model inverted vibrational distributions of nascent products from elementary chemical reactions[7,27,28,29,30]. This model assumes a sudden transition from the "dressed" precursor, *e.g.* AB in the parent molecule ABCD, to the "undressed" diatomic photofragment and calculates the probability, P(f), of forming nascent AB in vibrational state, $|f>$,

$$P(f) \sim (4\pi^2/h)|<i|f>|^2\rho(E), \qquad (9)$$

where $|i>$ is the initial "dressed oscillator" state, corresponding to SO in the parent molecule, *e.g.* SO in Cl_2SO, $\rho(E)$ is the density of the final states and h is Planck's constant. Morse oscillator functions are used for $|f>$ and $|i>$. Application of this model to the photofragmentation of Cl_2SO at 193 nm reveals the bond length for the "dressed" S=O moiety prior to the dissociation of this tetratomic molecule. Unlike in the case of SO_2[7], the S=O bond length in the ground state Cl_2SO ($d_{SO} = 1.44$Å)[31] with a trial vibrational frequency of 1200 cm^{-1} leads to close agreement with the LIF measured SO vibrational distribution, as shown in Fig. 3. This result suggests a direct dissociation mechanism, *i.e.* excitation of the ground state to a repulsive state, may be operative. A direct dissociation is consistent with the following: (i) our observation of unity spin state distribution ratios are consistent with a direct dissociation mechanism where no potential surface crossing, which may produce spin

polarization[25], is operative; (ii) the Cl_2SO absorption band near 193 nm is assigned to $n_{Cl} \rightarrow \sigma^*_{S\text{-}Cl}$[6,10] which may lead to an immediate rupture of both S-Cl bonds; (iii) the hypothesis is also consistent with the Baum *et al.* claim that the anisotropy of all the fragments from the photodissociation of Cl_2SO at 193 nm could be accommodated by one initially excited state of A" symmetry[8]. On the other hand, if a predissociation via an excited state with a *different* SO bond length was assumed, then $d_{SO} = 1.61$Å and $v = 1100$ cm^{-1} would be required to fit our LIF observation. Such a significant (12%) elongation of the S=O bond is not likely since the $n_S \rightarrow \pi_{SO}^*$ transition which could lead to the elongation of the S=O bond is far to the red of 193 nm ($\lambda > 250$ nm[6]). A small difference between the observed and predicted distributions exists and may suggest the involvement of final state interactions. Further investigation, especially the rotational state distribution dependence on the initial thermal conditions of the parent molecule[32], is needed to clarify whether the Cl_2SO dissociation is direct or indirect.

Besides the major dissociation channel, there may be some minor photochemical pathways which are also responsible for the production of nascent SO in the photodissociation of Cl_2SO at 193 nm. One could be the secondary dissociation of the SOCl intermediate, while another could be the molecular elimination channel (2)[8]. Following the radical elimination channel, a further cracking of SOCl into SO and Cl is possible, either via a unimolecular decay or via a secondary photodissociation. The latter is ruled out in the experiments of Baum *et al.*[8]. Much lower photolysis laser fluences are used in our experiments (0.25 mJ/mm^2) in comparison with theirs (700 mJ/mm^2), which allows us to also rule out such a possibility. Furthermore, our observed signal intensities are linear with respect to

photolysis laser fluence. Since we observe an inverted vibrational distribution with almost no nascent population in $v''=0$, it is not likely that the SOCl thermal decay contributes significantly. Baum *et al.* report that as much as 17% of the photoactivated Cl_2SO dissociates via elimination of Cl to produce SOCl[8]. Decay of this SOCl should yield an observable population in the $v''=0$ state, since most of the $SO(X^3\Sigma^-)$ produced by SOCl decay would be expected to produce the ground vibrational state. For the photodissociation of dimethyl sulfoxide (DMSO) at 193 nm, 14% of the nascent $SO(X^3\Sigma^-)$ population is found in the vibrational ground state under similar photolysis conditions, which serves as an indicator of the LIF measurability of $SO(X, v''=0)$[33]. No nascent population was measured for $v''=0$ in the photodissociation of Cl_2SO at 193 nm, even when the (2,0) and (3,0) transitions were used to probe the ground state. The Franck-Condon factors for these transitions are reported to be 4-10 times larger than for the (1,0) transition[20]. We estimate that less than 5% of the nascent $SO(X^3\Sigma^-)$ produced in the 193 nm photolysis of Cl_2SO has population in $v''=0$, by comparison with the signal of the same bands following the photolysis of DMSO at 193 nm[33].

The molecular elimination channel may produce $SO(X^3\Sigma^-) + Cl_2(B^3\Pi^+)$, which is allowed under spin selection rules,[8,34] and has been studied by Baum *et al.* to have a quantum yield of 3%[8]. Following the molecular elimination, Cl_2 may undergo further dissociation to yield Cl + Cl. However, no electronically predissociative states of Cl_2 in the accessible energy range are available, and tunnelling the centrifugal barrier of a rotational metastable state is not likely for chlorine due to its large reduced mass[8]. Therefore, besides the primary three body dissociation, the most likely production chemical for $SO(X^3\Sigma^-)$ is molecular elimination of Cl_2[8].

Our experiments still fail to account for the fate of all the photoactivated Cl_2SO. Baum *et al.* found direct evidence for the presence of OSCl (*m/e* = 83) following 193 nm photolysis of Cl_2SO, most of which they believed to be in an electronically excited state. Another possibility is that this discrepancy could be ascribed to the production of nascent SO in other electronic states, such as $a^1\Delta$ state, investigated by Kanamori *et al.* with an infrared diode laser[15], or the $b^1\Sigma$ state. Further studies are still needed to clarify this issue.

2. *248 nm PHOTODISSOCIATION*

Photodissociation of Cl_2SO at 248 nm can proceed energetically along the same three pathways as at 193 nm, but Baum *et al.* claim that only the molecular elimination of Cl_2, **(2)**, and/or the radical elimination of SOCl, **(1)**, are operative[8]. No further fragmentation of SOCl, deriving from the initial photoactivation, was found in their experiments. However, nascent $SO(X^3\Sigma^-)$ has been observed in our experiments for the same photodissociation, and is produced with a bimodal vibrational distribution. The production yield for the total nascent $SO(X^3\Sigma^-)$ has been measured as $13 \pm 7\%$ in this case and the first three vibrational levels ($v'' = 0,1,2$) accounted for 94% of the nascent $SO(X^3\Sigma^-)$ population. The nascent $SO(X^3\Sigma^-, v'' = 0\text{-}2)$ was found to observe a Boltzmann distribution, suggesting a stepwise mechanism involving the unimolecular decay of SOCl into SO and Cl. The vibrational temperature of the nascent $SO(X^3\Sigma^-)$ for $v'' = 0\text{-}2$ has been found to be, T_{vib} 1000 ± 200K. To further characterize the dissociation mechanism, the experimental data were fit to a prior distribution calculated by an information theoretical model, in which the total energy conservation is considered and the conservation of angular momentum is

neglected[35,36,37]. The pure statistical expectation for the nascent vibrational distribution for a chemical reaction involving AB + C has been formulated as follows[35],

$$P^o(v''|E_{tot}) = (E_{tot} - E_{v''})^{3/2}/\Sigma (E_{tot} - E_{v''})^{3/2}, \quad (10)$$

where E_{tot} is the operative excess energy (set as a trial variable) in the spontaneous dissociation of SOCl → SO($X^3\Sigma^-$) + Cl, $E_{v''}$ is the vibrational energy corresponding to the individual vibrational levels and $P^o(v''|E_{tot})$ stands for the prior expectation for the vibrational population. The observed vibrational distribution was fit by a calculated distribution from the above model by varying E_{tot}. The excess energy, E_{tot} = 9.1 kcal/mol, was found to give the best fit of the data (see Fig. 4), v'' = 0-2, which is in close agreement with the excess energy (7 kcal/mol) for the process: Cl_2SO + hν(248 nm) → SO + Cl + Cl[8]. The small difference between the fit value and the thermodynamic data may correspond to the contribution of the zero-point energy prior to the secondary fragmentation. Higher excess energy, E_{tot}, can lead to population in the higher vibrational states, *e.g.* v'' = 3. However, no calculated distribution containing population in v'' = 3 was found in close agreement with our observed LIF data, indicating E_{tot} = 9.1 kcal/mol is the best fit excess energy. The nascent population in the vibrational levels of v'' = 3 and higher are not likely to be produced via the unimolecular fragmentation of the OSCl intermediate.

The information content is defined as[35]

$$I = \Sigma - P(v''|E_{tot}) \cdot \ln[P(v''|E_{tot})/P^o(v''|E_{tot})], \quad (11)$$

which serves as a direct measure about the deviation of the observed vibrational distribution, $P(v''|E_{tot})$, from the statistical prior expectation, $P^o(v''|E_{tot})$. In the limiting case, where the observed distribution matches the prior expectation in all the

The average vibrational energy of the SO fragment via the molecular elimination of Cl_2 was calculated to be 15.5 kcal/mol by using the same procedure as for the case of the photolysis at 193 nm, assuming that no population in the vibrational levels of $v''=0$-2 was produced from channel (2). The nascent rotational state distributions of the SO fragment were not probed directly, but we assume the results of $E_{rot}=3.1$ kcal/mol from the 193 nm case as an estimate. The total translational energy for SO + Cl_2 was taken from the peak value (24 kcal/mol) of ref. 8. The only energetically allowed state of Cl_2 is the ground state, $X^1\Sigma^+$ [8,39]. An energy balance analysis leaves 21.3 kcal/mol to be disposed into the internal states of the nascent Cl_2. This large amount of internal energy into Cl_2 is consistent with the large change in Cl-Cl distance in going from Cl_2SO (3.09Å)[31] to Cl_2 (2.44Å)[39] via a three center transition state. Consequently, significant vibrational excitation may result from the formation of the Cl-Cl bond in the 248 nm photodissociation of Cl_2SO.

Summary and Conclusions

Following the 193 nm photodissociation of Cl_2SO, the nascent vibrational state distribution of $SO(X^3\Sigma^-, v''=0$-6) is found to be inverted with a population maximum at $v''=2$ by using laser induced fluorescence (LIF) spectroscopy of $SO(B^3\Sigma^- - X^3\Sigma^-)$ in the region of 237-295 nm. The nascent rotational state distributions of $SO(X^3\Sigma^-)$, for $v''=1,2$, and 3 have been obtained, and can be characterized by a single temperature distribution. The spin state distributions have been found to be unpolarized (F_1/F_2 = 0.9-1.2 error = ±0.4) for all the vibrational states measured. The primary quantum

yield for the production of $SO(X^3\Sigma^-)$ was measured to be $\Phi^{193\,nm} = 0.73 \pm 0.10$. The single temperature rotational state distributions and uniform spin state distributions suggest that one primary dissociation channel is responsible for the nascent $SO(X^3\Sigma^-)$. The inverted vibrational state distribution of the nascent $SO(X^3\Sigma^-)$ fragment indicates that this dissociation channel is a concerted process in which both S-Cl bonds cleave within *ca.* 10^{-12} s. Quantum yield measurements and an energy disposal analysis support the concerted three body fragmentation to produce SO + Cl + Cl, as the major dissociation channel. A Franck-Condon/golden rule model elucidates the dissociation geometry as similar with the equilibrium structure of the ground state Cl_2SO, suggesting a direct dissociation. The unity spin state distribution ratios are also consistent with a direct dissociation mechanism. Other minor dissociation channels, such as molecular elimination of Cl_2 and the production of SO in electronic states other than $X^3\Sigma^-$ cannot be ruled out.

Photolysis of Cl_2SO at 248 nm produces a nascent vibrational state distribution of $SO(X^3\Sigma^-)$ that is characterized as bimodal. The data is consistent with production of $SO(X^3\Sigma^-)$ by two different processes, a stepwise fragmentation of the S-Cl bonds and a molecular elimination of Cl_2 via a three center transition state. The two channels are well-separated in the production of the nascent $SO(X^3\Sigma^-, v'')$ in different vibrational levels (v'').

The detailed results described here have provided valuble insight into the nature of multiple bond photofragmentation processes. The two wavelengths employed delineate distinct photochemical behaviors, and are suggestive of possible state-selective behavior. Future studies aimed at exploring the wavelength region in between those used here, may provide crucial information towards a greater

understanding of multiple bond photofragmentation. These experiments are ongoing in our laboratory.

Acknowledgments

The experiments performed here were done in conjunction with the Puerto Rico Laser and Spectroscopy Facility at the University of Puerto Rico, under the auspices of NSF-EPSCoR Program. We would also like to kindly acknowledge the Air Force Office of Scientific Research which has generously supported this research.

Table I: The experimentally obtained vibrational state distributions of the nascent $SO(X^3\Sigma^-)$ following the photodissociation of Cl_2SO at 193 and 248 nm. No nascent population in the $SO(X^3\Sigma^-, v''=7)$ state has been measured following the photolysis of Cl_2SO at 193 nm.

	Relative Population (%)	
v''	at 193 nm	at 248 nm
0	≤ 5	71 ± 9
1	30 ± 8	20 ± 5
2	35 ± 6	3 ± 1
3	20 ± 4	.5 ± .2
4	7 ± 1	2 ± .3
5	2 ± .5	2.5 ± .3
6	1 ± .2	.8 ± .2
7	(0)	.2 ± .1

Table II: Energy disposal into different degrees of freedom of the nascent SO photofragment following 193 nm photodissociation of Cl_2SO *assuming a concerted three-body dissociation*. The available energy is 39.7 kcal/mol.

MODE	THIS WORK	PREVIOUS WORK[a]
E_{vib}^{SO}	7.2	---
E_{rot}^{SO}	3.1	---
E_{trans}^{SO}	< 11	---
E_{trans}^{SO+2Cl}	< 28	26
E_{total}	< 38.3	---

a. Reference 8

Figure Captions

Figure 1: A schematic energy diagram for the photodissociation of Cl_2SO at 193 and 248 nm.

Figure 2: LIF spectrum of nascent $SO(X^3\Sigma^- - B^3\Sigma^-)$ following the 193-nm photolysis of 0.020 Torr of Cl_2SO. The delay between the photolysis and probe laser was 400 ns. The origins of the vibrational bands have been assigned from reference 19.

Figure 3: Vibrational state distribution of the nascent $SO(X^3\Sigma^-, v'')$ fragment following the photolysis of Cl_2SO at 193 nm. The filled symbol, ■, represents the experimentally observed distribution, while the open symbol, □, stands for a calculated distribution by using a Franck-Condon/golden rule model (see text).

Figure 4: Vibrational state distribution of the nascent $SO(X^3\Sigma^-, v'')$ fragment following the photolysis of Cl_2SO at 248 nm. The round symbols, ● and ○, represent the experimental measurements, the ■ stands for the prior statistical distribution from an information theoretical analysis. The insert is the expanded portion of $v'' = 3\text{-}7$. ○ is the experimental data and □ is the predicted distribution from the Franck-Condon/golden rule model (see text).

Figure 5: (a) Laser induced fluorescence excitation spectrum of the (1, 2) band of the $SO(B^3\Sigma^- - X^3\Sigma^-)$ transition following the photolysis of 0.020 Torr Cl_2SO at 193 nm. A probe delay of 400 ns was used. (b) Simulated spectrum, assuming a Boltzmann rotational state distribution ($T_{rot} = 1400K$) and a Gaussian spectral line profile (FWHM = 0.25 cm^{-1}). For more information on simulation parameters, see text.

Figure 6: (a) A portion of the expanded laser induced fluorescence spectrum of the (1, 1) band of the SO(B-X) transition following the photolysis of 0.020 Torr Cl_2SO at 193 nm. A probe delay of 400 ns was used. (b) Simulated spectrum assuming a Boltzmann rotational state distribution ($T_{rot} = 1800K$) and a Gaussian spectral line profile (FWHM = 0.25 cm^{-1}).

Figure 7: (a) Nascent rotational state distributions of the SO(X, $v'' = 1\text{-}3$) measured at 400 ns following the 193-nm photodissociation of 0.020 Torr Cl_2SO. (b) Semi-log plot of relative population in the rotational levels of the $SO(X^3\Sigma^-, v'')$ state, corrected to the rotational degeneracy, $g(N'') = (2N'' + 1)$, versus the rotational energy, E_{rot}. The solid lines are linear least square fits to the data in the vibrational states of $SO(X^3\Sigma^-, v'' = 1\text{-}3)$ and each corresponds to a Boltzmann temperature (see text).

Figure 8: (a) Nascent rotational state distributions of the $SO(X^3\Sigma^-, v'')$ measured at 400 ns following the 193-nm photodissociation of 0.020 Torr Cl_2SO. ○ represents the population in the spin state F_1, or the average in both F_1 and F_3 when the two states cannot be resolved in the region of N = 10-30. The insert shows the comparision of the population in F_1 (○), and F_3 (●), states.
(b) The spin state distribution ratio of F_1/F_2 for $SO(X^3\Sigma^-, v'' = 1\text{-}3)$. The dashed line, ----, represents the error (2σ). The averaged F_1/F_2 ratio is found to be 1.0 ± 0.4 for $v'' = 1$.

Figure 9: A schematic diagram showing the different primary dissociation mechanisms for the photodissociation of Cl_2SO at 193 and at 248 nm.

References

(1) Rosker, M.J.; Dantus, M.; Zewail, A.H. *J. Chem. Phys.* **1988**, *89*, 6113,6128.

(2) Schinke, R. *Comm At. Mol. Phys.* **1989**, *23*, 15.

(3) Trentelman, K. A.; Kable, S. H.; Moss, D. B; Houston, P. L. *J. Chem Phys.*, **1989**, *91*, 7498.

(4) Borden, W. T.; Loncharich, R. J.; Houk, K. N. *Annu. Rev. Phys Chem.*, 1988, *39*, 213.

(5) Strauss, C.E.M.; Houston, P.L. *J. Phys. Chem.*, **1990**, *94*, 8751.

(6) Kawasaki, M.; Kasatani, K.; Sato, H.; Shinohara, H.; Nishi, N.; Ohtoshi, H.; Tanaka, I. *Chem. Phys.* **1984**, *91*, 285.

(7) Chen, X.; Asmar, F; Wang, H; Weiner, B. R. *J. Phys. Chem.*, **1991**, *95*, 6415.

(8) Baum, G.; Effenhauser, C.S.; Felder, P.; Huber, J.R. *J. Phys. Chem.* **1992**, *96*, 756.

(9) Suzuki, S.; Yamaguchi, M.; Onda, M; Sakaizumi, T.; Ohashi, O. Yamaguchi, I. *J. Mol. Struct.*, **1981**, *73*, 41.

(10) Uthman, A.P.; Demlein, P.J.; Allston, T.D.; Withiam, M.C.; McClements, M.J; Takacs, G. A. *J. Phys. Chem.* **1978**, *82*, 2252.

(11) Yamabe, T.; Nagata, S; Kikuzono, Y. Fukui, K. *Bull. Chem. Soc. Japan*, **1975**, 1349.

(12) Okabe, H. *J. Am Chem. Soc.*, **1971**, *93*, 7095.

(13) Donovan, R. J.; Husain, D. Jackson, P. T. *Trans. Far. Soc.*, **1969**, *65*, 2930.

(14) Donovan, R. T. *Chemical Bonds and Bond Energies*, Academic Press, New York, **1978**.

(15) Kanamori, H.; Tiemann, E.; Hirota, E. *J. Chem. Phys.* **1988**, *89*, 621.

(16) Stuart, B. C.; Cameron, S. M. and Powell, H. T. *Chem. Phys. Lett.*, **1992**, *191*, 273.

(17) Bersohn, R. in *Molecular Photodissociation Dynamics*, Ashford, M. N. R., Baggott, J. E., Eds; Royal Society of Chemistry: London, **1987**; 1-30.

(18) Barnhard, K. I.; Santiago, A; He, M.; Asmar, F. Weiner, B. R. *Chem. Phys. Lett.* **1991**, *178*, 150.

(19). **a**. Colin, R. *J. Chem. Soc. Far. Trans.* 2, **1982**, *78*, 1139
b. Colin, R. *Can. J. Phys.* **1969**, *47*, 979

(20) Smith, W.H.; Liszt, H.S. *J. Quant. Spect. Radiat. Trans.* **1971**, *11*, 45

(21) Gu, X.; Chen, X; Martinez, F.; Weiner, B. R. *to be published.*

(22) Hertzberg, G. *Molecular Spectra and Molecular Structure, Vol I: Spectra of Diatomic Molecules*, 2nd ed., Van Nostrand Reinhold, New York, 1950.

(23) Kim, R-H. *Ph. D. Dissertation*, Cornell University, Ithaca, New York, **1984**.

(24) Hönl-London factors for $^3\Sigma$-$^3\Sigma$ transition were calculated according to formulae in Tatum, J.B. *Can J. Phys.* **1966**, *44*, 2944.

(25) Kanamori, H.; Butler, J.E.; Kawaguchi, K.; Yamada, C.; Hirota, E. *J. Chem. Phys.* **1985**, *83*, 611.

(26) Chiu, C. L; Pan, S. C.; Ni, C. K. *J. Chem. Phys.*, **1986**, *85*, 10.

(27) **a**. Berry, M. J. *Chem Phys. Lett.* **1974**, *29*, 323.
b. Berry, M. J. *Chem Phys Lett.*. **1974**, *29*, 329.

(28) Berry, M. J. *Chem Phys.* 1974, *39*, 3114.

(29) Schatz, G. C.; Ross, J. *J. Chem. Phys.*, **1977**, *66*, 1037.

(30) Mukamel, S.; Jortner, J. *J. Chem. Phys.*, **1974**, *60*, 4760.

(31) Hargittai, I.; in *The Chemistry of Sulphones and Sulphoxides,* Eds. Patai, S.; Rappoport, Z.; Stirling, C.; John Wiley & Sons, New York, **1988**, pp. 33-54

(32) Andresen, P., Ondrey, G. S., Titze, B., Rothe, E. W. *J. Chem. Phys.*, **1984**, *80*, 2548.

(33) Chen, X.; Wang, H.; Weiner, B. R.; Hawley, M.; Nelson, H. H. *J. Phys. Chem.*, see following paper.

(34) Okabe, H. *Photochemistry of Small Molecules*, Wiley-Interscience, New York, **1978**.

(35) Levine, R. D.; Bernstein, R. B. *Molecular Reaction Dynamics and Chemical Reactivity,* Oxford University Press, New York, **1987**.

(36) Tamagake, K.; Setser, D. W. and Sung, J. P., *J. Chem. Phys.*, **1980**, *73*, 2203.

(37) Kaplan, H. D.; Levine, R. D.; Manz, J., *Chem. Phys.*, **1976**, *12*, 447.

(38) Campbell, J; Schlag, E. W., *J. Am. Chem. Soc.*, **1974**, *6*, 855.

(39) Huber, K.P.; Hertzberg, G. *Constants of Diatomic Molecules*, Van Nostrand Reinhold, New York, **1979**.

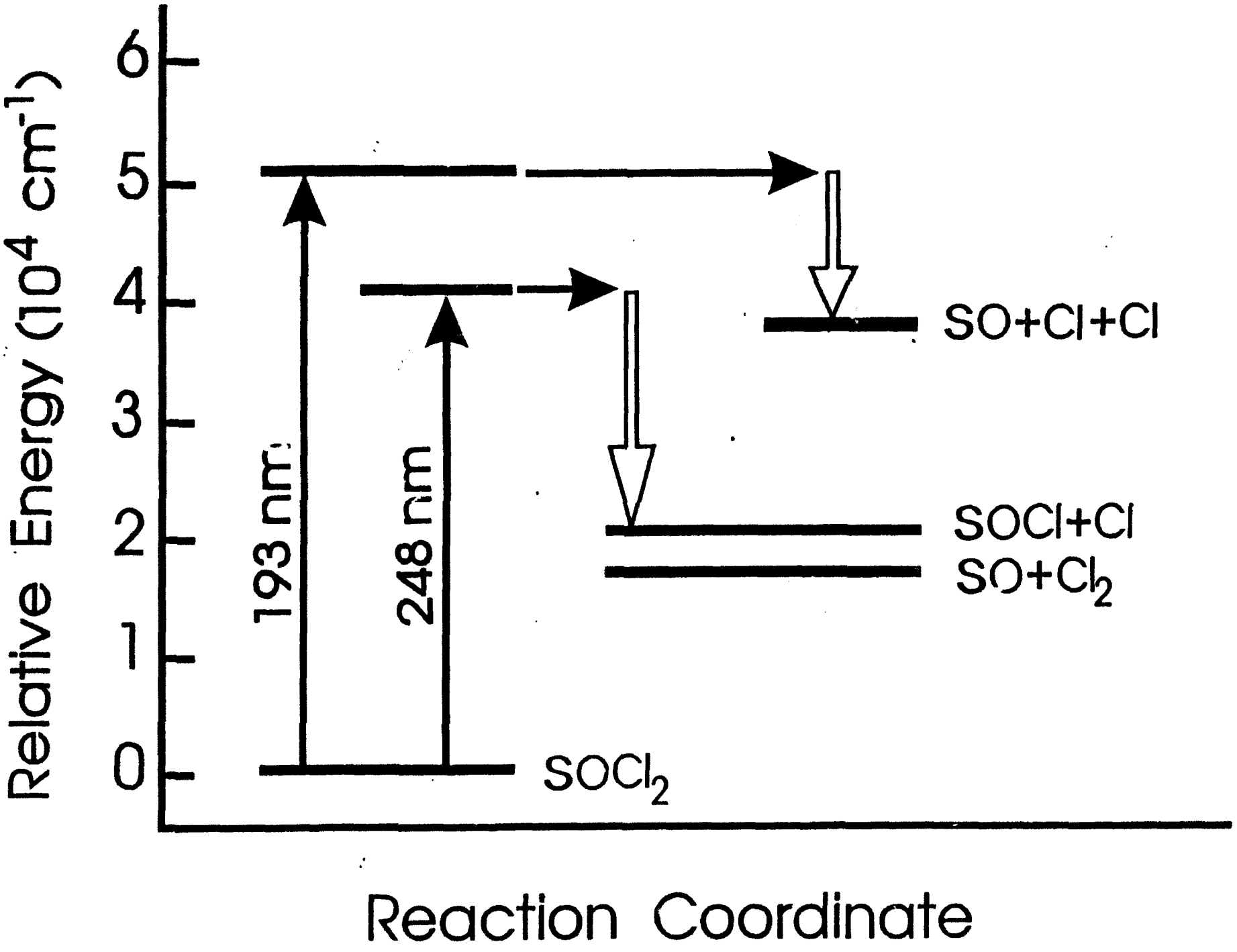
Relative Energy (10^4 cm^{-1})
6
5
4
3
2
1
0
193 nm
248 nm
$SOCl_2$
SO+Cl+Cl
SOCl+Cl
$SO+Cl_2$
Reaction Coordinate

Figure 1

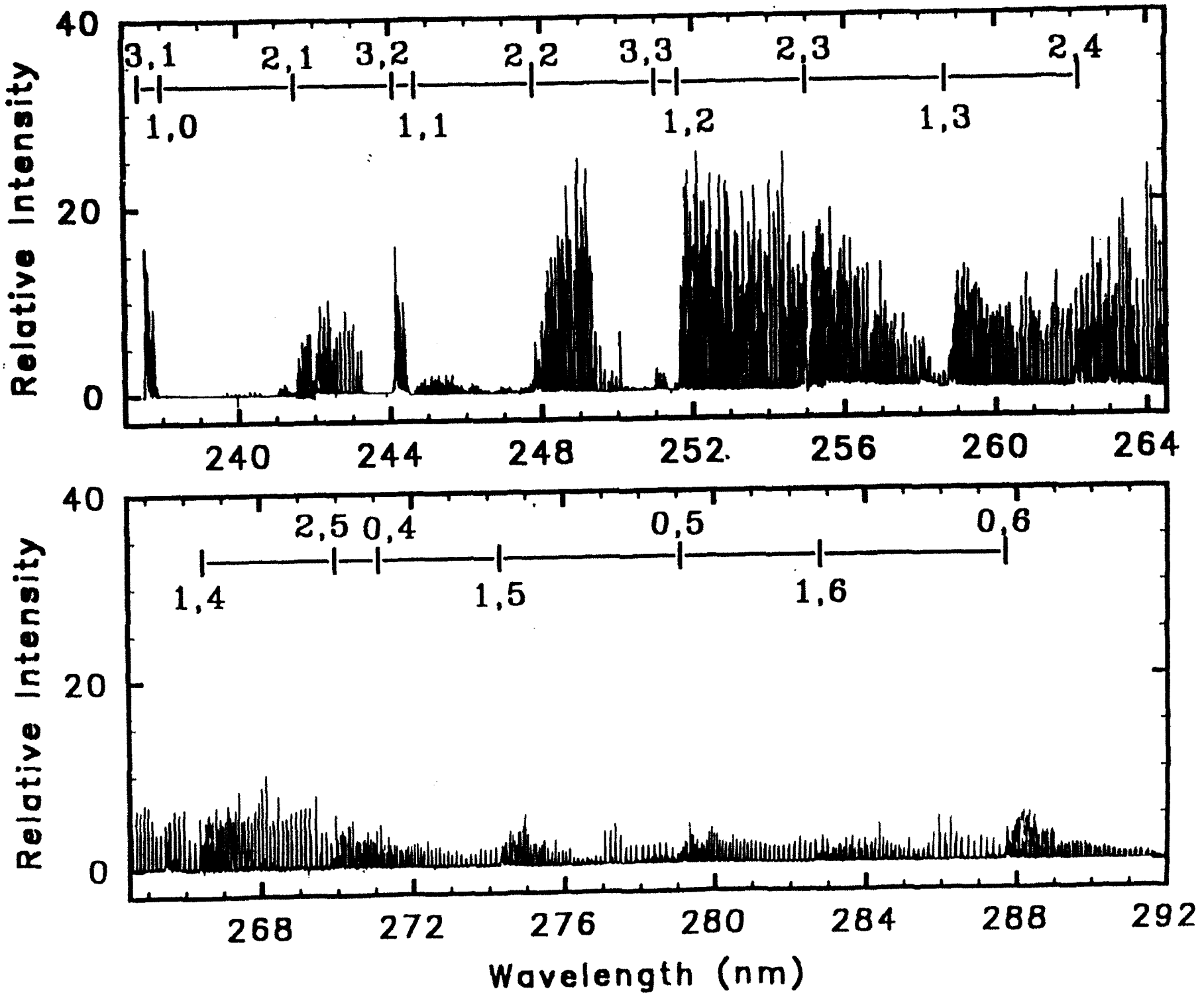
Relative Intensity
40
20
0
3,1
2,1
3,2
2,2
3,3
2,3
2,4
1,0
1,1
1,2
1,3
240
244
248
252
256
260
264
Relative Intensity
40
20
0
2,5
0,4
0,5
0,6
1,4
1,5
1,6
268
272
276
280
284
288
292
Wavelength (nm)

Figure 3

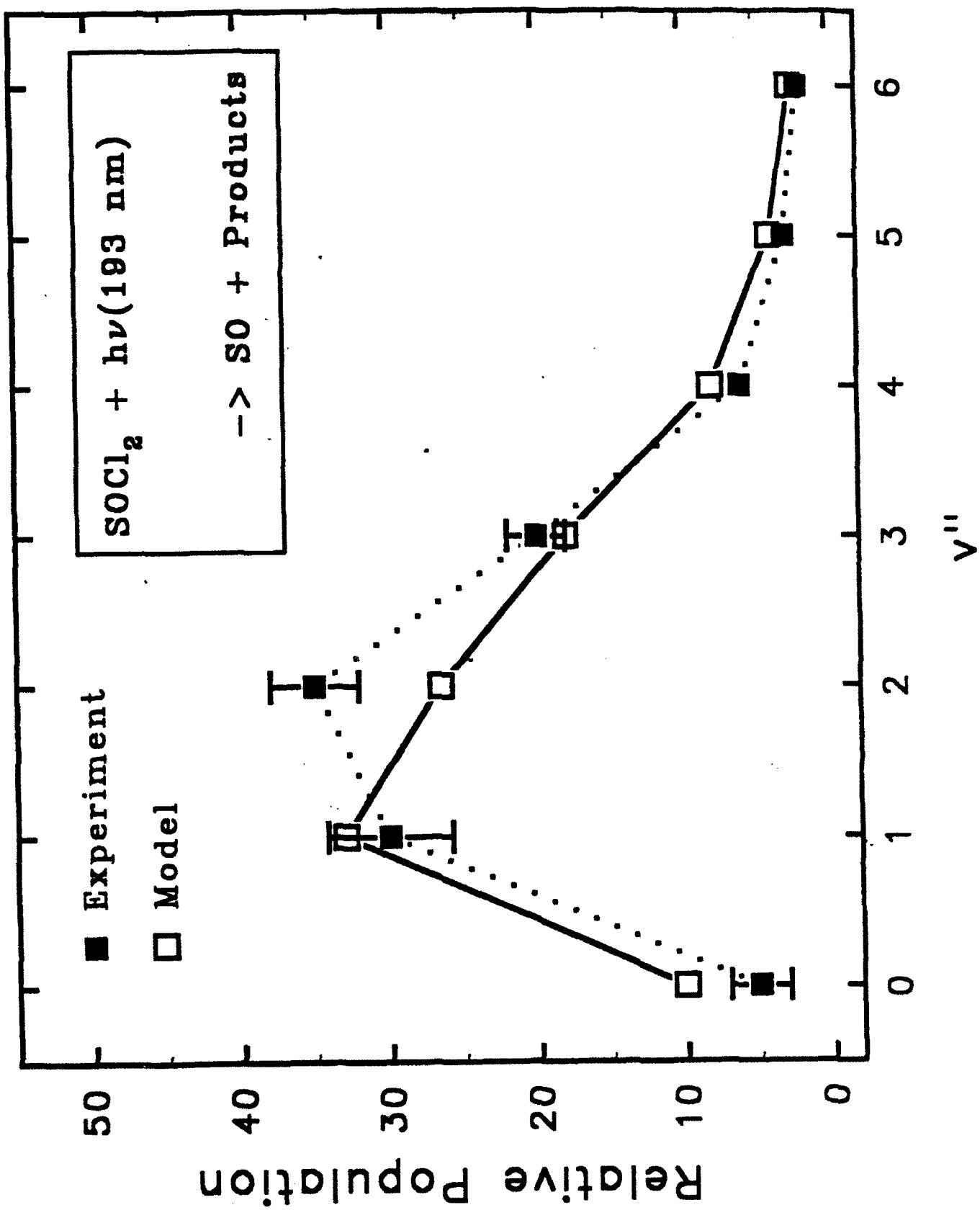
SOCl2 + hν(193 nm)
-> SO + Products
Experiment
Model
Relative Population
v''
0
10
20
30
40
50
0
1
2
3
4
5
6

FIGURE 4

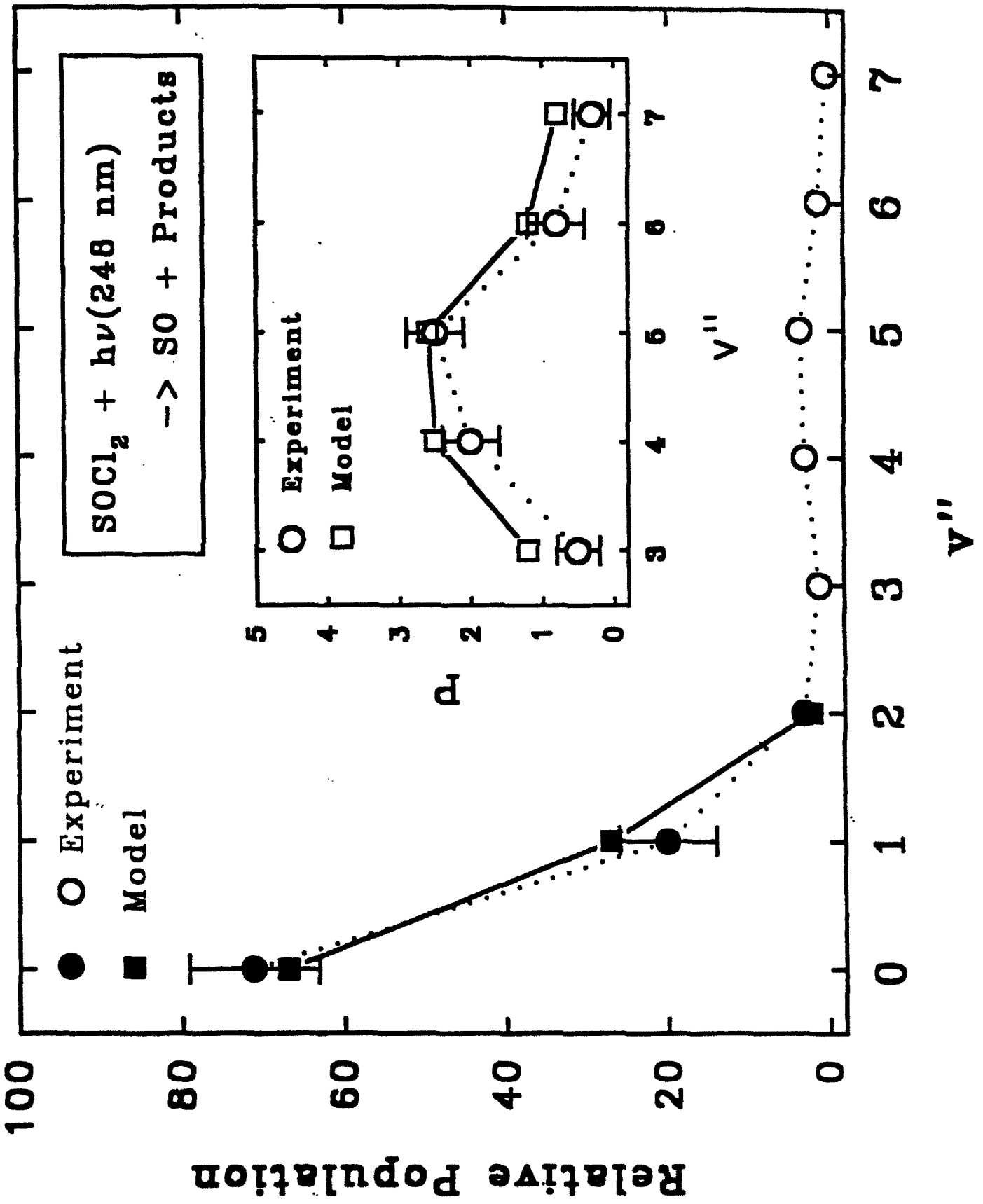
Relative Population
100
80
60
40
20
0
0 1 2 3 4 5 6 7
v''
O Experiment
Model
$SOCl_2$ + hν(248 nm)
-> SO + Products
P
5 4 3 2 1 0
3 4 5 6 7
v''
O Experiment
Model

FIGURE 5

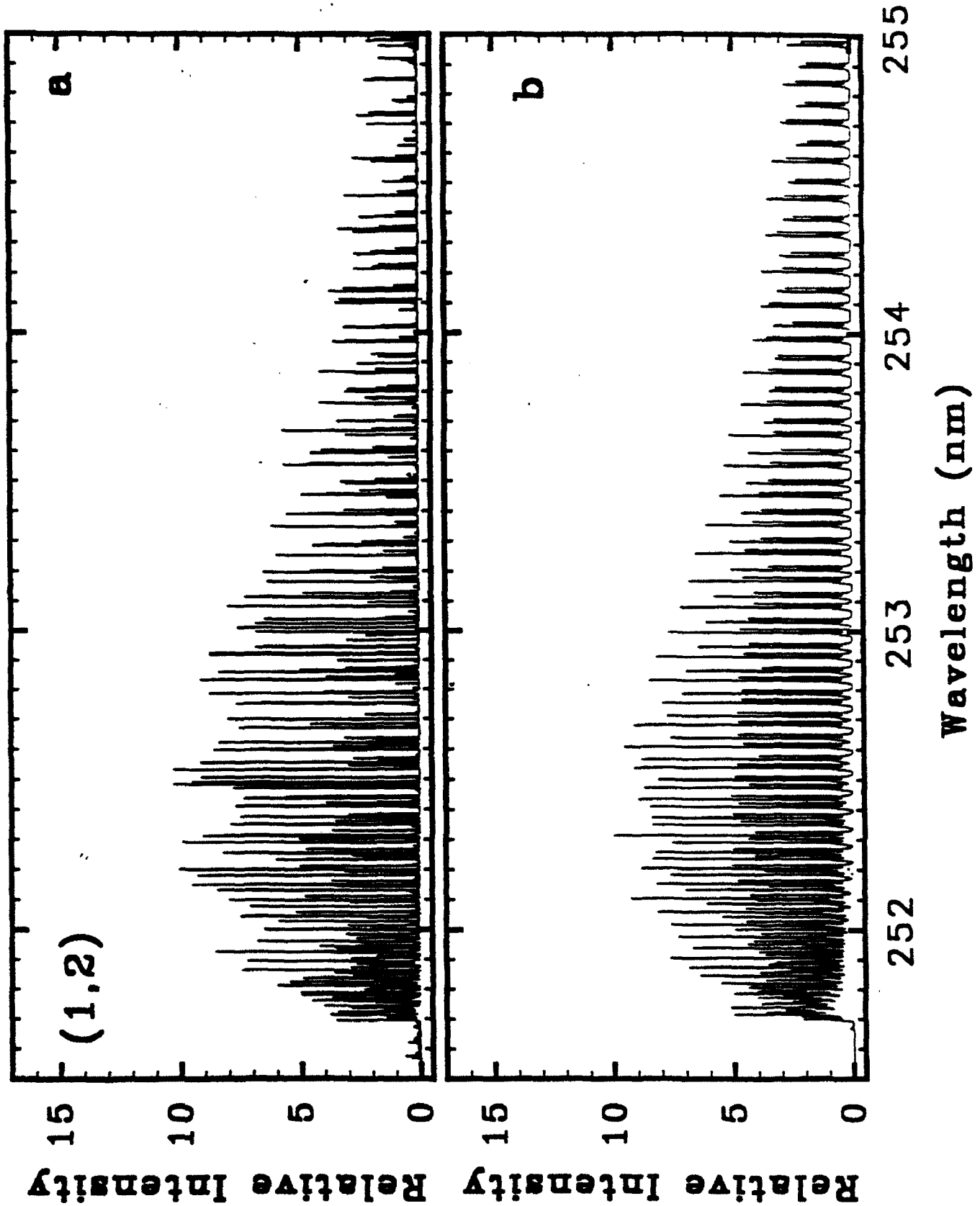
a
(1,2)
b
Relative Intensity
Relative Intensity
0
5
10
15
252
253
254
255
Wavelength (nm)

FIGURE 6

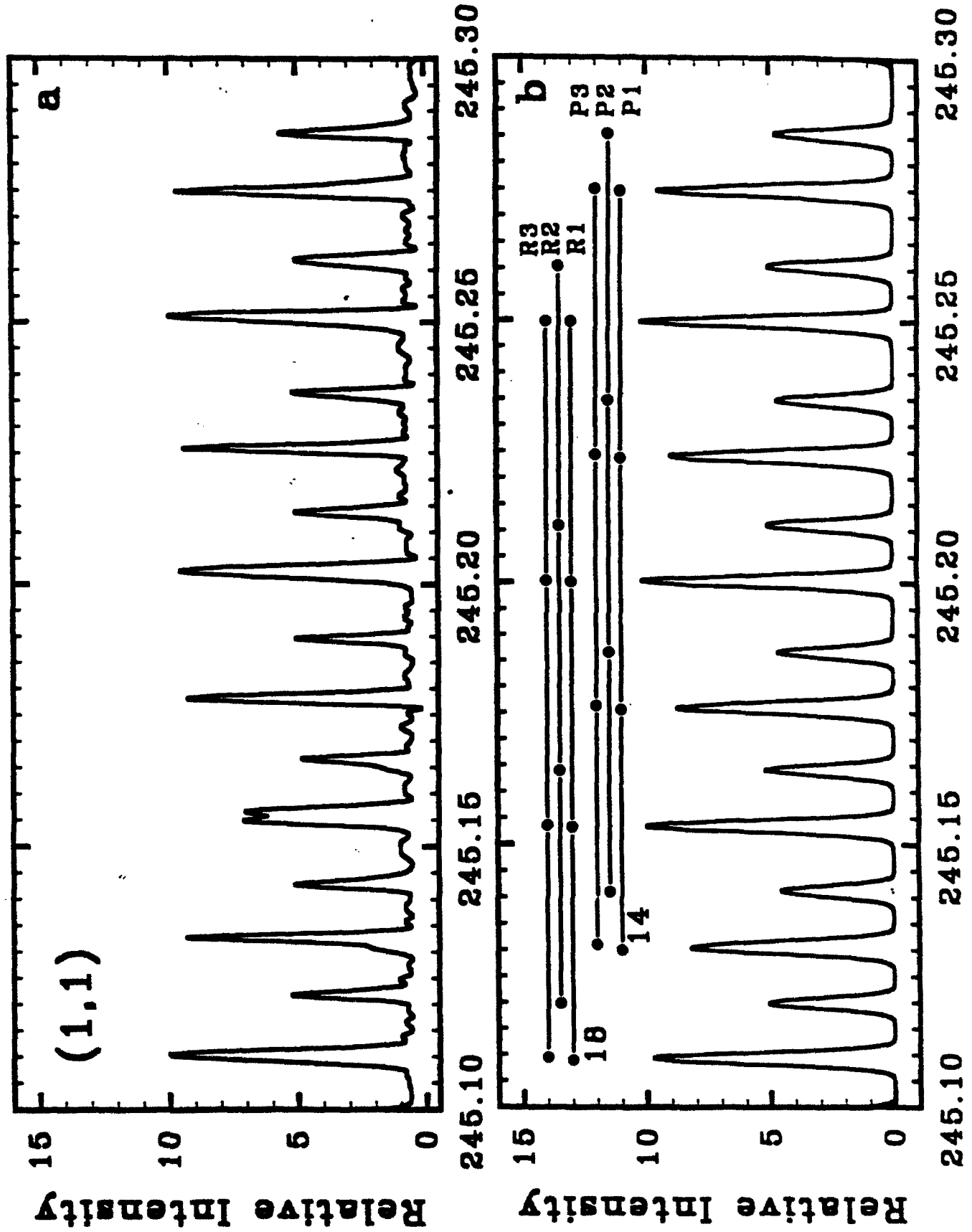
a
(1,1)
b
R3
R2
R1
P3
P2
P1
18
14
Relative Intensity
Wavelength (nm)
245.10
245.15
245.20
245.25
245.30
0
5
10
15

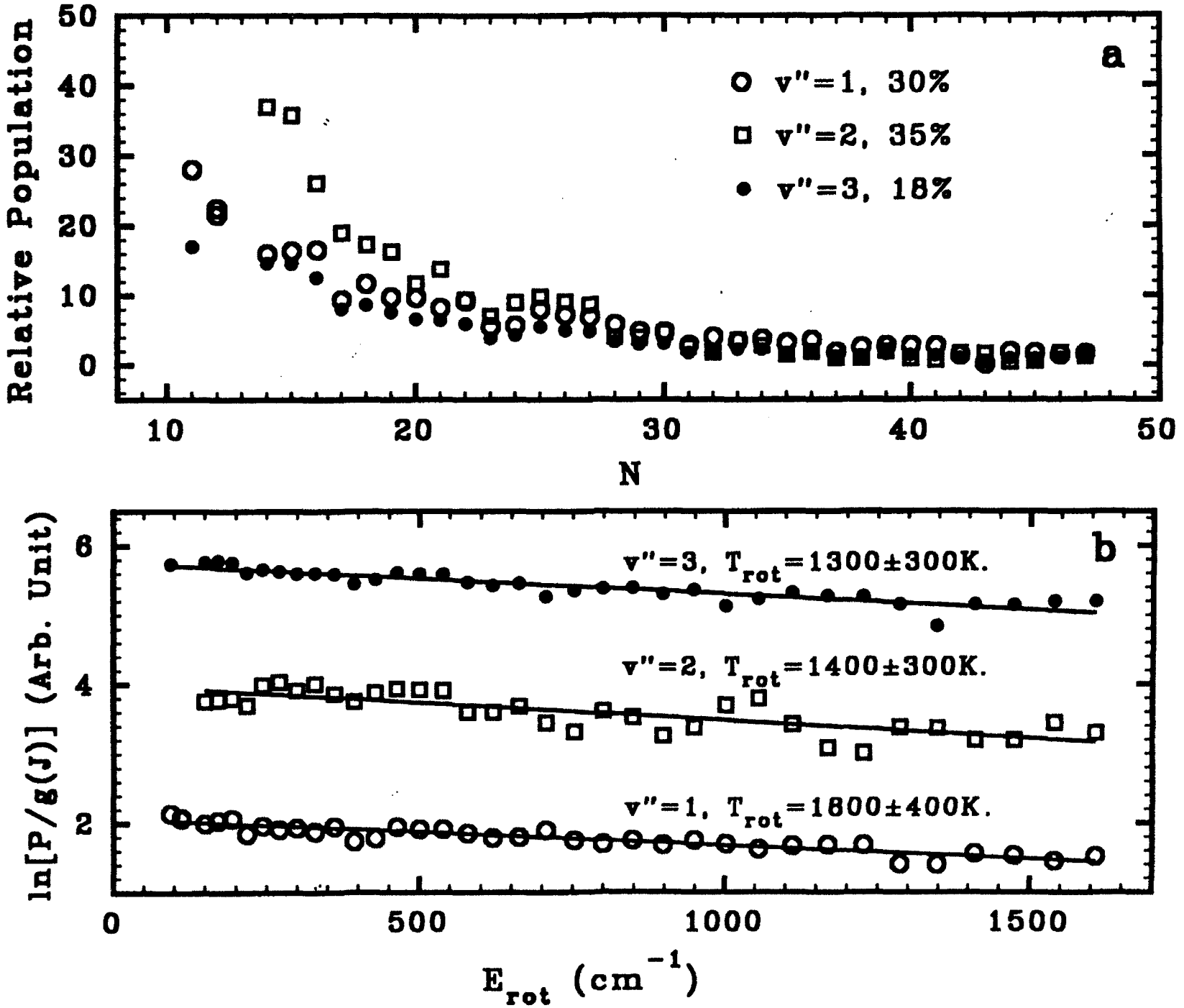
a
Relative Population
N
v"=1, 30%
v"=2, 35%
v"=3, 18%
b
ln[P/g(J)] (Arb. Unit)
E_{rot} (cm^{-1})
v"=3, T_{rot}=1300±300K.
v"=2, T_{rot}=1400±300K.
v"=1, T_{rot}=1800±400K.

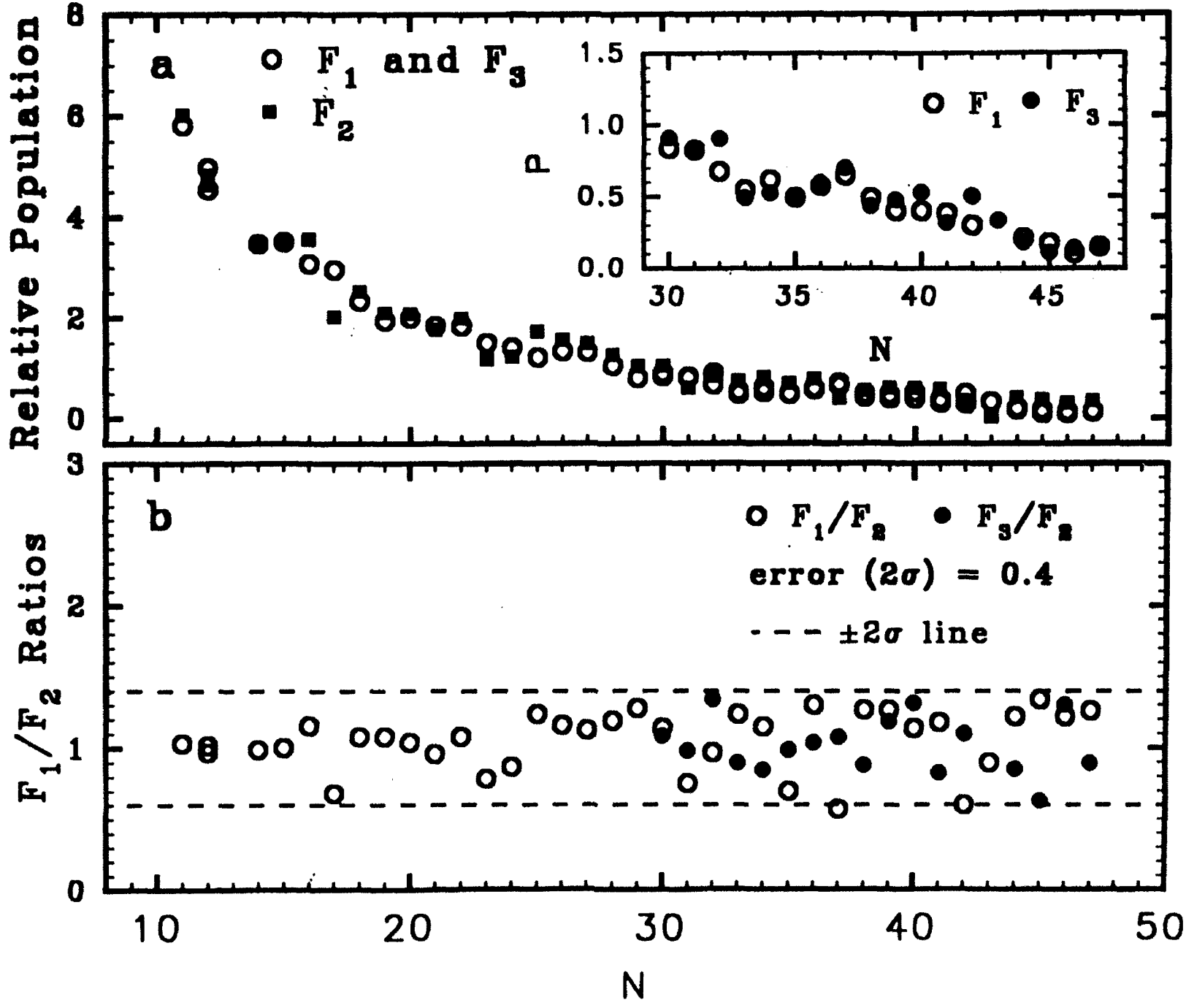
a
F_1 and F_3
F_2
Relative Population
n
N
b
F_1/F_2 F_3/F_2
error (2σ) = 0.4
$\pm 2\sigma$ line
F_1/F_2 Ratios
N

FIGURE 3

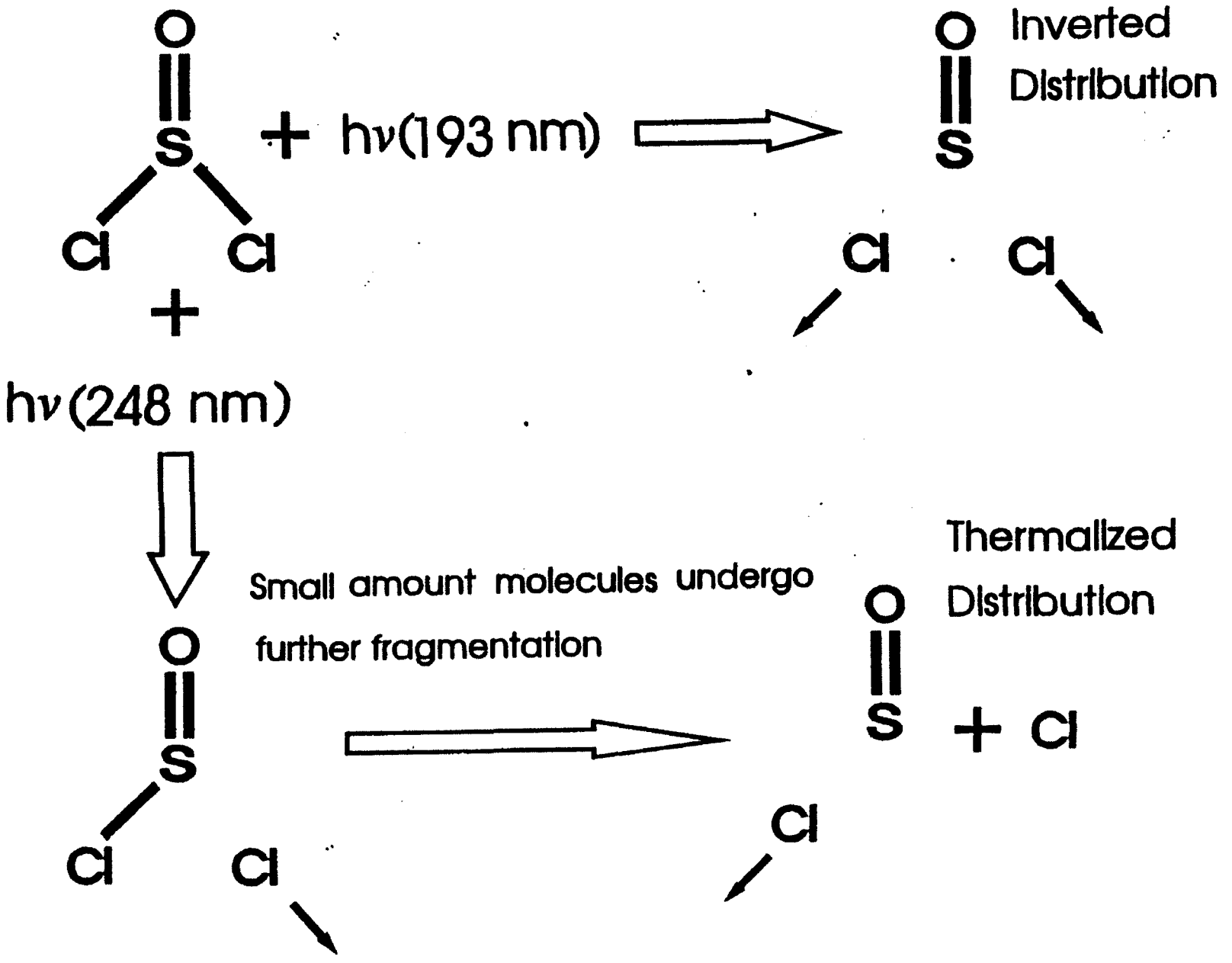
+ hν(193 nm)
Inverted
Distribution
hν(248 nm)
Small amount molecules undergo
further fragmentation
Thermalized
Distribution
+ Cl

Figure 9

J. Phys. Chem.
in press

PHOTODISSOCIATION OF DIMETHYL SULFOXIDE AT 193 nm IN THE GAS PHASE

Xirong Chen, Hongxin Wang and Brad R. Weiner*

Department of Chemistry and Chemical Physics Program
University of Puerto Rico
Box 23346 UPR Station
Río Piedras, Puerto Rico 00931

Michael Hawley[a] and H.H Nelson

Chemistry Division, Code 6110
Naval Research Laboratory
Washington, D.C.20375

Abstract

The photodissociation dynamics of the reaction, $(CH_3)_2SO + h\nu(193\ nm) \rightarrow 2CH_3 + SO$, have been examined by laser spectroscopic techniques. Relative vibrational and rotational state energy distributions of the nascent SO photofragment have been determined by using laser induced fluorescence spectroscopy on the ($B^3\Sigma^- - X^3\Sigma^-$) transition. The same technique has also been employed to establish the quantum yield, $\Phi_{193}[SO(X^3\Sigma)] = 1.02 \pm 0.12$. The nascent vibrational state distributions in the ν_1 and ν_2 modes of the methyl radical have been determined by using 2 + 1 resonance enhanced multiphoton ionization spectroscopy via the ($3p\ ^2A_2'' \leftarrow 2p\ ^2A_2''$) transition.

[a] NRC/NRL Postdoctoral Research Associate

* To whom correspondence should be addressed.

PHOTODISSOCIATION OF DIMETHYL SULFOXIDE AT 193 nm IN THE GAS PHASE

Introduction

Understanding the detailed photodissociation dynamics of polyatomic molecules containing more than five or six atoms remains a complicated problem. This complexity arises from the possibility of multiple product channels, and the large number of degrees of freedom available for energy partitioning. The measurement of the internal state distributions of the photofragments produced by laser induced fragmentation of polyatomic molecular species can be useful in elucidating the detailed mechanism of the photodissociation process itself.[1] In order to understand the photodissociation of polyatomic molecules at a detailed microscopic level, it is often necessary to evaluate the energy content of more than one of the primary products.[1] For the case of larger molecules, where more than two fragments are produced, the concertedness and/or synchronicity of the multiple bond-breaking needs to be addressed.[2]

Dimethyl sulfoxide (DMSO), a widely used solvent, presents an interesting test case on several different levels. As the simplest sulfoxide, DMSO can serve as a model photochemical system. As the sulfur analog of ketones, the unimolecular chemistry of alkyl sulfoxides may provide insight into the molecular orbital bonding picture.[3] $(CH_3)_2SO$ has been postulated as a possible intermediate in the atmospheric sulfur cycle, *i.e.* in the oxidation of reduced alkyl sulfides to sulfur dioxide.[4] In the laboratory, DMSO has been utilized routinely as a thermal source of methyl radicals,[5]

and can now be used to photolytically produce the SO radical,[6] an important member of the isovalent series that includes O_2 and S_2.

Photochemical studies of dimethyl sulfoxide in the ultraviolet are limited. Gollnick and Stracke[7] reported indirect evidence for

$$(CH_3)_2SO + h\nu \rightarrow CH_3SO + CH_3 \quad (1)$$

as the primary process for DMSO photolysis at 254 nm in solution. Chen, *et al.*, favored this mechanism as the primary step leading to the gas phase photoproduction of SO at 193 nm, but could not prove it conclusively.[6] The alternative mechanism,

$$(CH_3)_2SO + h\nu \rightarrow SO + 2CH_3 \quad (2)$$

where the parent sulfoxide undergoes simultaneous three body fragmentation is also a possibility, but the three-center molecular elimination to produce ethane and sulfur monoxide in concert, has been ruled out previously.[6]

As stated above, DMSO is the sulfur analog of acetone, $(CH_3)_2CO$. The 193 nm absorption band of acetone has been well-studied, because $(CH_3)_2CO$ provides a model system for a polyatomic molecule which produces three fragments on photodissociation. The direct measurement of the absorption spectrum of acetone suggests that the dissociation occurs by excitation first to a molecular Rydberg state, which is then followed by rapid internal conversion and dissociation into two methyl radicals and a CO molecule.[8] The nascent fragment quantum state distributions have been well-studied in this case. The internal vibrational and rotational state energy distributions, along with the translational energy release into the photoproducts have been experimentally measured for both the methyl and CO fragments.[9] The most recent experimental data and the complimentary information-theoretic analysis suggest

that the dissociation occurs by a mechanism, which is in between stepwise and concerted.[2,9d] This cooperation between experiment and theory interprets the dissociation for this model species as occurring by a two-step process, where the initially formed acetyl intermediate has a lifetime comparable to its corresponding rotational period.

The internal and translational energy distributions of nascent SO fragments produced by the photodissociation of SO_2[6,10], Cl_2SO[6,11,12,13,14] have been the subject of several experimental investigations. In a recent letter, Chen, *et al.* reported nascent vibrational distributions for the 193 nm photodissociation of SO_2, $SOCl_2$ and $(CH_3)_2SO$ by using the $SO(A^3\Pi\text{-}X^3\Sigma^-)$ transition to probe the diatomic photoproduct.[6] In this work, we use the $SO(B^3\Sigma^-\text{-}X^3\Sigma^-)$ transition to probe the nascent photofragment following the 193 nm photolysis of DMSO, because it allows us to probe higher ground state vibrational levels due to the relatively large Franck-Condon factors,[15] and because the rotational structure is much less congested than in the A-X transition. This allows the accurate measurement of nascent rotational state distributions. From the data obtained here, the relative vibrational and rotational state population distributions, and the quantum yield of the nascent $SO(X^3\Sigma^-)$ state are measured, as well as an upper limit for the kinetic energy imparted to the SO photofragment during the photodissociation process. Furthermore, we have used REMPI spectroscopy to probe the internal energy of the methyl fragments produced by this photodissociation. Previously, REMPI has been used to detect the vibrational state distribution of methyl fragments from photodissociation of other species, including acetone.[9c,16] This spectroscopic method provides the nascent state population distribution for a few

vibrational modes directly. An estimate of the rotational energy content of the methyl fragments produced from the dissociation of DMSO has also been obtained by band contour analysis. By measuring the rovibrational energy content of the three fragments, it will be shown that a more detailed picture of the photodissociation dynamics of DMSO at 193 nm, than that previously described, can now be unraveled.

Experimental

Two different experimental apparati were used in this study: (i) An excimer laser photolysis/LIF system at the University of Puerto Rico (UPR); and (ii) an excimer laser photolysis/REMPI experiment with mass-resolved detection at the Naval Research Laboratory (NRL).

UPR Experiments

The LIF apparatus used to measure the nascent energy of the sulfur monoxide photoproduct has been described previously.[6,17] In brief, DMSO, either neat or in a buffer gas, is flowed through a stainless steel reaction chamber, equipped with scattered light reducing extension arms and fused silica windows. DMSO partial pressures (10-200 mtorr) are limited by the room temperature vapor pressure of the compound. All pressures are measured by a capacitance manometer at the cell exit.

The two laser beams, photolysis and probe, are collinearly counterpropagated along the entire length of the cell to ensure maximum overlap in the center of the

reaction chamber. Dimethyl sulfoxide is photolyzed at 193 nm by an excimer laser (Lambda Physik LPX205i) operating on the ArF transition. Nascent SO photofragments are monitored by LIF on the ($B^3\Sigma^- - X^3\Sigma^-$) transitions in the 237-295 nm region of the spectrum. The probe laser light in this region was generated by frequency doubling (β-BaB_2O_4 crystal) the output of a Lambda Physik FL3002 tunable dye laser (bandwidth = 0.25 cm^{-1}), which is pumped by a Lambda Physik LPX205i excimer laser at 308 nm. To cover the entire frequency range of the SO B-X signal, three laser dyes, Coumarin 480, 503 and 540 A (Exciton, Inc.) were used. The LIF signal was found to be linear over a range of photolysis laser fluences (10-50 mJ/cm^2), indicating that the production of SO occurs by single photon absorption.

Fluorescence is viewed at 90° relative to the laser beam axis by a high gain photomultiplier tube (PMT) through a long-pass filter (Schott WG295). The output of the PMT is processed and averaged by a gated integator (SRS Model SR250), digitized (SRS Model 245), and sent to a microcomputer for display, storage, and analysis. The delay time between the two lasers was controlled with a digital delay pulse generator (SRS Model DG535). For a fixed delay time between photolysis and probe laser, the frequency-doubled output of the dye laser was scanned while collecting the total fluorescence signal to obtain a nascent excitation spectrum. Data were typically collected at 40 Hz.

$(CH_3)_2SO$ (MCB Reagents, 99.9%) was subjected to three freeze-pump-thaw cycles prior to use. Sulfur dioxide (Air Products, 99.8%) was used directly as supplied as a calibrant and as an actinometer in the quantum yield experiments.

NRL Experiments

The data for these experiments were obtained in a supersonic free jet, Time of Flight Mass Spectrometer (TOFMS), equipped for photoionization. The parent molecule, DMSO, is expanded in a buffer gas of helium through a flat, free-jet nozzle (0.05 cm diameter, General Valve). Total backing pressures were between 100 and 600 torr, and the expansions were between 0.2 and 1% in DMSO. These low backing pressures were chosen to prevent the formation of clusters in the free jet. No systematic correlation of the experimentally measured methyl spectrum as a function of backing pressure was observed, leading us to conclude that clusters are not contributing significantly to our detected signals. The gas mixture was allowed to expand unskimmed between the two extraction plates (spacing = 4 cm) of the TOFMS into a chamber pumped by a 10" diffusion pump. The entrance aperture of the mass spectrometer lies 5 cm below the nozzle at right angles to both the free jet axis and the laser axis. At the point where the mass spectrometer and jet axes intersect, rotational cooling of the precursor has effectively ceased, and an excimer laser (Lambda Physik EMG 101) operating on the 193nm ArF transition (30 mJ/cm^2) intersects the expanding free jet and photolyzes the DMSO precursor molecules. A second probe laser, delayed by 400 ns with respect to the first, detects the methyl photofragments by REMPI spectroscopy before they can be collisionally relaxed. The transition used is the well-known 2 + 1 ($3p\ ^2A_2'' \leftarrow 2p\ ^2A_2''$) REMPI transition.[5] The probe laser is a frequency-doubled Nd:YAG pumped dye laser (Quantel 581/DL) operating on DCM dye. The output from this laser in the UV is maintained at *ca.* 0.5 mJ per pulse to avoid broadening of the CH_3 REMPI transitions. The probe laser is

focused with a 15 cm focal length lens, and counterpropagates with the photolysis laser.

The mass spectrometer is of the standard Wiley-McLaren design[18]. In our specific case, the two stage extraction field is followed by two sets of parallel deflector plates. The first set of plates remove the initial jet velocity the ions possess, while the second set deflects them onto the ion detector which is a 1" diameter multichannel plate at the end of a 1.4 m drift tube. The mass spectrum can be observed on a 125 MHz transient digitizing oscilloscope (Lecroy 9400), and REMPI spectra are recorded by sequentially stepping the laser wavelength while averaging the signal in a boxcar integrator (Stanford Research SR250) which is gated for the arrival time of m/e = 15. The entire experiment is synchronized by a computer which steps the laser wavelength and collects the data.

Results

1. Internal Energy Distribution of SO($X^3\Sigma^-$)

a. Vibrational state distribution

Under collision-free conditions (DMSO: 0.02-0.03 torr; probe laser delay = 400 ns), the relative vibrational population of the nascent electronic ground state SO ($X^3\Sigma^-$) from the DMSO photodissociation at 193 nm has been determined by using LIF excitation spectra of SO($B^3\Sigma^-$-$X^3\Sigma^-$) transitions in the region of 237-295 nm (see figure 1). The bandheads of this electronic transition have been assigned by using the spectroscopic constants reported by Colin.[19] In order to obtain the relative vibrational population of SO ($X^3\Sigma^-$, v'' = 0-6), the integrated areas under the (1,0), (1,1), (1,2),

(1,3), (1,4), (1,5) and (1,6) vibrational bands are measured, and subsequently normalized for their respective Franck-Condon factors.[15] The nascent vibrational population distribution is shown in figure 2. The observed vibrational distribution is inverted and peaked at $v''=2$, in agreement with previous measurements.[6] The increased sensitivity at higher vibrational levels, now attainable with the B-X transition, can be seen when compared to the previous measurement.[7] No signal for the (1,7) band was detected, even though we have observed it for other photofragmentation cases.[14]

b. Rotational state distribution

The rovibronic transitions of SO ($B^3\Sigma^-$-$X^3\Sigma^-$) have been used for the measurements of the rotational state population distribution. The rotational levels of each of the $^3\Sigma^-$ electronic states are split into three spin components, F_1 for $J=N+1$, F_2 for $J=N$ and F_3 for $J=N-1$, primarily by the second order spin-orbit interaction. There is no Q branch in the $^3\Sigma^-$-$^3\Sigma^-$ transition due to the selection rule: $\Delta N = 0$ is forbidden.[20] Moreover, only $\Delta J = 0$ (*i.e.*, F'_1-F''_1 , F'_2-F''_2 , F'_3-F''_3) transitions have significant intensity for $N > 10$, because the Hönl-London factors for $\Delta J \neq 0$ transitions decrease rapidly with increasing N.

A portion of the rotationally resolved LIF excitation spectrum of SO ($B^3\Sigma^-$, $v'=1$-$X^3\Sigma^-$, $v''=1$) transition is shown in Fig. 3. The assignment of the spectrum is based on the calculated line positions using Colin's spectroscopic constants.[19] The difference between the calculated line positions and our experimental measurements are $\leq$ 0.005 nm.

The relative rotational state populations within a given vibrational band, P(N"), can be determined by normalizing the intensity of the transition by the Hönl-London factor and the rotational degeneracy. The integrated area of a given spectral peak is used as the measure of the intensity in these experiments. Hönl-London factors for $^3\Sigma$-$^3\Sigma$ transitions were taken from Smith and Liszt.[15]

A rotational distribution in a single vibrational level can, in many cases, be described by the Boltzmann expression,

$$P(N") = (2J" + 1) \exp[-BN"(N" + 1)/ kT_R] \quad (3)$$

where B is the rotational constant of the ground state, k is the Boltzmann constant, and T_R is the rotational temperature. A plot of $\ln[P(N")/2J" + 1)]$ vs $BN"(N" + 1)$ will give a straight line with slope, $-1/kT_R$, and the least-square fits of these points to this form will yield the rotational temperature T_R. Figure 4 is a Boltzmann plot of the nascent rotational state populations of $SO(X^3\Sigma^-, v" = 0, 1, 2$ and 3) that results from DMSO photodissociation at 193 nm. We emphasize that our Boltzmann plots are not rigorously linear (i.e. they cannot be characterized as rotational temperatures), and that linear least squares fits to the data points yield rotational temperatures that are only approximations of the rotational distributions. We present the data in this form only because it serves a useful purpose in comparison of this work with other related studies (see below). The rotational state populations of $v" = 0$-3 can be fit by a straight line with rotational temperatures, T_R, in the range of 750-1450K. In the case of $v" = 1$, the nascent rotational state distribution is not as well-represented by a single line as in the other cases.

2. *Quantum Yield Determination*

Since more than one electronic state of SO is thermochemically accessible in the 193 nm photodissociation of DMSO, we have measured the primary quantum yield of $SO(X^3\Sigma^-)$ following excimer laser photolysis. In our experiments, the LIF signal of a given rotational line of $SO(X^3\Sigma^-, v'' = 2)$ has been used to make this measurement. As mentioned above, the LIF signal intensity of $SO(X^3\Sigma^-)$ was found to be linear with respect to the 193 nm photolysis laser fluence in our experiment indicating that the production of SO radical results from a single photon absorption by the parent molecule. To measure the photofragment quantum yield of $SO(X^3\Sigma^-)$, we compare the LIF signal intensity of a single SO rotational line following the 193 nm photolysis of both DMSO and SO_2. For example, the dye laser is fixed at 252.105 nm corresponding to the $R_{22}(20)$ line of $SO(B^3\Sigma^-, v' = 1 \leftarrow {}^3\Sigma^-, v'' = 2)$ transition. 0.02 torr of either DMSO or SO_2 is introduced into the reaction chamber, and the LIF signal intensity is averaged for 2000 laser shots. We repeat the experiment ten times and take the average for the quantum yield measurement. Assuming that the $SO(X^3\Sigma^-)$ produced by SO_2 photodissociation at 193 nm occurs with unit efficiency, the quantum yield of sulfur monoxide radical production from DMSO photodissociation at 193 nm is found to be, $\Phi_{193}^{DMSO}[SO(X^3\Sigma)] = 1.02 \pm 0.12$. The measurement was also repeated for several different rotational lines in the $v'' = 2$ manifold, yielding a similar result. In order to obtain these values, the experimentally obtained signal intensity was corrected for the measured nascent SO photofragment vibrational state distributions resulting from 193 nm photolysis of SO_2 and DMSO, and for their absorption cross-sections.[21] The nascent $SO(X^3\Sigma, v'' = 2)$ rotational state distributions

for DMSO and SO_2 are similar.[22] A quantum yield measurement was made for longer delay times, *i.e.* to allow rotational relaxation and relaxation of higher electronic states of SO, and a similar result, 0.91 ± 0.09, was obtained. We have also made quantum yield measurements of the production of $SO(X^3\Sigma^-)$ from the 193 nm photolysis of $SOCl_2$.[14] We obtain a value of $\Phi_{193}^{SOCl2}[SO(X^3\Sigma)] = 0.73 \pm 0.10$, in strong agreement with the previous measurement of 0.80 by Kanamori, *et al.*, using infrared absorption spectroscopy.[14]

3. *Kinetic Energy of the SO Fragment*

Typical linewidths (FWHM) of SO rotational lines measured in our experiments are 0.25-0.3 cm^{-1}, and are therefore laser limited (0.25 cm^{-1}). This linewidth can be used as the maximum value of the Doppler profile of SO rovibronic transitions, assuming the DMSO photodissociation to be isotropic, and the translational temperature, T_{trans}, of nascent SO(X,v") fragment can be estimated by the following relationship:

$$T_{trans} = (\Delta v / 2v_o)^2 mc^2 / 2k \ln 2 \qquad (4)$$

where Δv is the FWHM of the Doppler profile, v_o is the center frequency of the given line, m is the molecular mass and k is the Boltzmann constant. The translational temperature of nascent $SO(X,v'' = 1)$ is found to be $< 3500 \pm 500$K by this estimate, yielding an upper limit for the average translational energy $< 8.8 \pm 1.4$ kcal/mol.

4. *CH_3 Internal Energy Distribution*

A representative REMPI spectrum of the nascent methyl radicals, uncorrected for laser power, is shown in Figure 5. The m/e = 15 ion signal arising from the photoionization of methyl is directly proportional to the intensity of the excimer(pump) laser and depends quadratically on the intensity of the doubled dye (probe) laser as would be expected for a 2 + 1 REMPI process. We observe four vibrational bands in the spectrum, 0_0^0, 1_1^1, 2_1^1, and 2_2^2 as designated in figure 5. Excitation is only observed in the ν_2 (umbrella) mode and the symmetric C-H stretch ν_1 . This result is consistent with the previous product state distributions of photolytic methyl fragments from acetone,[8] methyl iodide[14] and nitromethane,[15] obtained by REMPI.

Figure 6 shows a plot of the observed vibrational population distribution for the methyl radicals produced from the 193 nm photolysis of $(CH_3)_2SO$. Relative populations are determined by integrating under the vibrational band, and then correcting for both the laser intensity and the vibrational Franck-Condon factors.[15] As has been pointed out previously, there are difficulties in assigning relative populations from intensities of REMPI transitions.[15] We have used the same approximations as Trentleman *et al.* in their analysis of acetone.[9c] Following this standard and fitting the population of the observed levels in the ν_2 mode to a Boltzmann model produces a vibrational temperature of 600K. A rotational contour analysis[9,15] of the 0_0^0 band leads to an estimate of the rotational temperature of methyl in the origin band of 150K. As in the case of acetone, there may be vibrational modes populated which we cannot clearly observe, however, we believe that the relative distribution of the vibrational modes which we do observe is correct.

Discussion

The quantum yield measurement, demonstrating the production of ground state sulfur monoxide with unit efficiency, limits the number of possible photoreactions to:

$$DMSO + h\nu(193\ nm) \rightarrow SO(X^3\Sigma^-) + 2\ CH_3 \qquad \Delta H_{RXN} = 106.3\ kcal/mol\ (5)$$
$$E_{avail} = 41.7\ kcal/mol$$
$$\rightarrow SO(X^3\Sigma^-) + C_2H_6 \qquad \Delta H_{RXN} = 24.8\ kcal/mol\ (6)$$
$$E_{avail} = 123.2\ kcal/mol$$

While we have not directly measured the photochemical quantum yield of CH_3 radicals in this experiment, we assume (5) to be the only reaction pathway. This assumption is based on: (1) The inability to detect ethane in previous experiments;[6] and (2) the energy content of the photofragments (see below).

The total energy balance in these experiments is summarized in Table I, assuming that only reaction (5) is operative. Since we can only account for at most 52% of the available energy in the nascent photofragments, we must ask, where is the remaining energy? One possibility is that we have not accounted for all the internal energy in the CH_3 photofragments. Recently, experimental studies have shown that other vibrational states may also be populated which are not observed in our REMPI experiment. Donaldson and Leone, in infrared emission experiments have shown that the ν_3 mode of methyl is populated in the photodissociation of acetone.[6] No population is observed in the ν_3 mode in the REMPI spectrum of the methyl radical following 193 nm irradiation of $(CH_3)_2CO$ however.[8] Direct time-resolved infrared diode laser absorption spectroscopy experiments on dissociated acetone-d_6 show a rise in the ground vibrational state CD_3 population with a time constant suggesting that many

vibrational states may initially be populated,[9] again conflicting with the results of the REMPI study which suggests that most of the molecules are formed in the vibrational ground state. Despite this large discrepancy, the relative populations of the methyl rotational and vibrational states which are observed in both the REMPI and diode laser experiments agree. These important facts underscore the caution that must be exercised when one uses REMPI on a polyatomic molecule to measure state distributions. The REMPI spectrum provides incomplete information (much as an infrared spectrum does) on the vibrational population present, except in the most fortuitous cases. Therefore, population distributions determined from such a REMPI spectrum should be considered as a lower bound to the true vibrational excitation.

Even if the internal energy measurements of the nascent CH_3 photofragments are low, it is difficult to imagine that the remaining 48% of energy (*ca.* 20 kcal/mole) will be partitioned into the vibrational modes of the methyl product to which we are experimentally blind. More likely is that a significant fraction of the remaining energy is deposited into the kinetic energy of the methyl fragments. Similar effects have been observed in the photodissociation of acetone at 193 nm (see below), where the methyl fragments carry away over 40% of the available energy in their translational degrees of freedom.[9c] Our experimental apparatus is not suitable for measuring the kinetic energy deposited in the methyl fragments by the photodissociation.

The most striking result of this photodissociation is the production of a vibrational state population inversion in the nascent SO photofragments. This inversion has been observed previously, and in agreement with our results here, but this work extends the measurement to higher vibrational levels. Nevertheless, both

measurements indicate an inverted nascent vibrational distribution, peaked at $v'' = 2$. The observed vibrational distribution allows us to rule out direct photodissociation, *i.e.*, where absorption of a photon leads directly to a repulsive state, since the SO bond length in DMSO(1.49Å)[23] is almost identical to that in diatomic sulfur monoxide(1.48Å). A Franck-Condon analysis in the previous work was found to support a SO bond length of 1.55Å in the sulfoxide immediately prior to dissociation. Either an excited electronic state of DMSO or CH_3SO was postulated to be the precursor to the vibrationally excited SO moiety. The data reported here also fits this argument well.

The measurements of the sulfur monoxide rotational state distributions indicate a relatively cold nascent radical, that can be described by a temperature. The rotational temperatures are found to generally increase with increasing vibrational level, suggesting coupling between the rotational and vibrational motion in the transition state. We were not able to effectively measure the lower rotational levels ($N < 10$) due to spectral overlap, but simulations of these bands with the temperatures obtained from the higher levels, give reasonable agreement. The observation of the SO radical appearing with a single temperature distribution is consistent with the existence of only a single pathway to produce ground state SO, *i.e.* reaction (6) does not play a significant role.

We have thus far provided evidence that irradiation of DMSO at 193 nm proceeds along a single pathway to produce three fragments, two methyl radicals and ground state SO. But the question remains, does the three-body fragmentation occur by a concerted or stepwise mechanism? In this case, the lack of evidence for two

different types of methyl, along with the inverted vibrational distribution supports a concerted three-body fragmentation. The following scheme may be postulated: Absorption of a 193 nm photon by DMSO to give an excited state with a lengthened SO bond, which subsequently predissociates according to reaction (5).

To test this hypothesis, more data about the far UV spectroscopy of alkyl sulfoxides is necessary. Irradiation of DMSO at 193 nm is believed to be connected to a π-π^* type transition localized on the S-O chromophore. If this were the case, the excited state of DMSO would be expected to have a longer S-O bond length. Care must be exercised in assigning such localized bonding schemes in sulfoxides, because the d-orbitals of the sulfur atom can participate in forming the molecular orbitals, resulting in considerable electron delocalization.[7]

The similarities of the product state distributions from $(CH_3)_2SO$ and $(CH_3)_2CO$ seems to indicate that they may be dissociating by a similar mechanism. However, upon close examination of the product state distributions, small differences are indicative of the intermediate case (acetone) vs. concerted (DMSO) dissociations (see Table II). If the diatomic fragments from acetone and DMSO, CO and SO, respectively, are compared, small differences between the two cases exist. The CO fragment is produced with about one half the vibrational energy and five times more rotational energy than the SO fragment. This can be understood in the following way. The greater vibrational energy content (and the inversion) of the SO photofragment are the result of a fast predissociative process dominated by the Franck-Condon excitation in DMSO, while in acetone the dissociation, comparable with that of a rotational period, allows more time to thermalize the energy into the other polyatomic

fragments. The methyl rotational and v_2 vibrational distributions observed for DMSO both are slightly colder than those measured for acetone. Although some excitation was observed in the C-H stretch mode of methyl in the acetone dissociation, we see slightly more population in the case of methyl produced from DMSO.

The discrepancy between the two systems can be seen more clearly if one models DMSO in the stepwise dissociation limit. A simple extension of the impulsive model of Busch and Wilson[24] has been applied to the photodissociation of acetone, and reasonably reproduces the experimental data, even if one considers the possible excess energy in the methyl fragments (see Table II). This classical model supposes that the dissociation occurs by a two-step mechanism, and provides a rough estimate of the relative energies in each fragment. If this model is applied to DMSO, it predicts *ca.* 15% of the available energy will be partitioned into the internal degrees of freedom of the methyl radicals, and approximately 5% into rotation and vibration of sulfur monoxide. As can be seen in Table II, the model underestimates the amount of energy disposal into the SO photofragment, and overestimates the amount of internal energy in the CH_3 radicals. This analysis suggests that this dynamical effect may result from the concerted three-body dissociation following irradiation of dimethyl sulfoxide at 193 nm.

Recent evidence suggests that three-body concerted dissociations are not all that rare. The 193 nm photodissociation of thionyl chloride (Cl_2SO) is a particularly compelling case, because of its structural similarities with DMSO. Baum, *et al.* used photofragment time-of-flight spectroscopy to probe the 193 and 248 nm photodissociations of Cl_2SO. Their results indicate that following irradiation at 193

nm, 80% of the photoexcited Cl_2SO dissociates by a concerted three-body mechanism to give SO + Cl + Cl. Wang, *et al.* employed LIF spectroscopy to examine the quantum yield and energy disposal into the $SO(X^3\Sigma^-)$ fragment following 193 and 248 nm photolysis of Cl_2SO.[14] They concluded that 73% of the photoactivated Cl_2SO fragments via a concerted three-body dissociation to yield $SO(X^3\Sigma^-)$ following irradiation at 193 nm. Furthermore, the $SO(X^3\Sigma^-)$ produced from the 193 nm photolysis of Cl_2SO is born with an inverted vibrational distribution, peaked at $v'' = 2$.

Summary and Conclusions

The quantum yield, vibrational and rotational population distributions of the nascent $SO(X^3\Sigma^-)$ radical from the photodissociation of $(CH_3)_2SO$ in the gas phase at 193 nm have been measured by laser-induced fluorescence, while the internal energy of the resulting neutral methyl fragments have been studied by REMPI spectroscopy. The energy distributions of the nascent fragments are best described by a concerted three-body fragmentation. While some of our data are suggestive of a concerted synchronous dissociation of the two S-C bonds in DMSO,[2] we cannot conclusively determine the synchronicity from our results. Further studies of the photofragment angular distributions following 193 nm irradiation of dimethyl sulfoxide would be helpful in analyzing this aspect of the dissociation dynamics.

Acknowlegdments

We would like to acknowledge the generous support of this project by the Air Force Office of Scientific Research. Part of this research was carried out in the Puerto Rico Laser and Spectroscopy Facility, which operates under the auspices of the University of Puerto Rico and NSF-EPSCoR. HHN and MH thank the Office of Naval Research for funding the work done at the Naval Research Laboratory.

TABLE I: Distribution of available energy into the different degrees of freedom of the nascent photofragments following 193 nm photodissociation of dimethyl sulfoxide.

FRAGMENT	MODE	ENERGY (kcal/mol)	% Available Energy
CH_3	translational	Not measured	--
	internal	1.9	4.7
SO	translational	8.8[a]	21.1[a]
	internal	8.9	21.3
CH_3	translational	Not measured	--
	internal	1.9	4.7

a) Upper Limit

TABLE II: A comparison of the experimental and calculated relative energy distributions into the fragments following 193 nm photodissociation of acetone vs. dimethyl sulfoxide. Relative energies are obtained with respect to the total available energy for the photofragments. The calculated values are obtained from an impulsive model, and assume a stepwise cleavage of the bonds.

Fragment	Degree of Freedom	$(CH_3)_2CO$		$(CH_3)_2SO$	
		experiment[a]	model[b]	experiment[c]	model[b]
$CH_3(1)$	E_{int}	0.050	0.050	0.047	0.070
	E_{trans}	0.199	0.199	n.m.	0.291
CO,SO	E_{int}	0.172	0.195	0.213	0.052
	E_{trans}	0.163	0.190	0.211	0.157
$CH_3(2)$	E_{int}	0.050	0.068	0.047	0.081
	E_{trans}	0.199	0.299	n.m.	0.349
Total		0.833	1.000	0.518	1.000

a) Reference 9c
b) Adapted from reference 24
c) This work

Figure Captions

Figure 1: LIF spectrum of nascent SO($X^3\Sigma^-$) from the 193-nm photodissociation of 0.026 Torr of $(CH_3)_2SO$. The delay between the pump and the probe laser was 400 ns. The origins of the vibrational bands have been assigned from reference 19

Figure 2: Nascent vibrational state distribution of SO($X^3\Sigma^-$, v") from the 193 nm photodissociation of $(CH_3)_2SO$

Figure 3: A portion of the ($B^3\Sigma^-$,v' = 1←$X^3\Sigma^-$,v' = 1) transition showing the partial assignment of the rotationally-resolved LIF excitation spectrum used for measurement of the rotational population state distribution.

Figure 4: Semilog plot of the intensity of SO($X^3\Sigma^-$, v") rotational lines corrected for the Honl-London factors, measured 400 ns following the 193 nm photolysis of $(CH_3)_2SO$. The solid line is a linear least squares fit to the SO($X^3\Sigma^-$, v" = 0) data and corresponds to a Boltzmann temperature of 748 ± 24K.

Figure 5: 2 + 1 ($3p^2A_2"$←$2p^2A_2"$) REMPI spectrum of CH_3 radicals produced from the 193 nm photodissociation of $(CH_3)_2SO$ obtained by monitoring mass 15. This spectrum has not been normalized for laser power.

Figure 6: Relative vibrational state distribution for the observed vibrational modes of methyl radical produced from the 193 nm photodissociation of $(CH_3)_2SO$. The line is a Boltzmann fit to the ν_2 mode, which results in a vibrational temperature of 600K.

References

1. See for example, *Molecular Photodissociation Dynamics*, Eds. Ashfold, M.N.R.; Baggott, J.G. Royal Society of Chemistry, London 1987.

2. Strauss, C.E.M.; Houston, P.L. *J. Phys. Chem.* 1990, *94*, 8751.

3. a) Bock, H.; Solouki, B. *Angew. Chem. Int. Ed. Eng.* 1972, *11*, 436.
   b) Bock, H.; Solouki, B. *Chem. Ber.* 1974, *107*, 2299.

4. Plane, J.M.C. in *Biogenic Sulfur in the Environment, ACS Symp. Ser. 393*, Eds Saltzman, E.S.; Cooper, W.J. American Chemical Society: Washington, D.C. 1989, pp. 404-23.

5. Hudgens, J.W.; DiGiuseppe, T.G.; Lin, M.C. *J. Chem. Phys.* 1983, *79*, 571.

6. Chen, X.; Asmar, F.; Wang, H.; Weiner, B.R. *J. Phys. Chem.* 1991, *95*, 6415.

7. Gollnick, K; Strauss, H.U. *Pure Appl. Chem.* 1973, *33*, 217.

8. a) Gaines, G.A.; Donaldson, D.J.; Strickler, S.J.; Vaida, V. *J. Phys. Chem.* 1988, *92*, 2762;
   b) Donaldson, D.J.; Gaines, G.A.; Vaida, V. *J. Phys. Chem.* 1988, *92*, 2766.
   c) Hess, B.; Bruna, P.J.; Buenker, R.J.; Peyerimhoff, S.D. *Chem. Phys.* 1976, *18*, 267;
   d) Baba, M.; Shinohara, H.; Nishi, N. *Chem. Phys.* 1984, *83*, 221.

9. a) Donaldson, D.J.; Leone, S.R. *J. Chem. Phys.* 1986, *85*, 817.
   b) Woodbridge, E.L.; Fletcher, T.R.; Leone, S.R. *J. Phys. Chem.* 1988, *92*, 5387.
   c) Trentleman, K.A.; Kable, S.H.; Moss, D.B.; Houston, P.L. *J. Chem. Phys.* 1989, *91*, 7498.
   d) Hall, G.E.; Vanden Bout, D.; Sears, T.J. *J. Chem. Phys.* 1991, *94*, 4182.
   e) North, S.; Longfellow, C.; Lee, Y.T. *unpublished results.*

10. Felder, P.; Effenhauser, C.S.; Haas, B.M.; Huber, J.R. *Chem. Phys. Lett.* 1988, *148*, 417 and references therein.

11. Kawasaki, M.; Kasatani, K.; Sato, H.; Nishi, N.; Ohtoshi, H.; Tanaka, I. *Chem. Phys.* 1984, *91*, 285.

12. Kanamori, H.; Tiemann, E.; Hirota, E. *J. Chem. Phys.* 1988, *89*, 621.

13. Baum, G.; Effenhauser, C.S.; Felder, P.; Huber, J.R. *J. Phys. Chem.* 1992, *96*, 756.

14. Wang, H.; Chen, X.; Weiner, B.R. *J. Phys. Chem.* previous paper.

15. Smith, W.H.; Liszt, H.S. *J. Quan. Spectros. Radiat. Trans.* **1975**, *11*, 45.

16. a) Ogorzalek-Loo, R; Haerri, H.P.; Hall, G.E.; Houston, P.L. *J. Chem. Phys.* **1989**, *90*, 4222.
b) Moss, D.B.; Trentleman, K.A.; Houston, P.L. *J. Chem. Phys.* **1992**, *96*, 237.

17. Barnhard, K.I.; Santiago, A.; He, M.; Asmar, F.; Weiner, B.R. *Chem. Phys. Lett.* **1991**, *178*, 150.

18. Wiley, W.C.; McLaren, I.H. *Rev. Sci. Instr.* **1955**, *26*, 950.

19. a) Colin, R. *J. Chem. Soc. Far. Trans. 2* **1982**, *78*, 1139;
b) Colin, R. *Can J. Phys.* **1969**, *47*, 979.

20. Herzberg, G. *Molecular Spectra and Molecular Structure, I. Spectra of Diatomic Molecules,* (R.E. Krieger Publishing Company, Malabar, Florida, 1989).

21. The following 193 nm absorption cross sections were used: SO_2 (σ = 8.1 x 10^{-18} cm^2 $molecule^{-1}$; from Okabe, H. *Photochemistry of Small Molecules*, Wiley-Interscience, New York, **1978**, p. 249) and $(CH_3)_2SO$ (σ = 3.8 x 10^{-18} cm^2 $molecule^{-1}$; from reference 7).

22. Chen, X.; Wang, H.; Weiner, B.R. *unpublished results.*

23. Dreizler, H.; Dendl, G.Z. *Naturforsch.* **1964**, *19A*, 512.

24. Busch, G.E.; Wilson, K.R. *J. Chem. Phys.* **1972**, *56*, 3626,3638.

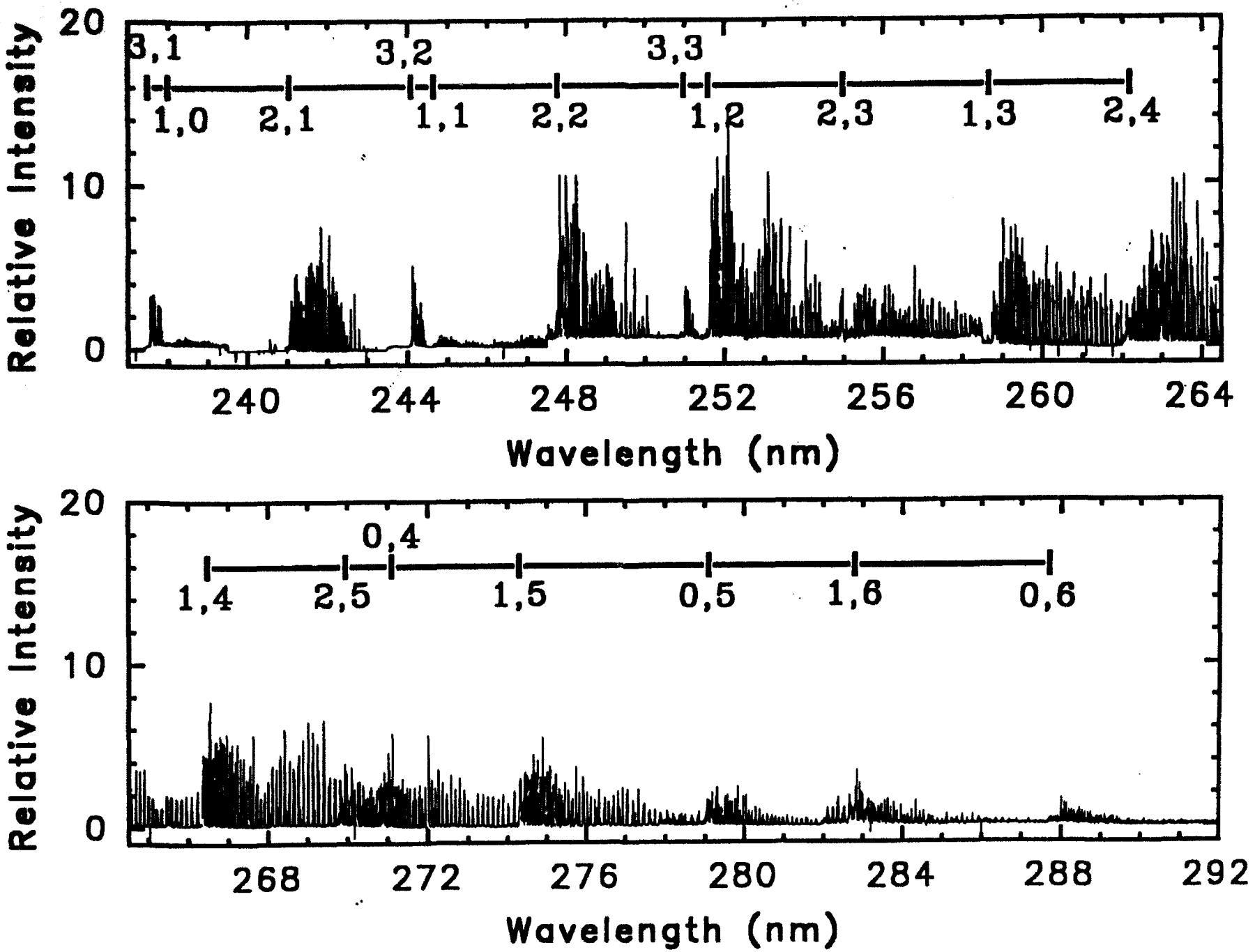
Relative Intensity
20
10
0
3,1
3,2
3,3
1,0
2,1
1,1
2,2
1,2
2,3
1,3
2,4
240
244
248
252
256
260
264
Wavelength (nm)
Relative Intensity
20
10
0
0,4
1,4
2,5
1,5
0,5
1,6
0,6
268
272
276
280
284
288
292
Wavelength (nm)

Figure 1

Figure 2

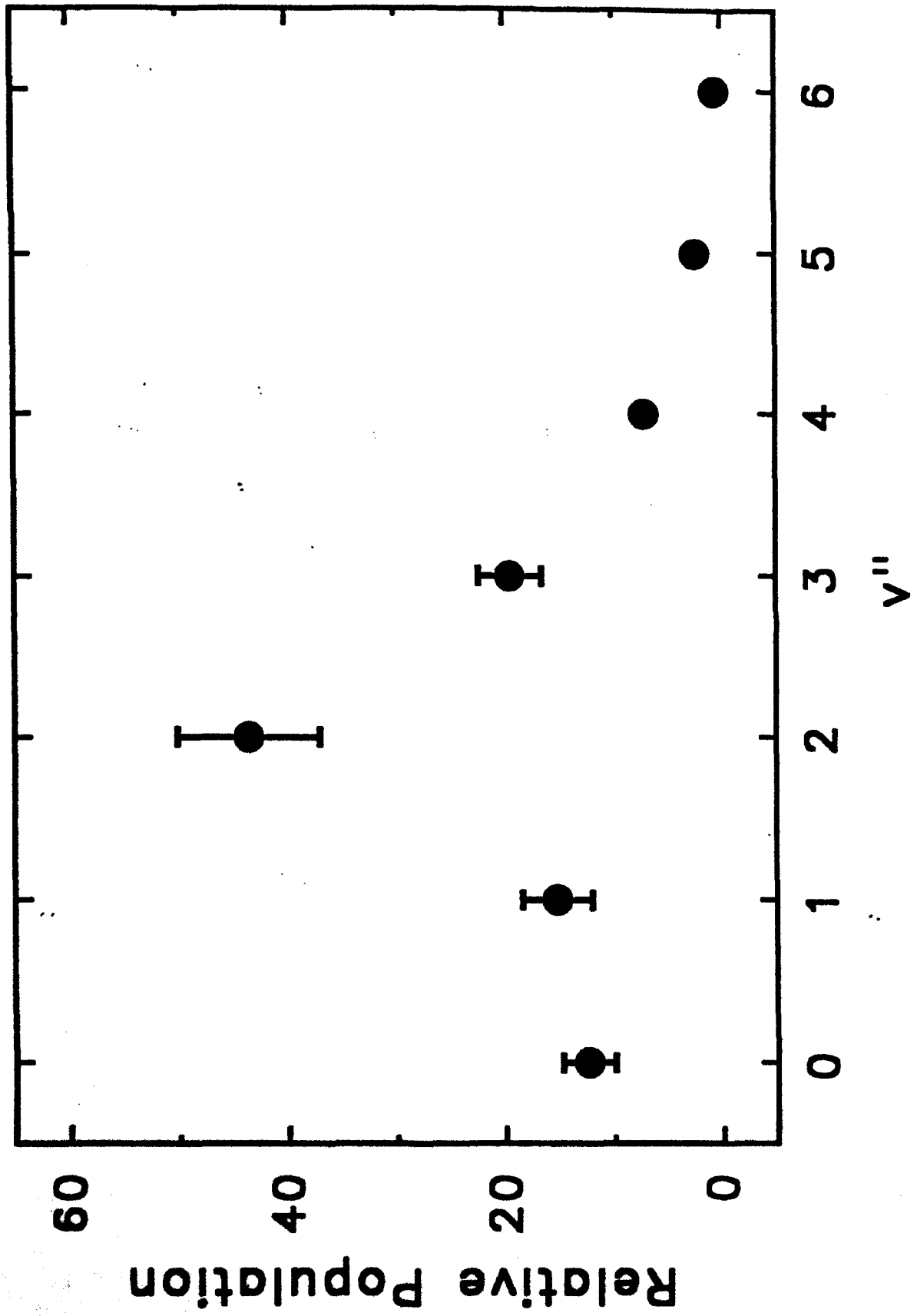

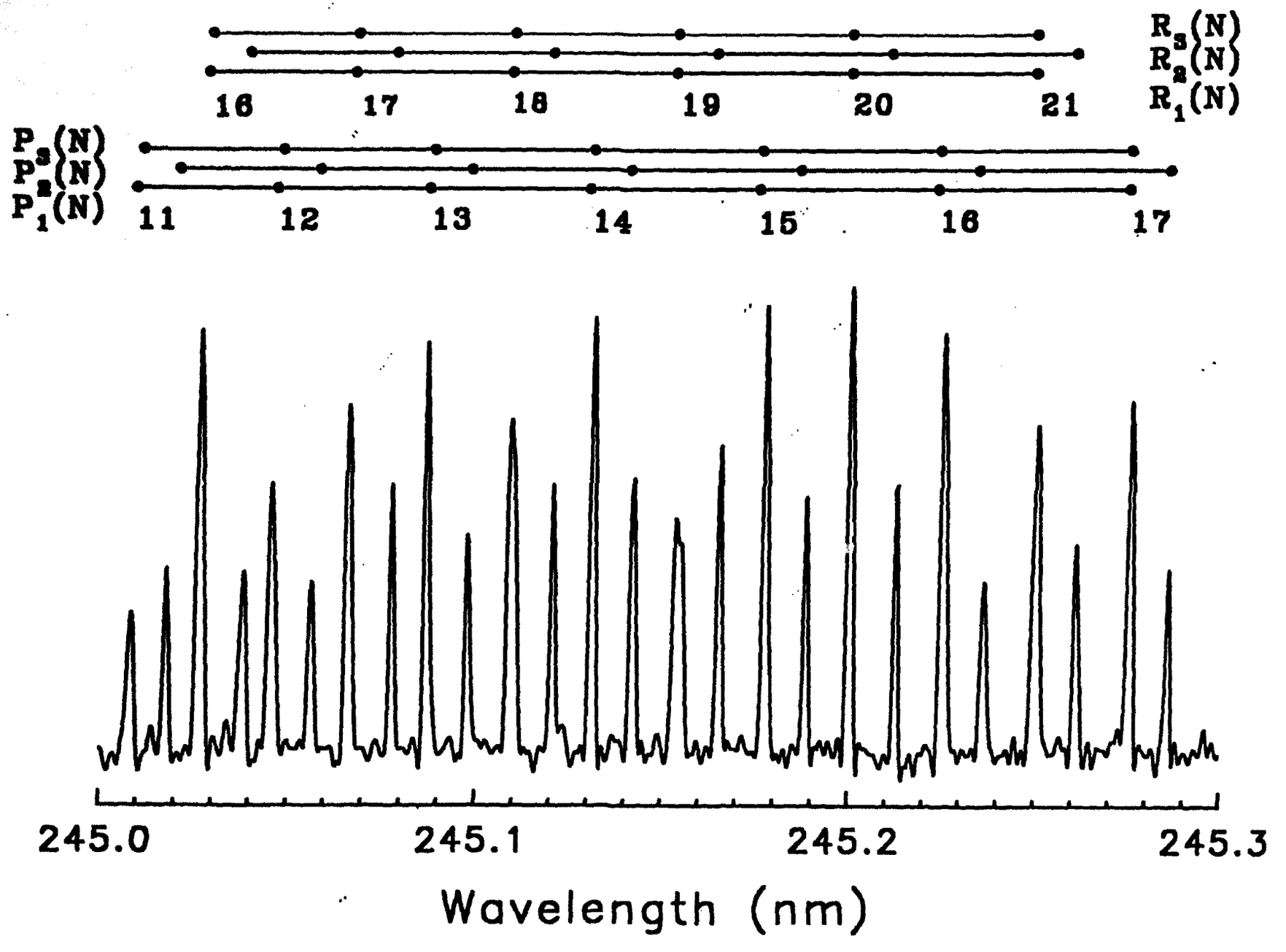
R3(N)
R2(N)
R1(N)
16
17
18
19
20
21
P3(N)
P2(N)
P1(N)
11
12
13
14
15
16
17
245.0
245.1
245.2
245.3
Wavelength (nm)

FIGURE 4

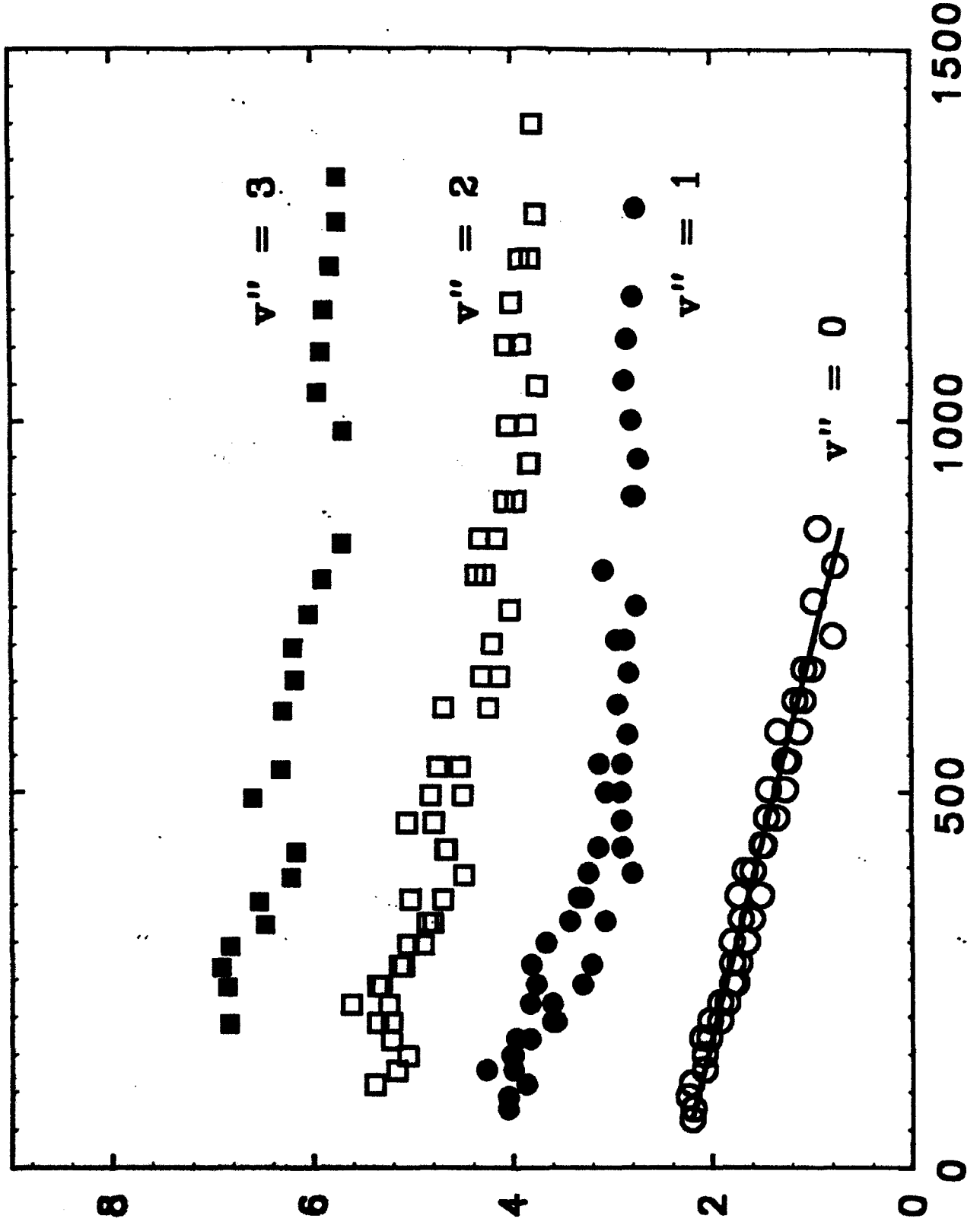

FIGURE 5

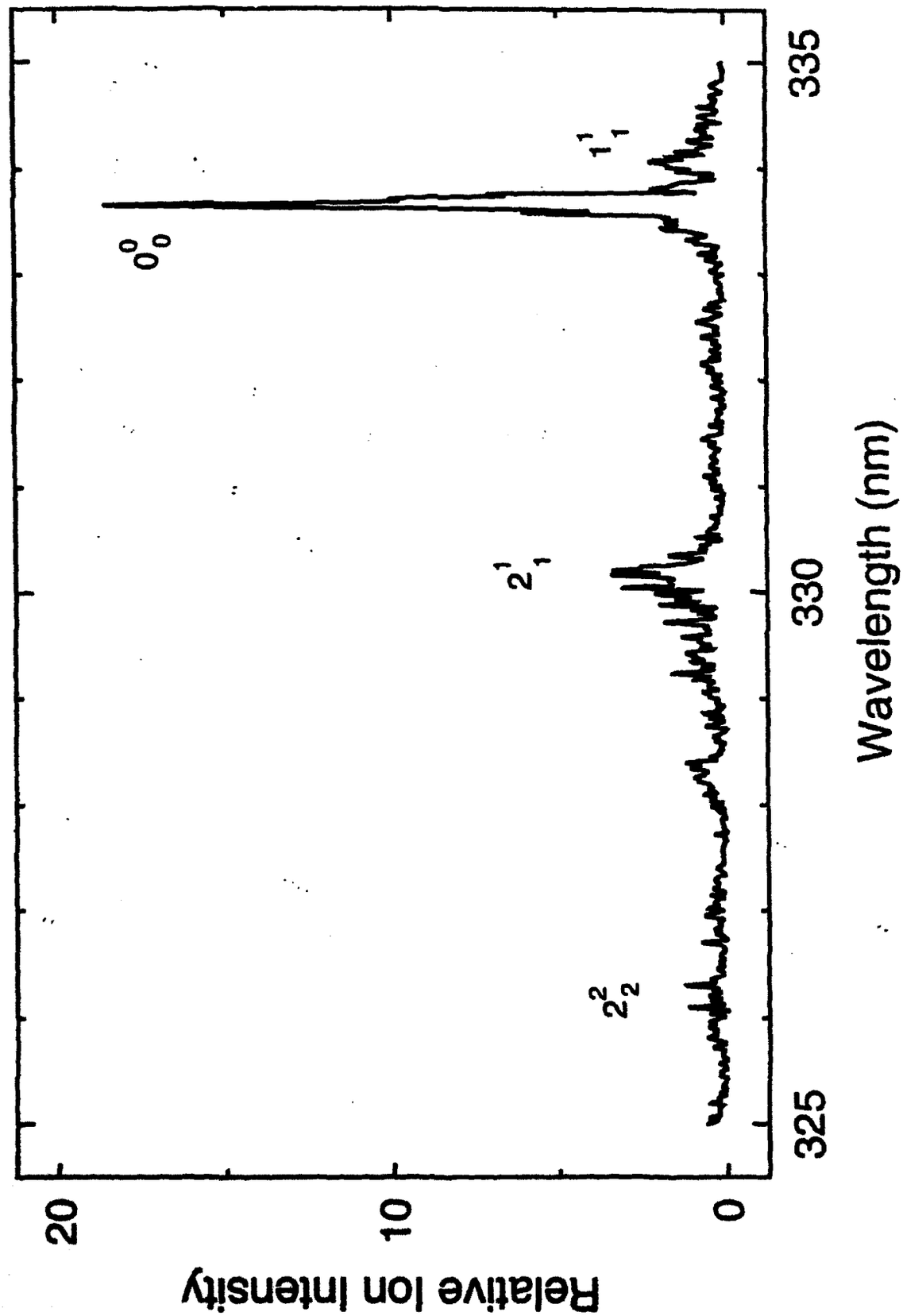
Relative Ion Intensity
20
10
0
325
330
335
Wavelength (nm)
0_0^0
2_1^1
1_1^1
2_2^2

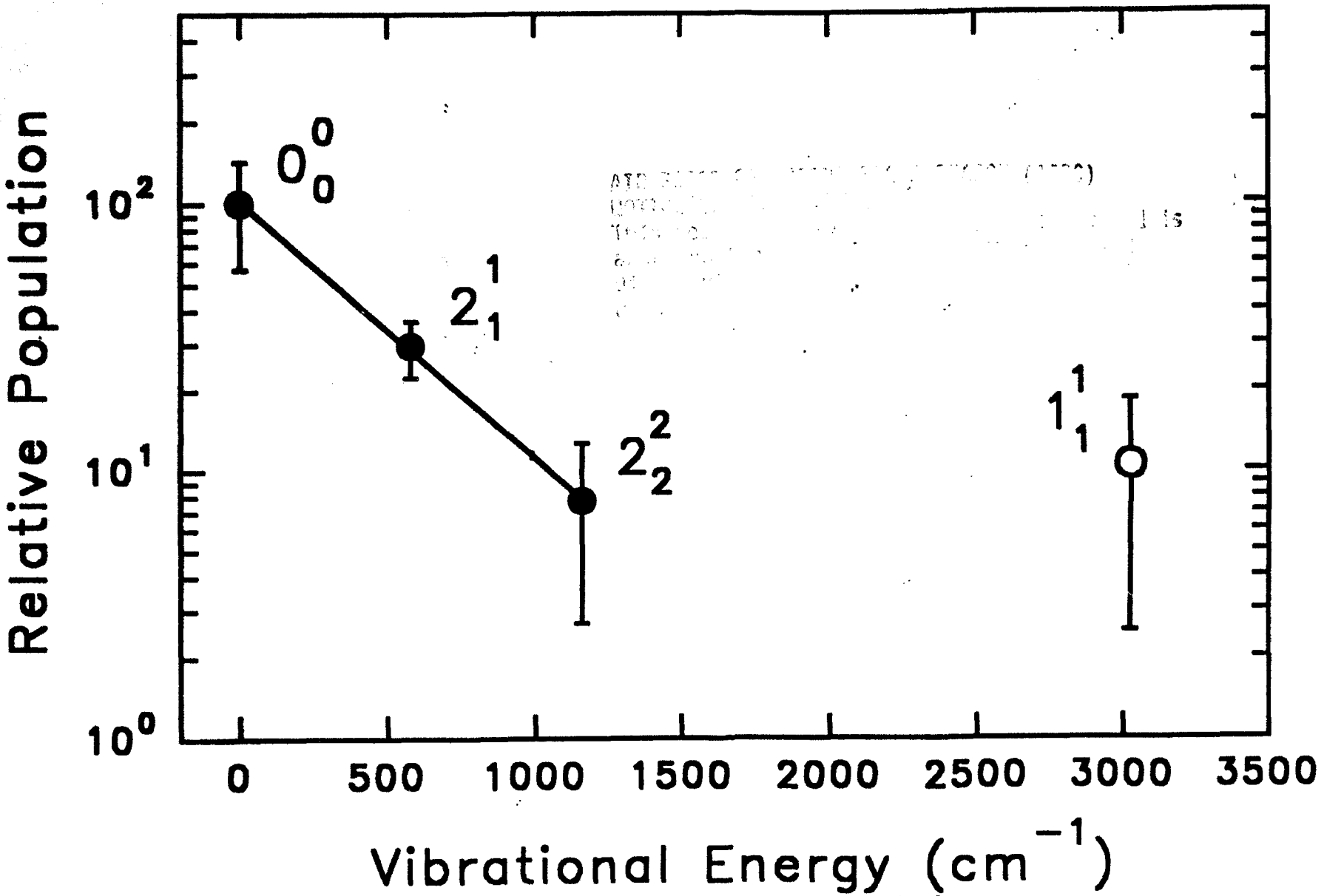
Relative Population
10^2
10^1
10^0
0_0^0
2_1^1
2_2^2
1_1^1
0
500
1000
1500
2000
2500
3000
3500
Vibrational Energy (cm^{-1})

Figure 6